IMPROVEMENT IN ACOUSTIC LINER ATTENUATION IN TURBOFAN ENGINES BY MEANS OF PLASMA SYNTHETIC JET ACTUATOR

CHRISTOPHER LOUIS BARNOBI

Thesis submitted to the Faculty of the
Virginia Polytechnic Institute and State University
in partial fulfillment of the requirements for the degree of

Master of Science
in
Mechanical Engineering

Chris R. Fuller, Chair

Alfred L. Wicks

Cory M. Papenfuss

July 2, 2010
Blacksburg, Virginia

KEYWORDS: noise control, acoustic liner, turbofan, plasma synthetic jet actuator,

IMPROVEMENT IN ACOUSTIC LINER ATTENUATION IN TURBOFAN ENGINES BY MEANS OF PLASMA SYNTHETIC JET ACTUATOR

Christopher Louis Barnobi

Abstract

Despite many advances in aviation noise control over the past 50 years, the industry is continually striving to reduce noise emissions. Turbofan engine acoustic liners are efficient attenuators of engine noise. Plasma actuators have been used as flow control devices in other settings and will now be studied as an enhancement for acoustic liners. A plasma actuator can excite oscillatory flow or a single direction (bias flow). Both flow types are studied as possible means to excite turbofan liners in order to improve the acoustic performance.

Experiments revealed the oscillatory flow as the dominant factor in controlling resonator performance. The phase control of the actuator signal is an important parameter when dealing with the oscillatory flow. The actuator is first applied to a single resonator and then a set of six resonators. The experiments show that with the correct phase, the actuators improved the performance of a single resonator by 3 dB to 5 dB. The results for the array of actuators/resonators mirror the results of a single device.

Beyond the improvements in performance, a number of other factors affect the usefulness of the plasma actuator technology in a turbofan environment. The ability of the actuator to produce plasma is susceptible to small imperfections in the device, and this property will likely be amplified in a perforated sheet with embedded actuators. Additional weight and energy consumed by the actuators is another factor to consider. Finally, plasma actuator operation produces ozone, so environmental effects deserve consideration as well.

Table of Contents

List of Figures

Index of Tables

1 Introduction

1.1 *Objective/Motivation*

In the United States, the FAA regulates the amount of noise that aircraft can produce with a major focus on take off and landing [8]. This regulation on noise can be an important limiting factor for airline operators and is sometimes the reason less flights are conducted in a day. Therefore, the aircraft manufactures have a powerful monetary incentive to lower the noise propagated from their product.

Several advances have been made in the area of noise control, dealing with aeronautical vehicles. Producing hulls and air foils with less air drag and insulating the hull have reduced noise pollution from the point of view of bystanders and passengers. Overall precision and efficiency of the engine have reduced unnecessary noise, also. The transition from the jet engine to the turbofan engine has reduced excessive turbulence and the accompanying noise. Despite the advances in the field, significant opportunity remains for further research.

The installation of acoustic liners has been proven to be an effective approach to mitigate the excessive noise produced by turbofan engines. Further improvements to conventional acoustic liners are desired to further reduce the radiated noise. Through a knowledge of cavity acoustics, an acoustic liner can be effectively broken down into a Helmholtz resonator analogy. A Helmholtz resonator functions as a single element of acoustic liner. As this thesis pursues new

methods of implementing acoustic liners, Helmholtz resonators receive focused attention. The combination of Helmholtz resonator methodology and plasma actuator technology provides the means to improve levels of attenuation already provided by acoustic liners.

This work aims to present a novel approach for improving the performance of acoustic liners employed in turbofan engines. Although the addition of an active component to a Helmholtz-style resonator has been previously attempted, the focus of this research uses a synthetic jet plasma actuator as the active device. These research efforts strive to improve the performance of turbofan acoustic liners as a sound attenuator. The method requires the investigation of both acoustic liner and plasma actuator technologies with the aim of combining those technologies. The 1kHz – 2kHz acoustic frequency range is the focus bandwidth for the research and investigation. This range lies within the larger problematic frequency range that Pratt and Whitney must consider when designing turbofan engines. These research efforts strive to improve the performance of turbofan acoustic liners as a sound attenuator.

1.2 *Approach*

This thesis seeks to investigate and document the combination of Helmholtz resonators and plasma actuator technology to acoustic liners. The acoustic liner is composed of perforated sheet with a honeycomb cell backing. The behavior of one single element of this liner operates in the same manner as a Helmholtz resonator. Before applying the plasma actuator technology to the complex acoustic liner, the simple Helmholtz resonator will be tested. A device is designed and constructed that will combine the active components of the plasma actuator and the

attenuating affects of the Helmholtz resonator. This construction is hereon referred to as the "actuator/resonator device" or "resonator/actuator".

Experiments are developed and employed that characterize the effects the actuator has on the attenuation of a single resonator. While these experimental efforts produced noteworthy results, great efforts were also committed to modeling and simulating these experiments. The models are built to fully embody and understand the components that are controlling the resonator-actuator device's capabilities to attenuate sound. A finite element method is used to model the actuator-resonator device. Abaqus CAE was the choice for finite element solver. The well known spring-mass analogy for lumped-parameter acoustic resonators was addressed and altered in order to show the effects of the plasma actuator. After preliminary testing and modeling, the actuator-resonator device was further developed. The final device was developed to reflect the array of Helmholtz resonators which combine to act as a turbofan jet acoustic liner.

1.3 *Summary*

This chapter has introduced the efforts to research and study the application of a plasma actuator. The motivation for this research has been discussed, as well as the possible benefits that may arise from the research. A brief summary of the entirety of the work done has also been outlined. The next chapter will detail the technical workings of the Helmholtz resonator as well as the plasma synthetic jet actuator with a brief review of previous literature relating to these concepts.

2 Background and Literature Review

An overview of previous work that relates to the research conducted on plasma synthetic jet actuators as a means of improving the performance of turbofan acoustic liners will be presented beginning with a summary and discussion of jet acoustic liners in turbofan engines. The acoustic liner is then broken down into its most basic element: a Helmholtz resonator. The Helmholtz resonator is characterized and explored as an excellent source of knowledge on how the acoustic liner operates. Then, the workings of a plasma actuator are explained. A short history of the development of this technology is explored. Finally, active noise control is explained. The fundamentals of active noise control enable the combination of these two technologies as method to improve the acoustic liner performance.

2.1 *Turbofan Jet Acoustic Liners*

Turbofan engines are currently the most feasible propulsion method for commercial aircraft due to their high power and low fuel consumption. These engines use a series ducted fans and jet exhaust nozzles as the core components of operation, which can be seen in the basic rendering of the engine in Figure 2.1. Such designs typically require less maintenance than other typical engines types. However, with the vast array of noise regulations imposed upon aircraft, manufactures must consider exterior flight noise a major design consideration.

Acoustic liners are an excellent means to reduce noise propagation from a turbofan engine and this method will be a main focus of this report. Liners are usually placed at the inlet

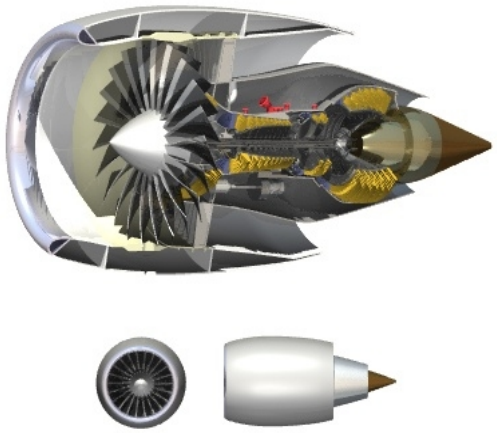

Figure 2.1: Turbofan Jet Engine[1] used

with permission of John MacNeil, 2010

and/or outlet of the engine. A single layer acoustic liner, composed of a perforated sheet with a honeycomb core, can be seen in Figure 2.2, with labels on the most crucial elements. This arrangement produces an array of single degree of freedom resonators. The basic mechanism that allows an acoustic liner to reduce the outwardly propagating sound from a turbofan engine parallels the workings of a Helmholtz resonator (also referred to as “HR” throughout this thesis). Some liners have used multiple layers of honeycomb and perforated sheets to produce multiple degree of freedom resonators, with more than one neck and volume cavity, which will be discussed later.

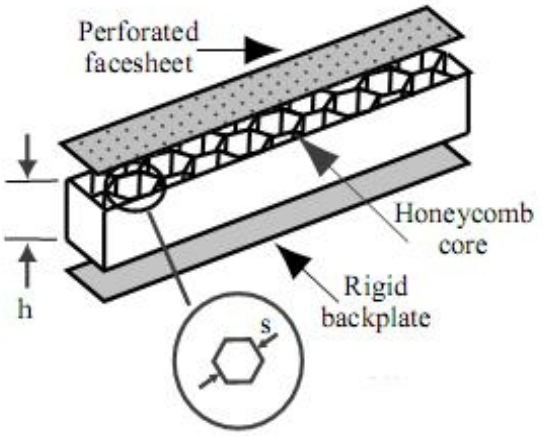

Figure 2.2: Acoustic Liner Sketch [2] used with permission of Michael G. Jones, 2010

2.2 *Helmholtz Resonator*

Hermann von Helmholtz invented the Helmholtz resonator and authored the book, "On the Sensations of Tone as a Physiological Basis for the Theory of Music"[9]. His work produced the first scientific study regarding the operation of an acoustic resonator. An acoustical resonator's operation depends on the physical characteristics of the cavity containing air. Section 3.1 discusses the theory behind Helmholtz resonators in more detail. When an incident acoustic wave interacts with a resonator, the pressure inside the cavity will fluctuate. Since the Helmholtz resonator acts like a band-stop filter, some specific frequencies will be strongly attenuated, while others will not. The width of that band-stop frequency range is controlled by viscous dissipation, like a dampener in a spring mass system.

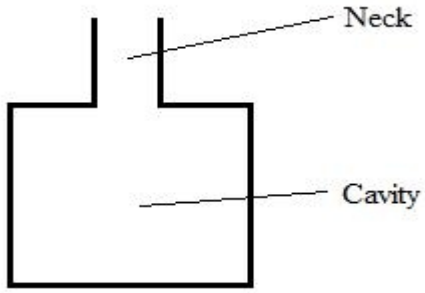

Figure 2.3: Helmholtz Resonator

Another classic acoustician, Lord Rayleigh, produced a work entitled, “The Theory of the Helmholtz Resonator” [10] in the mid 1910's. This work offers an early and rigorous mathematical model of operation of a Helmholtz resonator. This work included a derivation of the resonant frequency of a Helmholtz resonator based on the radius of the cavity (which was assumed to be a sphere shape), the radius of the neck opening (which was assumed to be circular or oval in shape), and the volume of the spherical cavity. Shortly after Rayleigh's publication, F. Puryer White published a conference proceeding which attempted to expand on that previous work. White sets out to “carry [Rayleigh's] result, by a slightly different assumption for [the normal velocity], to a higher approximation” [11] in his work “The Period of a Spherical Resonator with a Circular Aperture”.

Since these early studies of the operation of acoustic resonators, generally accepted models have focused on the volume of the cavity, the cross sectional area of the neck opening, and the length of the neck as the dominate dimensions impacting the resonant frequency of a Helmholtz resonator [12] [13].

2.3 *Basic Review of Acoustical Liners*

A little over half a decade before Rayleigh and White published their works, the Wright brothers were preforming their legendary test glides and flights on the North Carolina shores. While they may have not been the first to achieve flight, these bicycle mechanics are certainly worthy of being called pioneers of the sky. From those humble beginnings at Kitty Hawk, the aviation industry has matured and expanded. With the invention and incorporation of the aircraft engine, the problem of aircraft noise control became clear to society. Currently, the most effective combatant of airplane noise is acoustic liners for engine nacelles.

Intuitively, the best place to combat aircraft engine noise is in the design phase, but throughout the twentieth century and up to date, the state of the art engines do not operate with acceptable noise levels by design alone. Aircraft designers began looking for alternative methods to attenuate engine noise by lining the nacelle with an acoustic treatment. As early as the mid-1970's works had been published that focused on the optimization of acoustic liners and segmenting of acoustic liner [14] [15]. During this decade, NASA and Boeing worked together to study the possible effectiveness of acoustic liners placed in turbofan engine nacelles by conducting parametric studies [16]. As a result, Atvars and Mangiarotty reported that the significant parameters controlling the acoustic lining performance are the “acoustic impedance, treatment length, depth, core-cell dimensions, channel width, number of walls lined, number of layers in the lining, air velocity, and direction of flow with reference to sound propagation” [16]. This research was conducted under a number of metrics limiting the physical application of Helmholtz resonator systems. A list of these limiting factors are presented in Table 2.1. While

an excellent starting point for research pertaining to acoustic liners, this paper has a focused range for the experimental data collected. The bandwidth (800 Hz to 10 kHz for [16]) of interest exceeds the bandwidth of experimentation included in this thesis.

Metric	Range	Units
Duct Size	4 – 12	in.
Lining Cavity Depth	¼ – 1	in.
Flow Mach Number	-0.4 – 0.4	-

Table 2.1: Previous Research Metrics [16]

Additionally, the dimensions of a acoustic liner have been the focus of a number of works [17] [18]. Different methods of optimization can focus on variations in the treatment depth, core-cell dimensions, and number of layers in the lining. Once the extent of the passive optimization was reached, studies in active methods developed to further improve upon the success of the passive liner. Active in this context refers to a method which requires the addition of energy into a system. Dividing the acoustic liner into segments is a method that has been found to improve attenuation of the liner, and an excellent review of the major works that contributed to this knowledge is authored by W. R. Watson [19].

2.3.1 Resonator/Liner with Flow Interaction

Flow associated with the massive amount of air passive through a turbofan engine has a significant effect on the performance of acoustic liner. Parrott Watson and Jones astutely declare “the effective impedance of a duct liner beneath a boundary layer usually depends upon

both the intrinsic impedance of the liner and its interaction with the local aeroacoustic environment" [20]. Fluid flow interaction with acoustic liner has been the focus of numerous studies. These studies are particularly interesting because the plasma actuator has the potential to control local fluid flow. Therefore, an intimate understanding of the fluid-flow and Helmholtz-resonator interaction will better equip acoustic liner manufacturers to design acoustic liners with embedded plasma actuators.

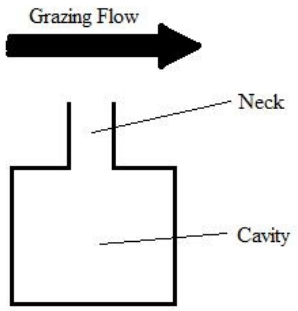

Figure 2.4: HR with Grazing Flow

Fluid flow can interact with a resonator in one of two ways: grazing flow or bias flow. Grazing flow results from the medium of fluid flowing across the face of the liner, not through the neck, as shown in Figure 2.4. For a Helmholtz resonator, the flow transverses the opening or aperture. The engine of an aircraft will pull air across the face of the liner during normal operation, and this air flow will produce grazing flow. Beyond grazing flow, another important flow interaction can impact the performance of the turbofan liner. Bias flow refers to the flow of air through the perforations in the face sheet of the liner or simply through the neck of a resonator.

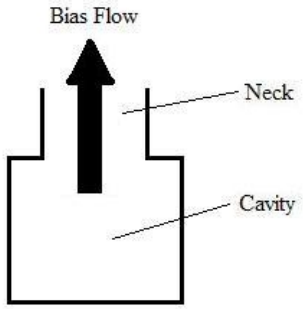

Figure 2.5: HR with Bias Flow

A number of studies on the effect of the grazing flow on the acoustic liner performance have been conducted [20] [21]. Understanding bias flow interaction with acoustic resonators will aid in the implementation of plasma actuators as an active component to the acoustic liner system. Bias flow interaction has also been the focus of research [22] [23]. The plasma actuator will have an effect on this "local aeroacoustic environment", and this effect will also change the impedance.

Investigations into the effect of bias flow on acoustic liner began in the 1970's with P. D. Dean's work [24]. Dean's study focused on the effects bias flow has on several types of acoustic liner, with particular focus on the impedance as the main response variable. Dean concentrated his efforts on narrow band, engine operational frequencies [22]. On the other hand, Cataldi, Ahuja, and Gaeta showed that negative bias flow has the ability to improve broadband liner performance [25]. This previous research indicates that if a bias flow could be induced by a plasma actuator, then this active component has ability to improve the acoustic liner performance, theoretically.

2.3.2 HR / Acoustic Liner Analogies

The basic mechanism that allows an acoustic liner to attenuate sound, is the same as a Helmholtz resonator (HR). The two basic components of a HR are the cavity volume and the aperture of the neck. To illustrate the physical behavior of a Helmholtz Resonator, two analogies are commonly presented.

The first analogy is the spring mass system. The air in the neck of the resonator is treated as a single unit and the "mass" of the system. The air in the volume is equivalent to a spring, and other parameters make up the dampening (such as viscous effects). Figure 3.1 (in the next chapter) provides a visual illustration of these parameters. This analogy will be particularly helpful once the plasma actuator's operation is better understood.

The second of these two analogies is most useful to people with a strong background in electrical engineering design. This analogy applies the workings of an HR to an electrical circuit. Resistive, capacitive, and inductive elements are again based on the geometric and fluid properties of the resonator.

2.4 *Plasma Actuator Basics and Literature Review*

Beyond the Helmholtz resonator and acoustic liner, the other major technology that is relevant to this research is the technology of plasma actuators. Since the beginning of the study of electricity, a number of electrical discharges have been categorized and characterized. A common example of one of these discharges is the arc discharge, and a lesser known example is

the glow discharge. Under certain conditions, the glow discharge can produce a synthetic jet or induced flow in a gas. Electric wind, glow discharge, plasma synthetic jet, dielectric barrier discharge, ionic wind, and corona discharge are all terms used to describe the same electrical phenomenon, and these terms will be used interchangeably throughout this thesis.

2.4.1 Literature on Glow Discharge

An excellent history and summary of the state of the art up to the time of its publication is included in Movement of Air in the Electric Wind of the Corona Discharge [26], by Robinson. He says that this physical event "refers to the movement of gas induced by the repulsion of ions from the neighborhood of a high-voltage discharge electrode" [26].

In 1709, Hauksbee reported the first observation of induced fluid flow by means of electric discharge [27]. Over a century later, Faraday developed the first explanation for this phenomena [27]. Myron Robinson chronicles the development of this physics in "A History of the Electric Wind" [27]. Such great scientists as Newton, Faraday, and Maxwell spent some time investigating the corona discharge, but as the late 20th century has progressed, the attention given to this electric phenomenon has been sporadic [26].

Many of the more recent research efforts focus on specialized applications of the ionic wind, with little or no attention given to general purpose use. The most promising application of the plasma actuator is on aircraft airfoils. The actuator has proven to be an affective means of flow control for air accelerating around the foil. The induced flow by the actuator allows for

better control of the leading edge of turbulence on air foils [28]. Two other focused applications involve the food industry and the computer processor industry. T. Goodenough, P. Goodenough, and S. Goodenough explore the possibility of using ionic induced flow as a mechanism to dry food products in their 2006 paper "The Efficiency of Corona Wind Drying and its Application to the Food Industy". Confirming other previous work, Goodenough *et al.* show power usage of the actuators convert a mere 1-2% of the electrical energy consumed to kinetic energy of the air [29]. The plasma actuators "[show] significant drying enhancement at an overall efficiency comparable to [industry standard conventional] drying methods" [29]. An important and relevant finding by Goodenough *et al.* "is that the electrode placement is crucial for effective operation" [29]. Yang *et al.* investigated the possibility of using the induced flow from a high voltage corona discharge actuator as a device to cool microprocessors [30]. Similar to Goodenough *et al.,* Yang *et al.* found that the energy efficiency of the high voltage electrostatic air pump is "comparable" to the standard heat sink and fan used for many common computing devices [30]. Other applications are likely to arise, since the technology is still being developed by a number of independent researchers [5].

A few recent publications apply the plasma actuator technology to aeroacoustic problems. Huang *et al.* investigated the ability of a plasma actuator to "attenuate low-speed cavity flow-induced tones" [31]. Huang *et al.* focused their investigation on specifically studying the power efficiency of their actuators. The power usage by the plasma actuators will be a design constraint when implementing the technology in an acoustic liner. A low flow investigation involving a rectangular cavity is presented by Chan *et al.* in "Attenuation of Low-Speed Flow-Induced

Cavity Tones Using Plasma Actuators". The results show that "the dominate cavity mode and its harmonics were attenuated to broadband level" during actuating of the device [32]. Many other conclusions were derived from their experimental work, but this conclusion holds special relevance to this research. This reduction in the modes of a cavity closely resembles the turbofan and acoustic liner system. The circular cross section of turbofan engines have a mode which acoustic liners are designed to reduce.

2.4.2 Basic Components of Plasma Actuator

The basic elements that were used throughout this research to manufacture plasma synthetic jet actuators (PSJA) will be described in this section. A dielectric material makes up the base of the actuator. Two electrodes are adhered to opposite sides of the dielectric. A number of variations exist on the alignment of the electrodes, but they are commonly asymmetrically arranged, with some overlapping. Figure 2.6 shows an exemplary arrangement.

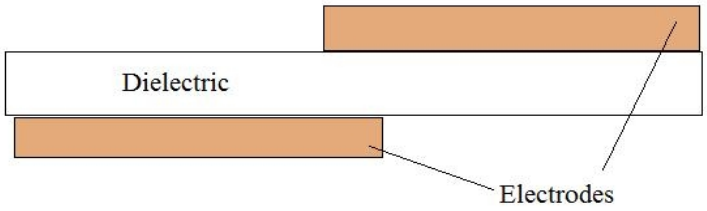

Figure 2.6: Dielectric and Electrodes

High voltage alternating current is the necessary electrical input for the electrodes to produce the desired glow discharge and induced motion of the local air. At a high enough

potential, the air in the local region becomes ionized, and carries electrons from one electrode toward the dielectric region which shields the opposite electrode. The direction of the ion flow is reversed at the frequency of the alternating current. Lorentzian collisions transfer the momentum from the ions to the neutral gas [31] [33] [34]. The properties of the dielectric used in the manufacturing of a plasma actuator can dictate the possible uses in industry. Roth and Dia's conference paper [7] contains a great amount of information on plasma actuator operation including a detailed summary of dielectrics. Their table of dielectric materials can be found in Appendix A.

The straight line configuration is the most common found in the literature, but does not lend itself well to embedding/coupling with a Helmholtz resonator. Further research revealed an alternative configuration of the electrodes. Arvind Santhanakrishnan and Jamey Jacob were the first to present a configuration of the plasma actuator that had a circular form [35]. Figure 5.1 shows the circular configuration, which serves as the basis for the original experiments outlined in Chapter 5.

2.5 *Active Noise Control*

Active noise control is an important connection between the passive acoustic liner and the plasma actuator technology. Active noise control manipulates a noise source by adding energy to the system in such a way that the source's intensity reduces. This noise control method takes advantage of the physics of sound and interference. A second sound source (speaker) is added to the system, and designed to emit the same amplitude as the noise source but with an inverted

phase. The two acoustic signals will then interact, and the resulting sound wave will have a reduced amplitude. The interaction of the two waves is commonly called interference.

Thompson first observed active noise cancellation in 1878 while working with two early telephones [36]. Coanda recorded his observations and applied for a patent in 1930 [36]. Lueg patented his idea to use active noise control in a duct to control low frequency [36]. Neither Coanda nor Lueg saw a working prototype of their ideas, and active noise control did not receive much attention for many years [36]. Olsen returned to these old ideas in the 1950s and attempted to apply the theories to rooms and headphones [36]. His efforts, like those of Lueg and Coanda, suffered from the infancy of many necessary electronics as well as relevant control theory.

Active noise control in duct work is a realm of research that is especially relevant to this thesis because the turbofan engine is modeled as a duct system. Trinder and Nelson were able to use a “detailed investigation of [a ducted] loudspeaker near field [which] enabled the optimum position of the microphone to be identified” [37]. Using a “ 'virtual earth' principle, feedback loop [with the goal of] driv[ing] the sound pressure to a minimum” they were able to see a “reduction of up to 20 dB in the amplitude of low frequency broadband noise at a position downstream of the cancelling [sic] source” [37]. This ability has been so well tuned that a company named NVH Technologies offers to design “active duct quieting (ADQ) systems” that can focus on the 40- 100 Hz frequency band in heating, ventilation and air conditioning (HVAC) networks [38].

Today, active noise control has become common to many people. The technology manifests itself in noise canceling headphones and in certain situations an active attenuator for

ventilation fans. A plethora of information is readily available to someone who desires to learn more about active noise control.

2.6 *Summary*

This chapter has been a brief introduction to the workings of acoustic liner, plasma actuators and their relationship within the construct of active noise control. Some history of the development of each technology is provided as a literature review. Chapter 3 will present a more complete and detailed explanation of these two devices.

3 Related Theory

This chapter presents the theoretical basis for the research and will relate the theory back to the problem of excessive noise propagation from turbofan engines. The chapter begins with a discussion of the Helmholtz resonator because this device is the basic single degree of freedom system that acoustic liner is built from. A Helmholtz resonator is the simplest element in an acoustic liner of a turbofan engine. Once introduced, the effects of flow interaction with acoustic liner will be presented. The chapter will then present a summary of the theoretical work conducted on synthetic plasma actuators with all of the relevant work highlighted. Finally the chapter will conclude with a look at the couple system of a Helmholtz resonator and plasma actuator device from a lumped parameters perspective.

3.1 *Helmholtz Resonator*

The classic Helmholtz resonator, in its simplest form, is a cavity with an opening. The opening is usually referred to as a neck, because in most cases this opening is small compared to the dimensions of the cavity. The air inside the cavity couples with the air that resides in the opening of the neck. These two volumes combine to produce a dynamic system with a resonant frequency.

When excited by an acoustic pressure fluctuation, air flows into the resonator, which increases the pressure in the volume. If the force pushing air into the resonator, is then removed, the higher pressure on the inside of the volume will cause air to flow out of the opening. Inertial effects cause the outward flow to continue beyond the equilibrium point. This motion, in turn, causes the volume to turn into a low pressure region. The cycle repeats as air flows back into the volume in an attempt to equalize the pressure.

Equation 3.1.1 shows how to calculate resonant frequency of a HR depending on some of the dimensions of the resonator. The f_h stands for the resonant frequency in Hertz, the c stands for the speed of sound in the medium, the A stands for the cross sectional area of the neck, the V_0 stands for the volume of the cavity, and the L represents the length of the neck.

$$f_h = \frac{c}{2\pi}\sqrt{\frac{A}{V_0 L}} \quad \text{(Hz)} \tag{3.1.1}$$

The resonant frequency of a HR is important parameter in the implementation of a coupled plasma actuator and HR device. One way to understand a HR is to consider it an acoustical band-stop filter with the f_h dictating a center point of the stop band. A more detailed explanation of the resonant frequency of a Helmholtz resonator is available in a number of sources, including Kinsler and Frey's Fundamentals of Acoustics [12] or Bies and Hanson's Engineering Noise Control: Theory and Practice [13].

3.1.1 Spring Analogy

A common analogy for the Helmholtz resonator is the spring mass system. The air in the neck of the resonator acts as a mass. The properties of the cavity act like a spring and damper system. The equations of motion are presented later in this chapter (3.4.1 Bias Flow Model).

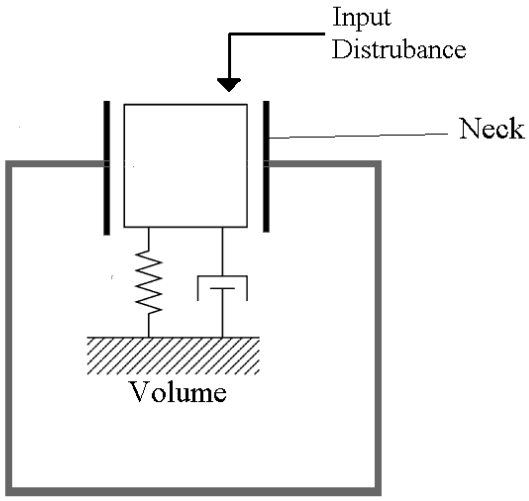

The spring-mass analogy provides an important method to analyze a HR system, using normal one degree of freedom vibration analysis. The resonant properties of the device allow it to amplify certain frequencies while attenuating others. The sound power transmission coefficient describes the sound power that will transmit effectively during the excitation of a Helmholtz resonator by some disturbance. The sound power transmission coefficient, T_π for a HR is given in Equation 3.1.2 [12].

$$T_{\pi}=\left(1+\frac{c^2}{4S^2(\omega\frac{L_e}{S_b}-\frac{c^2}{\omega V})^2}\right)^{-1} \tag{3.1.2}$$

The c term is the speed of sound in the fluid, the S term is the area of the opening of the neck, and the V term is the volume of the cavity. The L_e is an effective length of the neck where

$$\begin{aligned} L_e &= L+1.7\text{a} \quad (\textit{for outer end flanged}) \\ L_e &= L+1.4\text{a} \quad (\textit{for outer end unflanged}) \end{aligned} \tag{3.1.3}$$

L is the length of the neck, and a is the radius of the opening, for a cylindrical neck. When applying these equations to an acoustical liner, the neck is usually composed of a perforated sheet in which the thickness of the sheet is the length of the neck, the radius of the perforations is the radius of the opening, a. The **flanged instance is appropriate because the sheet usually has a percent open area less than 30%, and the surrounding perforations are small in radius as well.

Equation 3.1.3 shows that when $\omega = \omega_h$, the transmitted power falls to zero. This situation occurs when the frequency is equal to the tune frequency of the resonator. A flow motion, described in the following section, has important properties that can be exploited by the plasma actuator's operation.

3.2 *Bias Flow*

In the turbofan engine environment large amounts of air are being compressed and ignited. All of the moving blades together with the explosive chemical reactions produce high amplitude noise. Fast moving air is common throughout all parts of the turbofan engine,

especially at the exit and inlet. Acoustic lining is commonly placed at the inlet or exit, and a number of studies have focused their efforts on modeling and predicting the impact the flow field might have on the performance of the acoustic liner [21, 32, 39].

There are two common types of flow interaction with the acoustic liner (or array of Helmholtz resonators) in the literature. Grazing flow as shown in Figure 2.4 (in the previous chapter) is a flow field moving across the opening of the Helmholtz resonator.

Bias flow describes a single direction flow through an opening. In the case of the HR, the bias flow is traveling through the neck. Figure 3.2 is a close up of the interface between a waveguide wall and the neck of a HR.

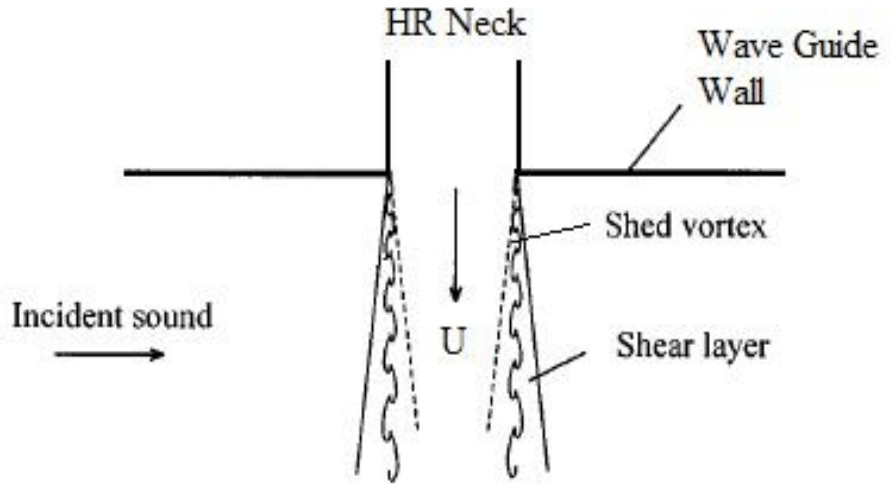

The mechanism that plays a major role in the acoustics of bias flow is vortex formation [3]. The incident acoustic energy is converted to flow energy once it has interacted with the fluctuating shed vortices shown in Figure 3.2. These vortices are created and dissipated by the

structural interaction with the bias flow traveling through the opening [40]. As the bias flow increases, the acoustic resistance will as well [41]. Figure 3.2 shows where the shear layer and vortex formation occur relative to the bias flow, U, and the incident acoustic sound. This figure shows an extreme close up of the waveguide and HR neck interface that receives further attention in both the modeling and experimental chapters.

Some amount of acoustic energy is dissipated during interaction with the bias flow vorxtices. A metric has been developed which can predict the amount of acoustic absorption which is undergone during this interaction. This absorption coefficient, Δ , for this bias flow situation can be calculated by using Equation 3.2.1 [3].

$$\Delta = \frac{\frac{8\alpha}{\pi M_c}\Delta_R \kappa R \cos\Theta}{\left|\kappa R\cos\Theta + \frac{4\alpha}{\pi M_c}(\Delta_R + i\Gamma_R)\right|^2} \tag{3.2.1}$$

With α standing for the open area of the neck, and M_c standing for the Mach number of the bias flow through that neck. κ is the thermal conductivity. The $\cos\Theta$ accounts for the angle of incidence of the acoustic wave. The absorption coefficient is dependent on the Strouhal number, *St*, where

$$St = \omega R / U_c \tag{3.2.2}$$

In this equation, ω is the angular frequency, R is the radius of the opening of the HR neck, and U_c is the speed of the bias flow. Howe's plot in Figure 3.3 shows the Strouhal number verses the absorption coefficient.

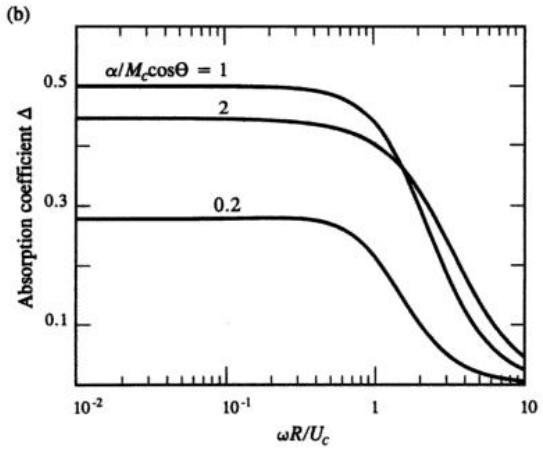

Figure 3.3:Sound Absorption with bias flow [3]

used with permission of M. S. Howe, 2010

The Δ_R and Γ_R terms of Equation 3.2.1 are related to the Rayleigh conductivity, K_R by Equation 3.2.3.

$$K_R = 2\mathrm{R}\,(\Gamma_R - i\,\Delta_R) \tag{3.2.3}$$

A normalized examination of these equations will offer some insight into the relationship between the Strouhal number and the absorption coefficient.

Figure 3.3 reveals that when the Strouhal number is less than 1, the attenuation is at a maximum [3]. The absorption coefficient drops for Strouhal numbers above one, and for Strouhal numbers above ten the absorption coefficient is nearly zero. Figure 3.3 shows that for a constant bias flow speed, U_C, the absorption coefficient declines as the frequency increases. The bias flow adds a high-pass filter component to the system.

Beyond the fluid-structure perspective, which focused on a single aperture, an alternative

bias flow explanation is worthy of exploration. For this method, the focus will be on the bias flow effects on an acoustic liner segment, instead of a single Helmholtz resonator. This approach will characterize the impedance of the acoustic liner, instead of absorption coefficient and power transmission coefficient.

Bias flow has an effect on the impedance of acoustic liners. Dean's Bias Flow Model is of particular interest in comparing with the attenuation coefficient [23]. This model is based on of the Hersh 75 impedance model with bias flow terms added [23]. Dean's model is split into two regions: one linear and the other nonlinear. In the following equations, θ stands for the normalized resistance, and χ stands for the normalized reactance [23].

$$\theta_{Dean}=\frac{1}{\sigma}\left[k(d+t)\left(\frac{0.4244\mathrm{v}_b}{C_D^2(1.0+\frac{t}{d})}\right)+\sqrt{\frac{1.0}{Re}}\right]\left[\frac{0.8488\mathrm{v}_b}{C_D^2(1.0+\frac{t}{d})}-1.01\sqrt{\frac{2}{Re}}\right]+\underbrace{[\frac{2\mathrm{v}_b}{c\,\sigma^2}\,or\,\frac{M_{gf}}{0.845\sigma}]}_{whichever\ is\ greater} \quad (3.2.4)$$

$$\chi_{Dean}=\frac{k(d+t)}{\sigma}\left[1.0+\frac{1}{\sqrt{(2Re)}}\left(1.0-\frac{0.8488\mathrm{v}_b}{C_D^2(1+\frac{t}{d})}\right)\right] \quad (3.2.5)$$

The ratio $\frac{v_b}{\sigma\,\omega\,d}$ determines whether the impedance is operating in a linear or non-liner fashion, the previous equations work when this ratio is less than one (linear operation), and the applicable equations for when that ratio is greater than one (non-linear operation) are Equations 3.2.6 and 3.2.7 [3]:

$$\theta_{Dean} = \frac{k(d+t)0.64\mathrm{v}_b}{\sigma C_D^2(1.0+\frac{t}{d})}\left[1.0-\left(\frac{1.03\mathrm{C}_D(1.0+\frac{t}{d})}{v_b}\right)^2\right]+\underbrace{\left[\frac{2\mathrm{v}_b}{c\,\sigma^2}\,or\,\frac{M_{gf}}{0.845\sigma}\right]}_{whichever\ is\ greater} \tag{3.2.6}$$

$$\chi_{Dean} = \frac{k(d+t)0.33}{\sigma C_D}\left[1.0+\frac{2.6\mathrm{C}_D(1+\frac{t}{d})}{v_b}\right]\left[1.0-\left(\frac{1.03\mathrm{C}_D(1+\frac{t}{d})}{v_b}\right)^2\right] \tag{3.2.7}$$

Equations 3.2.4 – 3.2.7 have a number of variables. For quick reference, Table 3.1 defines many of the variables in the previous equations.

θ_{Dean}	Dean's normalized Resistance
σ	Percent Open Area
k	Wave Number, $=\omega/c$
d	Perforated Hole Diameter
t	Perforated Thickness, or Neck Length
v_b	Bias Flow Velocity
C_D	Discharge Coefficient (steady flow)
Re	Reynolds Number
c	Speed of Sound
M_{gf}	Mean Grazing Flow Mach Number, $=v_{gf}/c$
χ_{Dean}	Dean's Normalized Reactance
ω	Circular Frequency, $=2\pi f$

Table 3.1: Term Definitions

These equations offer insight into the properties that control the impedance of acoustic liners. A major difference between these models for impedance and the previous explanations for absorption and transmission coefficients is that Dean's models make a distinction between operation in the liner or non-linear regions. This research will not address the non-linear operation, but its existence is still worth mentioning. The next section contains the theoretical

details which pertain to the plasma actuator. After the plasma actuator section, the theoretical basis for the proposed device will combine the liner and actuator technology.

3.3 *Plasma Actuator*

A brief description of a plasma actuator is delivered in the Background Chapter. In a gas, such as air, a high electric potential can cause the ionization of nearby air molecules. Once ionized, many of those molecules will conduct electrical current through that ionized path. Air normally acts like an insulator, but in the presences of a electric field strength exceeding 3 x 10^6 V/m, a breakdown in the insulating properties will occur, and air becomes temporarily conductive [42]. Air particles that flow away from the actuator quickly return to their neutral charge. The plasma produced by these actuators is sometimes referred to as a one atmosphere uniform glow discharge plasma (OAUGDP). When a spark or arc is formed in air, the color of

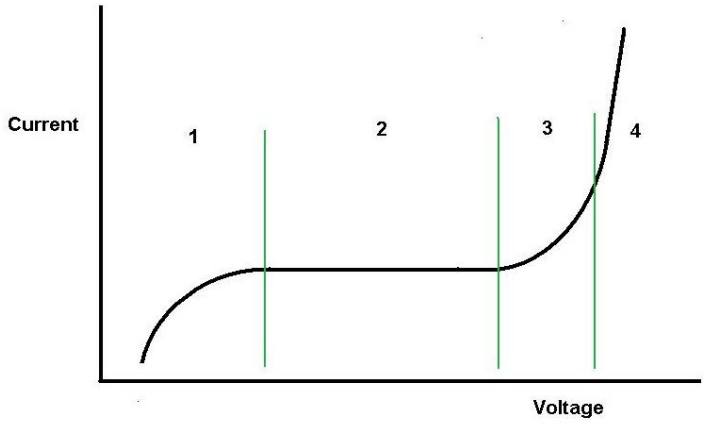

Figure 3.4: Voltage vs. Current near arc discharge

the discharge is dependent upon the composition of the local medium air [43].

The voltage-current relationship varies around the onset of arcing. A plot of the current and voltage relationship near values that would produce an arc is visible in Figure 3.4. Area 1 in Figure 3.4 is a region where some but not all local air molecules are charged and these ions can allow for some small level of current to flow through the otherwise insulating medium [43]. Region 2 shows a constant current for some range of voltage potential, and it is in this region where all of the nearby air molecules are ionized, and current can readily flow at that constant rate [43]. The final two regions in Figure 3.4 (Area 3 and Area 4) show the Townsend discharge zone which is dominated by electron avalanche breakdown [43]. This understanding of the electrical functioning of these discharges aids in the understanding of the overall plasma actuator.

For corona or arc discharge, a chemical reaction produces ozone out of the air used as a medium. This fact is noteworthy for any application of the plasma actuator which will have environmental consequences.

A plasma actuator in operation produces a zero-net mass flux (ZNMF) jet during operation. The theory on the flow induced by the plasma actuator relies on Lorentz forces. These forces transform electromagnetic effects into body forces acting on individual particles [31] [33] [34]. This force falls under the umbrella of electrohydrodynamics, which studies the motion of fluid with individually charged particles when those particles are interacting with electromagnetic fields. The Lorentz force is most concisely conveyed in equation form:

$$\boldsymbol{F} = q\left(\boldsymbol{E} + \boldsymbol{v} \times \boldsymbol{B}\right) \tag{3.3.1}$$

Equation 3.3.1 relates the force applied to a particle, $\boldsymbol{F}$, to four other parameters. $\boldsymbol{E}$ is the electric field (V/m). $\boldsymbol{B}$ is the magnetic field (teslas). The change is denoted by q, and v is the

velocity of the particle.

Robinson developed the first equation for the electric wind velocity, shown as Equation 3.3.2.

$$v_G = k \times \sqrt{\frac{i}{\rho_{gas}\mu}} \tag{3.3.2}$$

The "electric wind velocity" is represented by v_G. The k term is a constant developed from the geometry of the electrodes, i is the time-averaged discharge current, ρ_{gas} stands for the gas density, and μ represents the mobility of the ions [26].

Sigmond and Lagstadt built upon Robinson's work to reform Equation 3.3.2 into Equation 3.3.3.

$$v_G = \sqrt{\frac{i\, g_e}{\rho\, \mu\, A_G}} \tag{3.3.3}$$

Reusing many of the same terms as Robinson, this expression removes the k constant, and replaces it with the electrode gap, g_e, and the discharge cross-section, A_G [44].

Vortex motion and interaction play an important part in the jet formation[45]. The plasma produces an electrostatic body force on the local fluid. The force is dependent on the electric field, and Equation 3.3.4 [45] shows all the parameters that affect the force.

$$\boldsymbol{F} = -\left(\frac{\epsilon_o}{\lambda_D^2}\right)\phi\, \boldsymbol{E} \tag{3.3.4}$$

In this equation, ϵ_o is the permittivity of free space, ϕ is the net charge density, **E** is the strength of the electric field, and λ_D is the Debye length. The Debye length is defined in Equation 3.3.5 [45].

$$\lambda_D = \sqrt{\frac{k_{Bolt} T_e}{4 \pi e^2 \rho_e}} \tag{3.3.5}$$

In Equation 3.3.5, k_{Bolt} is Boltzmann's constant, T_e is the electron temperature, e is the charge on the electron, and ρ_e is the plasma density[46] [47].

The electrical signals that control the actuator can induce flow in two ways: bias flow or oscillatory. These equations for electric wind focus on the bias, or single direction, flow generated by the plasma actuator. The oscillatory flow is controlled by the operational frequency of the alternating current signal which feeds into the electrodes.

3.4 *Theoretical Design of Coupled Resonator Actuator*

The input electrical signals dictate the flow type: oscillatory flow and bias flow. The plasma actuator will be planted in the neck of the Helmholtz resonator; Figure 3.5 shows the combination device.

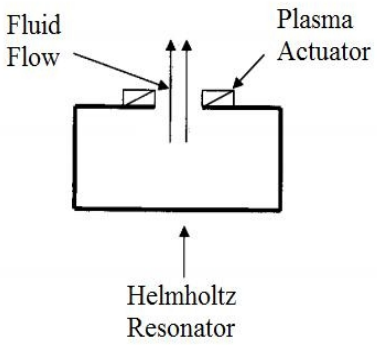

Figure 3.5: Plasma Actuator/ Helmholtz Resonator Device

The oscillatory flow will operate similar to a loud speaker. Active control of the signal is

key in this situation. Bias flow produced by the plasma actuator will operate differently. Bias flow will improve the performance of acoustic liner by inducing vortex shedding.

Using the spring analogy, the analysis of the resonator and actuator can be more fully developed. A number of excellent undergraduate vibration texts include a thorough exploration of the spring mass system [48]. It is useful to explore the plasma actuator and Helmholtz resonator device using these tools. The basic operation of the resonator as a spring mass system has already been briefly discussed in Section 3.1.1 with Figure 3.1 showing a helpful visual.

Now, since the important mechanisms that allow the plasma actuator to operate are understood, a model of the combined device can be developed. There are two common extensions of the spring mass system that can be applied here: a constant force acting on the mass (for bias flow) and an harmonic force acting on the mass (for the oscillatory flow).

3.4.1 Bias Flow Model

To model the resonator system, the air in the neck of the resonator is treated as one unit of mass. The volume of the cavity controls the spring-damper properties. The equation of motion for the system can then be written in the form of Equation 3.4.1 [12].

$$m\,\ddot{x}(t)+R_{total}\,\dot{x}(t)+k\,x(t)=0 \tag{3.4.1}$$

In Equation 3.4.1 m stands for the effective mass of the unit of air in the neck of the Helmholtz resonator. The effective mass of the unit of air in the neck of the resonator can be calculated for a cylindrical neck by Equation 3.4.2 [12].

$$m=\rho_0 S L' \tag{3.4.2}$$

The R_{total} term is the total resistance and is further broken down in Equation 3.4.3 [12].

$$R_{total} = R_{radiation} + R_{WallLosses} \tag{3.4.3}$$

$R_{radiation}$ is the radiation resistance, and $R_{WallLosses}$ is the resistance due to wall losses. Finally, the k term in Equation 3.4.1 is a stiffness term which can be calculated using Equation 3.4.4.

$$s = \rho_0 c^2 \frac{S^2}{V} \tag{3.4.4}$$

Equation 3.4.4 relates the stiffness term, s, in the equation of motion of the air mass system directly back to the density of air, ρ_0, the speed of sound, c, and the cross section area of the cylindrical neck, S, and indirectly to the volume of the cavity, V.

The addition of bias flow can be modeled in a manner similar to gravity, as a constant on the right hand side of Equation 3.4.1.

$$m\ddot{x}(t) + c\dot{x}(t) + kx(t) = F_{bias} \tag{3.4.5}$$

Assuming that system starts from equilibrium with no displacement or velocity, one form of the solution is shown in Equation 3.4.3.

$$x(t) = e^{-\zeta \omega_n t} \cdot \left(A\cos(\omega_d t) + B\sin(\omega_d t) \right) + \frac{F}{k} \tag{3.4.6}$$

$$A = \frac{-F}{k} \qquad B = \frac{F}{k\zeta \omega_n \omega_D} \tag{3.4.7), (3.4.8}$$

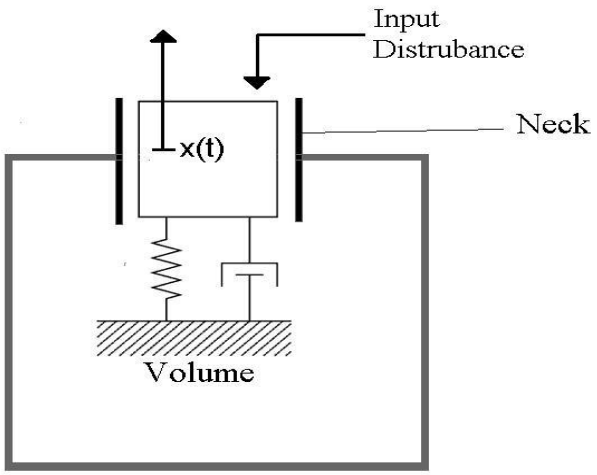

Figure 3.6: Helmholtz Resonator with Air Mass Origin

This solution for the motion of the mass of air in the neck can theoretically allow a HR design to be tuned for a specific band-stop frequency with the addition of bias flow.

3.4.2 Oscillating Flow Model

The model treats the oscillating induced flow like a harmonic excitation of the system. If the Helmholtz resonator is a damped system, then the displacement of the unit of air in the neck satisfies Equation 3.4.6.

$$m\ddot{x}(t)+c\dot{x}(t)kx(t)=F_0\cos\omega_{dr}t \tag{3.4.9}$$

The solution for this linear non-homogeneous equation is the sum of homogeneous and particular solutions. The system is assumed to be underdamped. The solution is shown in Equation 3.4.7.

$$x(t)=C\,e^{-\zeta\omega t}\sin(\omega_d t+\theta)+D\cos(\omega_{dr}t-\phi) \tag{3.4.10}$$

Again, this explanation focuses on the motion of the bulk mass of air inside the neck of the resonator. When the passive resonator is combined with an active driving component the solution to the system is different than the previously discussed cases.

Both the bias flow and oscillatory flow models account for only a single resonator. When applied to an acoustic liner, the models must account for a number of resonators tightly packed in a small amount of space.

3.4.3 Acoustic Impedance Considerations

The acoustic impedance of the turbofan liner must be near the impedance of the surrounding medium for best performance. When an incident sound encounters the liner, if the acoustic impedance is close to the impedance of the surrounding, then the incident sound will be absorbed, with a minimum amount of the incident wave reflected back since the impedance change is small.

To connect the acoustic impedance, $\boldsymbol{Z}$, back to the equations of motion Equation 3.4.11 is provided.

$$\boldsymbol{Z}=R+j\left(\omega M-\frac{1}{\omega C}\right) \tag{3.4.11}$$

A few more equations are required to connect this acoustic impedance equation back to the geometry of the Helmholtz resonator. Those equations are shown in Equations 3.4.12, 3.4.13, and 3.4.14 with the names of the parameters [12].

Acoustic Resistance: $R = R_m / S^2$ (3.4.12)

Inertance: $M = m / S^2$ (3.4.13)

Compliance: $C = S^2 / s$ (3.4.14)

These equations are only value for a situation in which the system can be treated like a lumped parameter system. For this assumption to be valid, the dimensions of the acoustic system must be small compared to the wavelengths of interest. At 2kHz, the wavelength of an acoustic wave is .1715 m. The most acoustic liners have dimensions on the order of centimeters or millimeters, so frequencies up to 2kHz can by analyzed using this method. The sponsor of this research requested that the focus bandwidth be between 1kHz to 2kHz. If the largest dimension of an acoustic resonator is 10cm, then the highest frequency that can be analyzed using this system is 3430 Hz, if the speed of sound is assumed to be 343m/s.

3.5 *Summary*

This chapter summarizes the major theoretical concepts which compose the operations of the Helmholtz resonator, and the plasma actuator. The major equations that dictate operation are presented and explained. The synthesis of the two devices is also presented with comments on the theoretical operation of the combined device. The theoretical model of the resonator/actuator requires restraints on the dimensions of the resonator to ensure the assumptions for a lumped parameter analysis are achieved.

4 Simulation of Resonator/Actuator

A number of models and prediction methods exist for predicting acoustic liner performance [49] [39] [50]. A finite element software suite was chosen as the tool for use in modeling and simulating the plasma synthetic jet actuator. The actuator is modeled to work in a similar manner as a speaker with an abnormal flexibility in its shape. A portion of a waveguide and an array of resonators were built with Abaqus CAE. Once verified by a parametric study of the passive resonator array, the model is then used to study the performance of the active system. The most common model of the actuator will be shown as an acoustic pressure source that is wrapped around the interior of cylindrical neck of the modeled resonator. This method specifically focuses on the oscillatory flow induced by the actuator. Bias flow is not accounted for in these models because early experiments showed the induced bias flow speeds were too low to show significant change in the attenuating of a resonator. Refer to Chapter 5 for further details on this experiment.

4.1 *Finite Element Method Background*

The finite element analysis (FEA) requires that the continuous real world system be broken down into discrete elements or nodes. Governing equations dictate the interaction of each element in the model during simulation. A number of texts focus on the finite element methods [51] [52].

4.1.1 Introduction to Abaqus

The Abaqus suite of software gives a user the ability to apply finite element method (FEM) with the aid of a graphical user interface (GUI) for ease of construction and visualization. Abaqus CAE controls the graphical components of the suite, while Abaqus Standard/Explicit deals with bulk of calculations that are completed while running a simulation.

4.2 *Construction of Model with Abaqus*

This section will include various details that pertain to the construction of the model in Abaqus. It will begin with the construction of the model, and go on to discuss the meshing method. Then it will discuss the boundary conditions focusing first on the anechoic termination, then on the disturbance speaker, and finally discuss the modeling of the plasma actuators.

4.2.1 Model Construction

Abaqus CAE's GUI uses basic 3-D shapes and various tools to allow a user to build any shape imaginable from simple parts for finite element analysis. The model is built to reflect the experiments. The majority of experimentation relies on a waveguide as the base of the system. A test subject is then mounted at the midpoint of the waveguide for testing. Refer to the Experimental Chapters for further details.

The basic elements of the model are intended to resemble the experimental setup. See Chapters 5 -8 for the details of the experiments. The waveguide used for experimentation is a

cylinder shape with a speaker as a disturbance source at one end. The size of the cross section of the waveguide is chosen so the cut off frequency of the duct lies above the bandwidth of interest. See Section 6.1.1 Waveguide and Duct Design for more details on the cut off frequency. This design consideration ensures that the bandwidth of interest will propagate down the duct as plane waves. The basic system is composed of a waveguide, with an anechoic (non-reflecting) termination at one end, and the disturbance speaker (input source) at the other end. Figure 4.1 shows the cylinder constructed in Abaqus CAE as the base of the model. An explicit dynamic model allows for the correct propagation and collection of data during simulation.

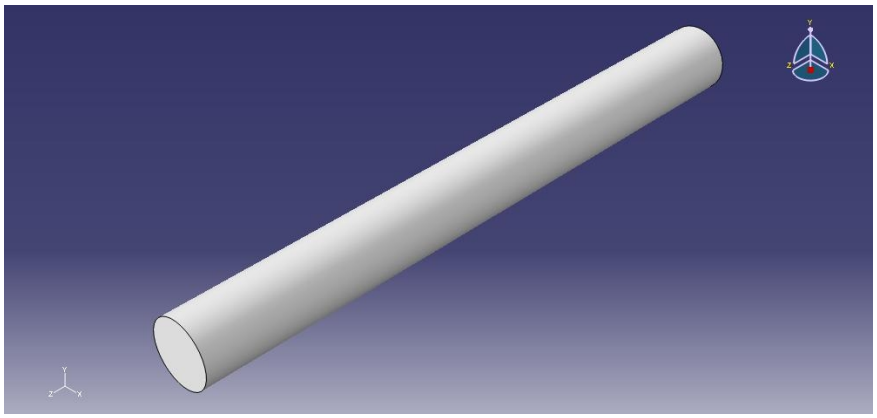

The test subject of interest for these simulations is an array of resonators, which are shaped similar to the ones tested in the Chapter 8. These resonators have a cylinder neck, which opens up to a wider diameter cylindrical volume. For ease of composition and visibility during the visualization of the results, they are spaced 90 degrees apart at three points along the length of the waveguide. The resonator/actuator array that is tested in the final experimental chapter has 3-pairs of devices (resonator/actuators) packed tightly together at a single mounting point on the waveguide. Despite the slight variations between the model and the constructed actuator

array, the information from the simulations will still be useful and relevant. This difference might affect the results if cross modes exist inside the waveguide, but both the model and the experimental waveguides were designed to allow only plane waves to propagate at the frequencies of interest. This simplification of only working with plane waves is one of the reasons the simulation is a good representation of the experimental work. Figure 4.2 shows the simulation resonators attached to the waveguide.

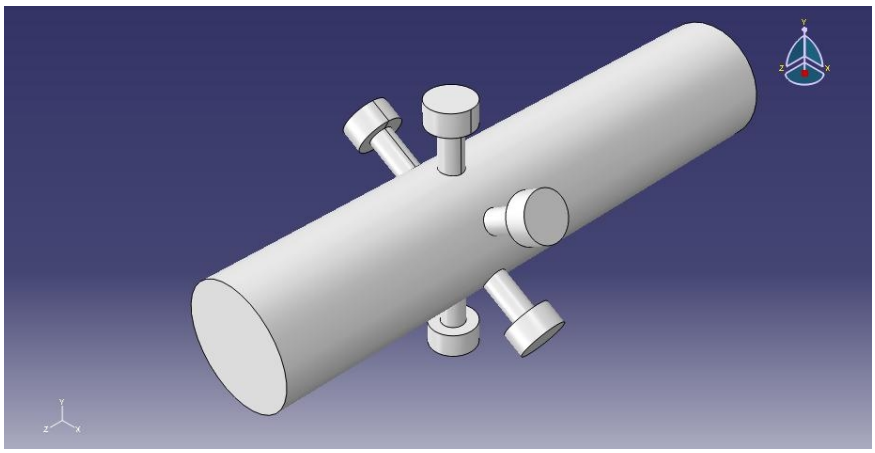

Figure 4.2: Simulation Waveguide with Resonators Attached

Abaqus CAE has multiple meshing procedures, which convert the geometry in Figure 4.2 to an array of nodes. An element type must be chosen which will dictate the geometry of the individual elements which make up the mesh of the waveguide and resonators. A dynamic explicit simulation requires a specific element set to construct the model. A "AC3D4" element set is chosen for meshing, because this element type allows for the simulation to operate as a fluid medium with acoustic perturbations. This type of element in Abaqus is composed of a 4-node linear acoustic tetrahedron.

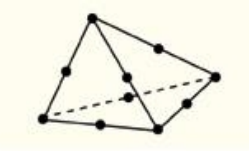

Seeding of nodes at corners of the model, continues the process of meshing. According to the Abaqus User Manual, a functional meshing must have six nodes of the mesh spaced within the smallest wavelength, and accuracy is vastly enhanced if ten or more inter-node intervals span the shortest wavelength [53]. The number of nodes is set during seeding so there would be more than 10 nodes per the shortest wavelength. The shortest wavelength of concern has a frequency of 2kHz. To calculate the approximate maximum inter-node distance, L_{max}, it will be assumed that the ideal spacing requires at least 10 nodes per wavelength of interest $(n \geq 10)$. For Abaqus the speed of sound, c, will be calculated from the material attributes of the bulk modulus, K_f, and the density of the medium, ρ_f.

$$c = \sqrt{(K_f / \rho_f)} \tag{4.2.1}$$

The bulk modulus of air, K_f, is set to 1.42 x 10^5 Pa, and the density of air is of 1.2 kg/m^3. These values allow the calculation for the speed of sound to produce 344 m/s, a generally accepted value for the speed of sound in air at standard temperature and pressure. The conditions in a turbofan engine will be quite different from these normal atmospheric conditions. However, these are the conditions chosen to model because the experiments were conducted at normal atmospheric conditions. The speed of sound calculated by Equation 4.2.1 affects the maximum inter-node distance. The inequality shown in Equation 4.2.2 relates the maximum inter-node distance to all of the relevant parameters.

$$L_{max} < \frac{c}{n_{min} f_{max}} \tag{4.2.2}$$

Input values used to calculate L_{max} include: c = 344 m/s, n_{min} = 10 nodes, and f_{max} = 2000 Hz. Calculating L_{max} shows that the spacing between nodes of elements in the mesh should be approximately 1.7mm. This more conservative calculation is used rather than the Abaqus User Manual recommendations for n_{min} = 12 and a maximum frequency of interest of 1000Hz. The Abaqus User Manual recommendation inter-node distance is less than 29mm [53].

This knowledge is particularly useful when seeding the constructed outline of the air inside the waveguide and Helmholtz resonator. Seeding a part places outline nodes on the intersection of two surfaces, and this process can be completed by specifying a number of nodes for a surface or setting an approximate distance between the nodes on a surface. After a single face or edge is seeded, Abaqus can extrapolate the mesh for the rest of the model. Throughout the various simulations conducted, a variation of 20-25 nodes were seeded at each facial intersection on the model. The diameter of the waveguide is 5.08cm, so this seeding method ensures enough nodes per wavelength. Figure 4.4 shows the meshed system.

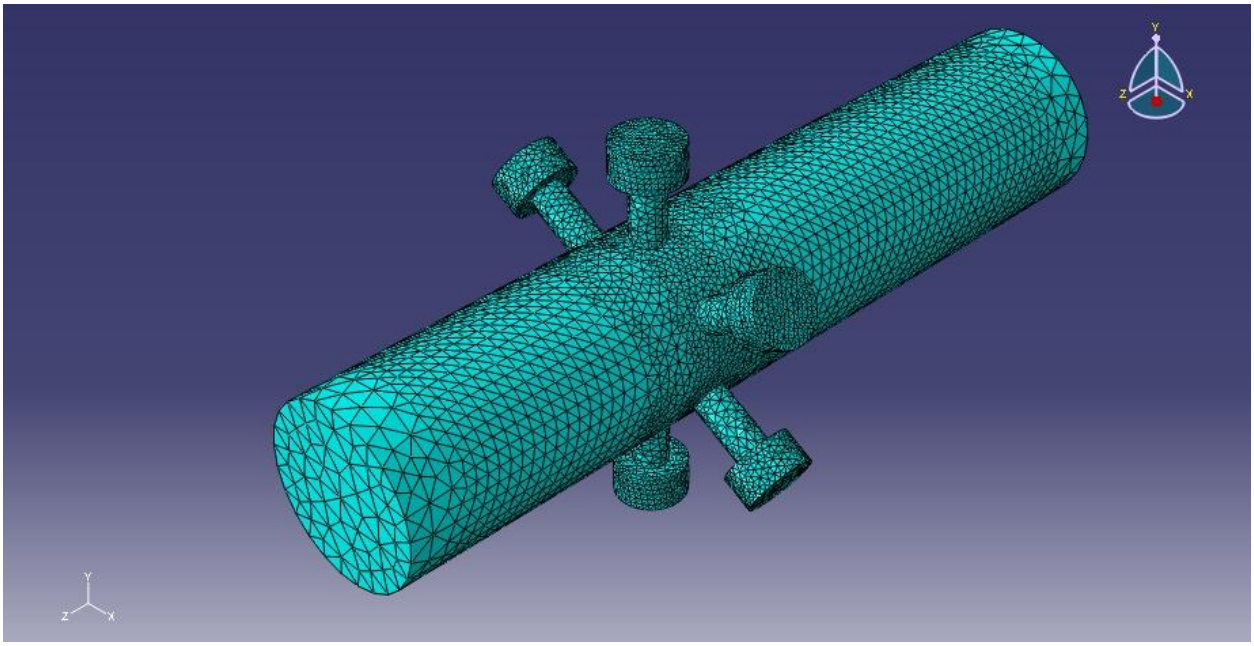

Figure 4.4: Meshed Model

4.3 *Abaqus Calculation Engine*

The online Abaqus Theory Manual, part of the Abaqus Documentation, provides a detailed summary of the theoretical background of how Abaqus employs FEA. The equation that Abaqus uses "for small motions of a compressible, adiabatic fluid with velocity-dependent momentum losses" [53] is shown as Equation 4.4.1.

$$\frac{\partial p}{\partial x}+\gamma(\boldsymbol{x},\theta_i)\dot{\boldsymbol{u}}^f+\rho_f(\boldsymbol{x},\theta_i)\ddot{\boldsymbol{u}}^f=0 \qquad (4.3.1)$$

In this equation, p represents the variation of pressure in the fluid, **x** is the placement of the individual fluid node. The $\dot{\boldsymbol{u}}^f$ term stands for the fluid node velocity and $\ddot{\boldsymbol{u}}^f$ is therefore the term for the acceleration of the focus fluid node. The density term appears as ρ_f , and the

γ represents the drag force in the form of force per unit volume per velocity. The θ_i and the i are terms for independent alternative variables including temperature, humidity, or composition of the air [53]. A second important equation that also aids in describing the system appears as Equation 4.4.2.

$$p = -K_f(\boldsymbol{x}, \theta_i)\frac{\partial}{\partial \boldsymbol{x}} \cdot \boldsymbol{u}^f \tag{4.3.2}$$

These two equations make up the basis for the calculations that Abaqus performs during the finite element analysis.

4.4 *Boundary Conditions*

The boundary conditions require the setting of special parameters for surfaces. One end of the waveguide has an anechoic termination, and a non-reflection boundary condition in Abaqus fulfills this condition. A test pulse confirmed the non-reflecting property of the "end" surface of the waveguide. This test entailed visually (through Abaqus CAE) confirming no reflection at the far end of the waveguide when the disturbance speaker perturbed the system with a short pulse. A single data point collected the pressure time history which also showed no reflections from the non-reflecting end of the waveguide.

The disturbance speaker and the actuators require a different boundary condition setting. A tabular input allows for definition of complex pressure functions. The tabulated data is forced

upon the nodes at the speaker surface at the times specified. The neighboring nodes see the changes which are imposed upon the speaker surface, and those nodal parameters are altered in the next time step. This process is repeated as the speaker input drives the system.

A desirable input function should cover the entire frequency range of interest, from 1kHz to 2kHz. A single short pulses made up the input signal used for all simulations. The Fourier transform, FT(t), of a pulse results in a sinc function defined in Equation 4.3.1.

$$FT(t_{pulse}) = \frac{\sin(x)}{x} \tag{4.4.1}$$

The theoretical frequency response of a pulse is shown in Figure 4.5, normalized by π. This plot was formed by using the same post processing matlab script employed on the simulation data. An arbitrary pulse vector was used as the input to the post processing script.

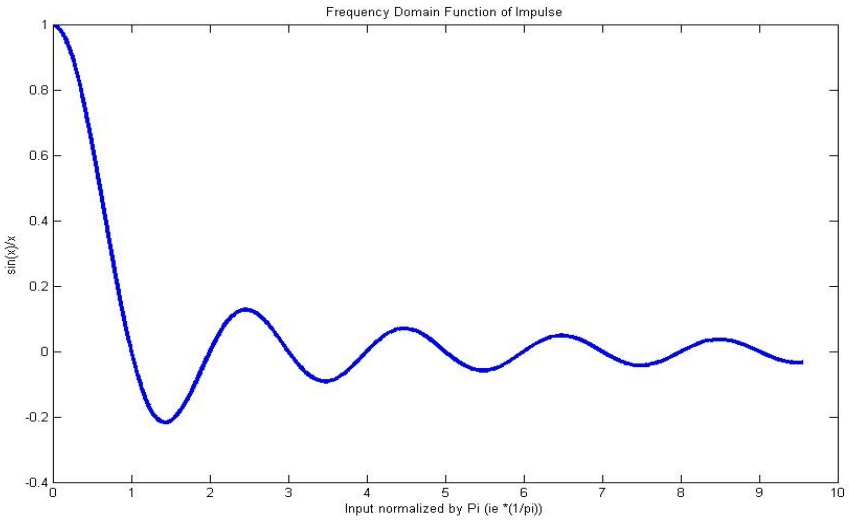

Figure 4.5 shows the basic shape that should be expected from the simple waveguide response. The next goal is to ensure proper frequency content is contained in the pulse. The

shorter the pulse, the greater the frequency content. The pulse used for simulations is shown graphically in Figure 4.6.

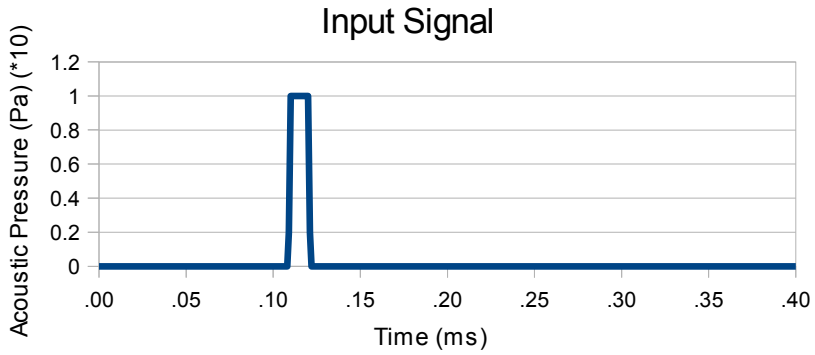

To confirm the appropriate amount of frequency content, a test simulation was run and the frequency response of the waveguide excited by this pulse are shown in Figure 4.7.

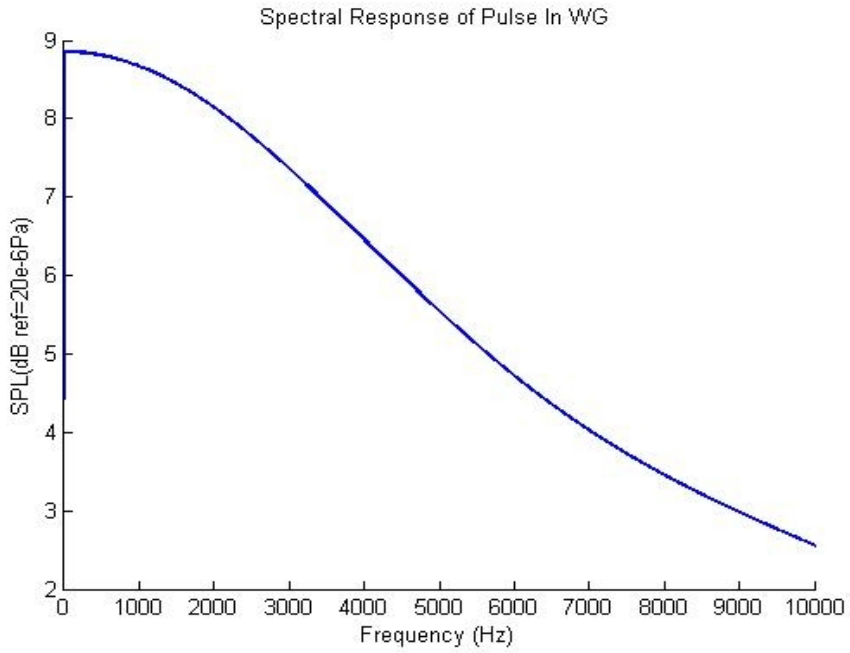

Figure 4.7: Frequency Response of Simple Waveguide Excited by Pulse

Figure 4.7 shows the roll off of the major frequency to occur between 1 and 2kHz. This will be an acceptable trend. Figure 4.7 also offers an important standard for comparison as resonators are added to the model, and tune frequencies are checked.

All other surfaces were set to a hard walled boundary condition to reflect the PVC waveguide used during experiments. This boundary condition forced the velocity of the outer nodes to not expand outward beyond their initial positions. The impulse propagating down the waveguide with minimal dissipation.

A single, unique node was chosen for the sample location for all of the simulations that had resonators. A different mesh was used when the HRs were not present, so the same node could not be used, but a similar location was chosen for data collection. The similar location was within 1mm of the usual sampling location. A sampling frequency of 50 kHz is used to collect data from the simulation at that single node point. The time history collected from the sampling node was then saved in an excel spreadsheet, and post processed in matlab to convert the time domain information into frequency domain data.

4.5 *Parametric Study and Model Validation*

A model was built of a simple waveguide with no resonators or actuators. The input driving pulse shown in Figure 4.6 was set to excite the waveguide from the speaker end of the tube. The end opposite the driving speaker was set as a non- reflecting condition. The FEA calculation time step was set to be no greater than .1 μs. The sampling frequency for the data

collected from the downstream node was set to 100 kHz. This vector of data was post processed in matlab to convert time domain information into the frequency domain.

To validate the model, an arbitrary resonator size was modeled and then altered. The basic dimensions of a "T" shaped cross section composed the resonator 2-d drawing. A basic sketch with related variables is shown in Figure 4.8. This two dimensional drawing is revolved around the pivot line called out in the figure to produce two coupled, cylindrical cavities. The dimensions h_N and r_N turn into the length of the neck of the resonator and the radius of the opening of the neck, respectively. The dimensions h_V and r_{HR} produce the depth of the cavity and the total radius of the cylindrical volume, respectively.

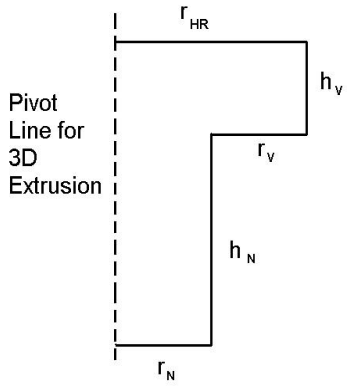

The r_N surface is the opening from the waveguide to the resonator. Since the waveguide is a cylinder, this interface will not be perfectly flat like the r_N surface. The curvature of the opening will be a source of error for the resonator tune frequency calculations. For the parametric study, the HR was build with the dimensions shown in Table 4.1.

r_N	5 mm
h_N	14.5 mm
r_V	15 mm
h_V	10 mm
r_{HR}	10 mm

Table 4.1: Initial Resonator Dimensions (Resonator A)

Using Equation 3.1.1 from the Theory Chapter, the theoretical tune frequency was calculated to be 1867Hz. This resonant frequency was confirmed by a simulation with six resonators arranged like Figure 4.4. A drop of nearly 20dB is observable with the local minimum at 1873Hz.

Two more resonators were tested with similar dimensions. The details of those dimensions are present in Table 4.2.

Resonator:	B	C
r_N	5 mm	5 mm
h_N	13 mm	9 mm
r_V	5 mm	10 mm
h_V	15 mm	15 mm
r_{HR}	10 mm	15 mm

Table 4.2: Alternative Resonator Dimensions

Resonator B was designed to have a tune frequency of 1580 Hz, and resonator C was designed for the lower frequency of 1180Hz. Both resonator arrays produced simulation results

which confirmed these resonant frequencies (See Figure 4.9).

The data collection and post processing deserve some attention before the results are shown. A node near the anechoic end of the waveguide mesh was sampled for its pressure time history data at a frequency of 10 kHz for the length of the simulation. The data was post processed in matlab with a pwelch function used to convert the time history data, into a density spectrum.

4.6 *Parametric Study Results*

The results are shown graphically in Figure 4.9. There are four curves plotted from 0 Hz to 2.1kHz. The solid black line is shown as a reference because this is the spectral density of the waveguide without any resonators attached. The other three curves show the spectral density of the simulations with different Helmholtz resonators attached to the waveguide.

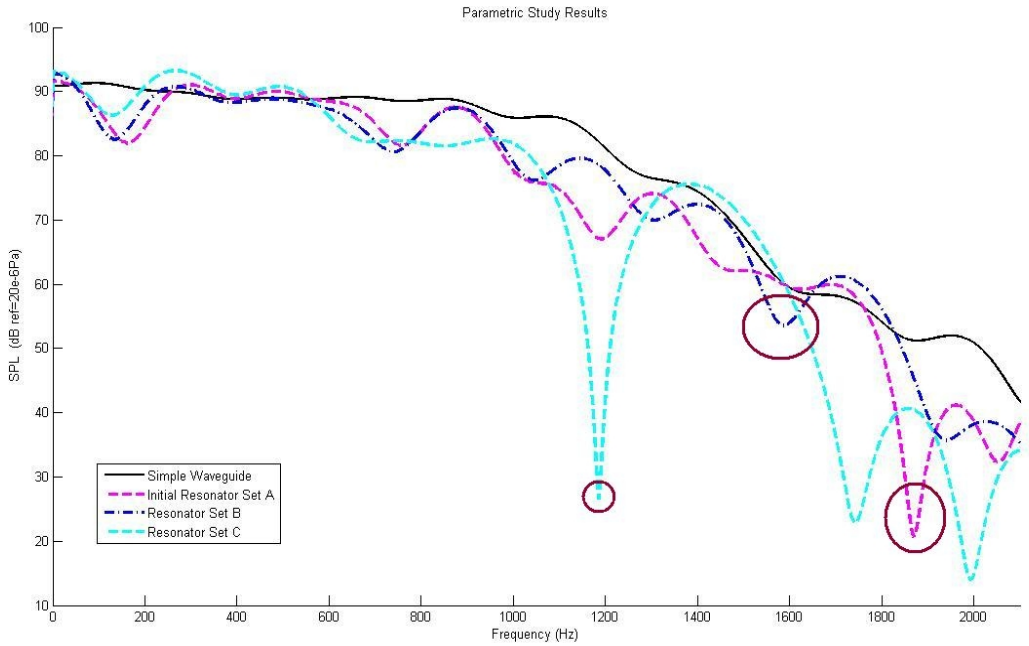

Figure 4.9: Parametric Study Results

Resonator	Designed Tune Frequency	Simulated Tune Frequency
A	1.867 kHz	1.84 kHz
B	1.58 kHz	1.60 kHz
C	1.18 kHz	1.195 kHz

Table 4.3: Resonators Design and Simulation Tuning

Each curve is identified by the legend, and for quick reference Table 4.3 is provided showing the designed tuned frequency and the local minimum near that tune frequency. The results of the simulations show that the resonators attenuate frequencies within 30Hz of the design tune frequency. This is a reasonable margin of error, and is likely due to the inexact

effective length of the neck of the resonator due to the curvature of the waveguide cross section. The attenuation each resonator produces varies widely. Resonator set C produced over 50dB of attenuation at the resonant frequency. Resonator set A produced over 20 dB of attenuation, and set B showed the smallest impact at the resonator frequency with about 5 dB difference at the tune frequency. These results validate the FEA model and provide a source of confidence in the results of the simulations.

4.7 *Active HR/PA Simulations*

To focus on the oscillatory motion, the plasma actuators were modeled as speakers. The inside surface of the neck of the resonator is where the actuator was placed on the Helmholtz resonator. This configuration reflects the actuator/resonator (*Res)* configuration sketched in Figure 5.10. The actuator signals were inversions of the input signal. An appropriate time delay was calculated knowing the distance from the disturbance speaker to the middle of each actuator. This time delay allowed the actuators to fire when the disturbance signal reached the position of the actuators, but was unlikely the exact time delay necessary to see the most optimistic active control results. Because of this, a number of tests were conducted to vary the time delay by fractions of the impulse time length. These time delays simulate varying the phase of the single in a similar manner to the phase variations conducted for the experiments chronicled in Chapters 6 and 7. Applying these pressure boundary conditions at the disturbance speaker face of the model, and also at the actuator faces produces a simulation of the waveguide, resonator, actuator

system with active control.

Before combining the disturbance speaker signal with the actuator signals, the actuators effect on the system. Various amplitudes of the actuator signals were simulated, and data was collected at a similar downstream position as other simulations.

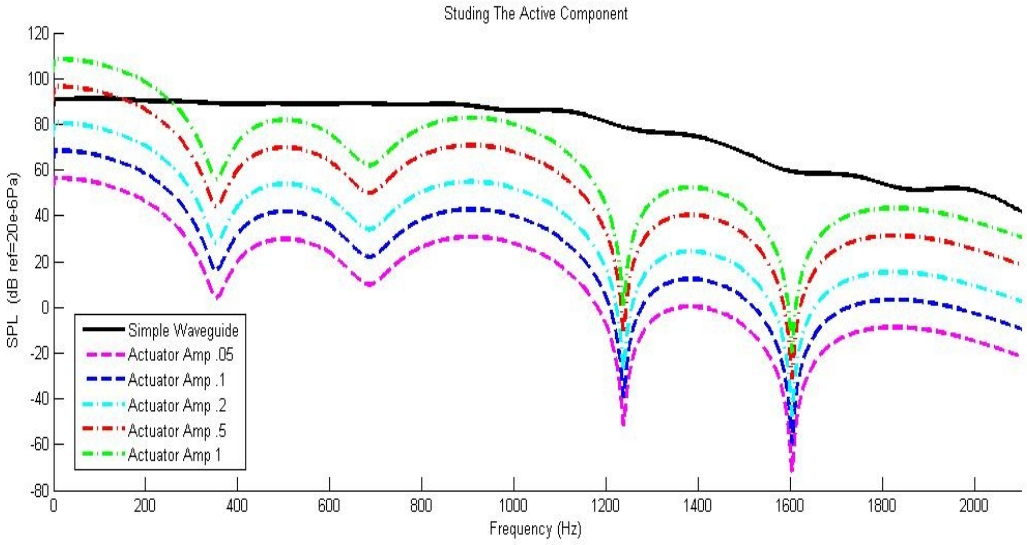

Figure 4.10 reveals some interesting information about the active signal originating from the neck of the Helmholtz resonator. First, the shape of the system response when excited by the actuators is a different shape from the signal which originated from the disturbance speaker. There is significantly less frequency content at 1240Hz and 1600Hz. These frequencies will not react well to active control, unless the reason for the lack of response at the 1600Hz is because the resonator is attenuating the actuator signal. Because of this lack of frequency content, only frequencies between 1320 Hz and 1550 Hz were the chief concern throughout the rest of the simulations, with close attention also given to the tune frequency. This frequency range is within

the bandwidth of interest from 1kHz to 2kHz and is likely to respond well to active control. These troughs of missing frequency content should not adversely affect the performance of the passive resonator. Figure 4.11 shows vertical lines at the tune frequencies of resonators A, B, and C. Since Resonator A was the resonator used for this series of simulations, it is possible that the resonator was attenuating the signal before it could propagate down the waveguide.

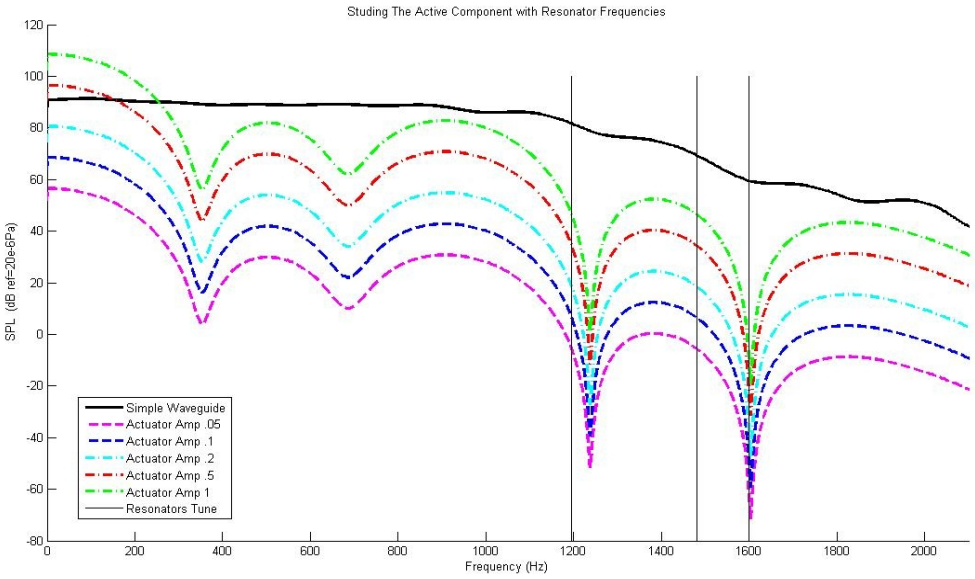

Resonator A, which is the resonator that was attached to the waveguide during this set of simulations, has a tune frequency of 1.84 kHz. This indicates that the resonator removed an extremely large amount of the energy at 1.84 kHz. A higher amplitude is required to make the amplitudes at most frequencies match which is necessary for the best active control results. The time arrivals will probably not affect this resonator/actuator device, because the actuator cannot excite the waveguide at the tune frequencies of the resonator. Now Resonator B, with a tune frequency of 1.6kHz, will be the subject of a time initiation study to see if the different in phase

of the active control system will impact the broadband cancellation. The frequency spectral at the downstream sampling node is shown in Figure 4.12. The combination of the two signals has significantly altered the system response. It appears that the dips in the actuator system response simulations had some negative effects in the 800 Hz to 1300 Hz range. This range is blocked in Figure 4.12. Reducing the amplitude of the actuator signals will reduce this negative effect, but may also reduce the added attenuation in the 1400 Hz to 1550 Hz range. It should be expected that the negative and positive will both be reduced in a directly portion-able manner.

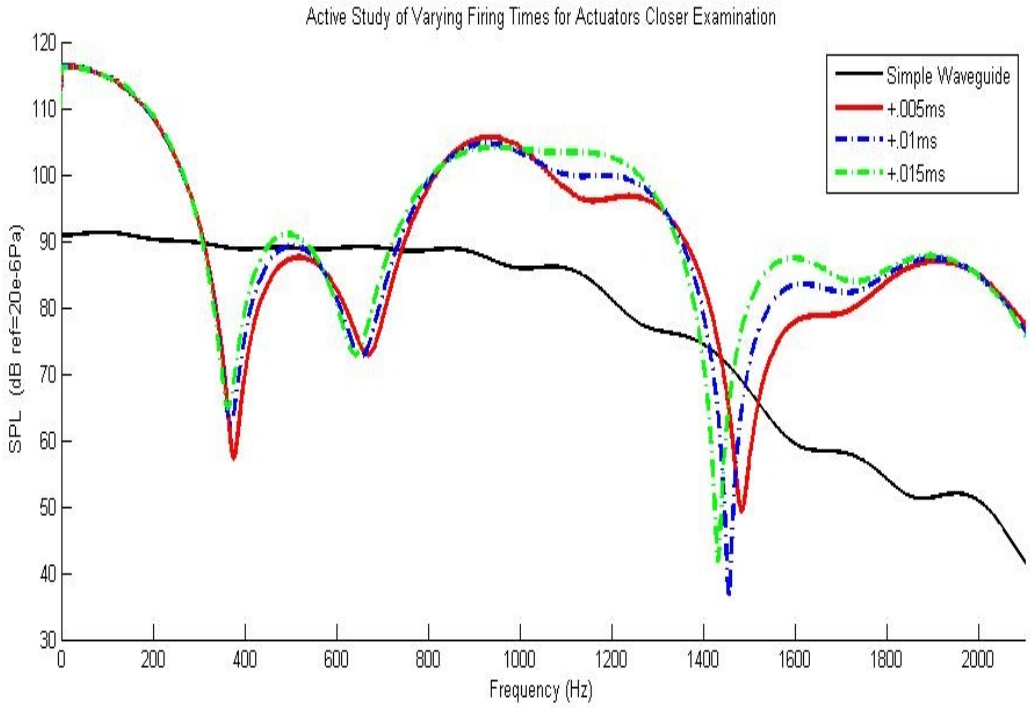

Figure 4.12: Active Study of Varying the Firing Times for Actuators, Close Examination

To confirm this assertion, the model with resonator set B, will have the amplitude reduced and the time of fire varied with more exactness. Reducing the amplitude of the actuator signal flatted the effects out. The 800 Hz to 1200 Hz band has +10 dB response in the active

simulations results shown in Figure 4.12. In Figure 4.13, this effect has dropped some, and is most pronounced around 1000 Hz with specific time delays for the actuator firing. Transfer function plots are provided in Appendix B.

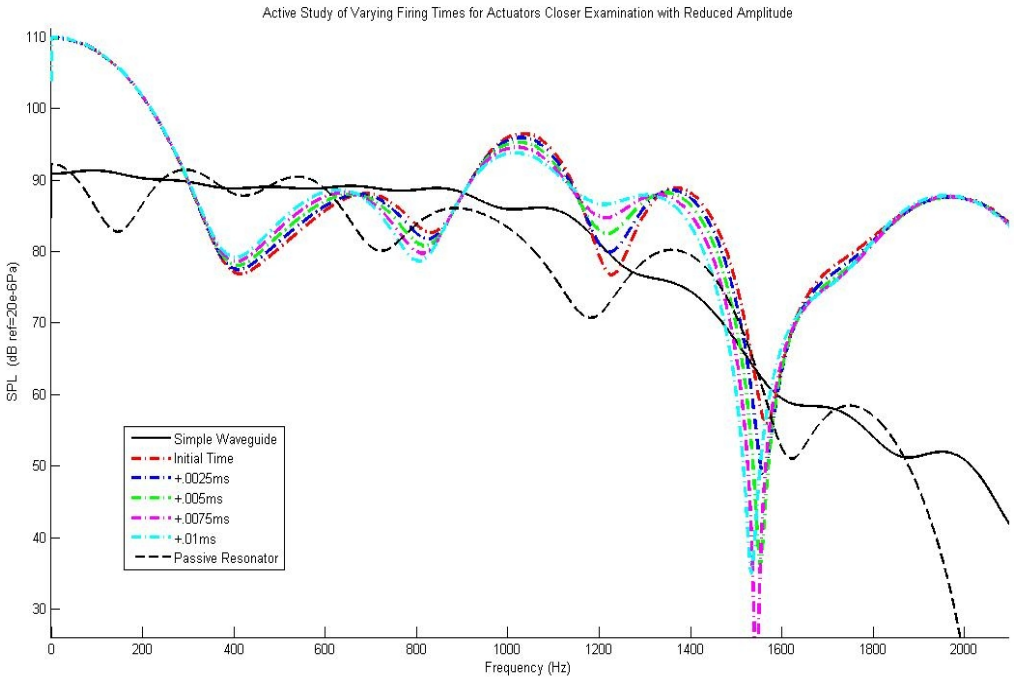

Figure 4.13: Active Study of Varying Firing Times for Actuators with Reduced Amplitude

Reducing the amplitude of the actuator signal allows a clearer comparison between the passive and the active systems. The shape of the frequency shows shifting of local minimums due to the active actuators. The apparent tune frequency of the resonator has been shifted left by approximately 150 Hz, depending on the time of fire of the actuator. The higher frequencies above 1.6 kHz show a 20 dB or more increased response.

4.8 *Simulation Conclusions*

The active simulations showed that across a narrow band of frequencies the active addition could be extremely effective with sound pressure level drops of greater than 20 dB. The active actuators cause some creep of local maximum and minimums. This shifting of the tune frequency could be used as a re-tuning mechanism. This would allow narrow band filters to follow a frequency shifting tone and reduce the propagation. The repercussion for this narrow band improvement in resonator performance comes at the higher frequencies.

5 Initial Experiments with Plasma Actuator

This section will relate and explain preliminary efforts regarding the plasma synthetic jet actuator (PSJA), in order to use the actuator as a means to improve the acoustic liners in turbofan engines. A discussion of the basic setup used to run a plasma actuator is followed with details of the evolution of the design of the actuator. Finally, a refined actuator design will be presented and highlighted for its attributes that display its effectiveness as a compliment to turbofan acoustic liners.

5.1 *Overview of Experiments*

5.1.1 Basis from Literature

The majority of literature that focuses on developing and testing PSJAs discusses one of two designs. Either the PSJA is a straight line configuration or in a circular configuration following the form presented by Arvind Santhanakrishnan and Jamey Jacob [35]. The straight line configuration does not immediately lend itself to working with a Helmholtz resonator. However, the circular configuration has a shape that will naturally interact with the neck of a Helmholtz resonator with only a small alteration in the dielectric base. An image of the circular configuration is shown in Figure 5.1.

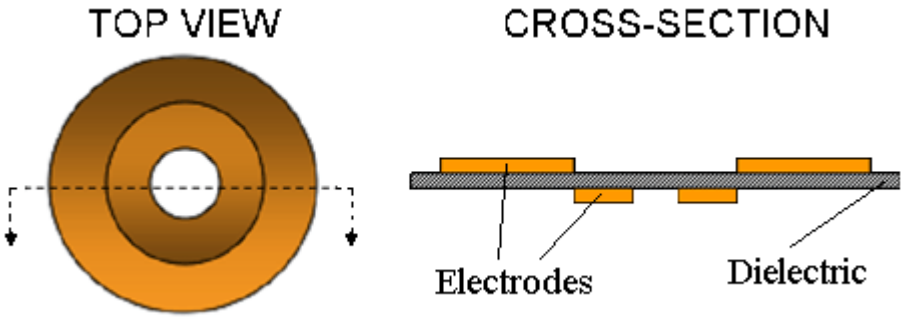

The basic components that combine to make a PSJA are two electrodes separated by a dielectric. In the cross section of Figure 5.1, the dielectric material is represented in gray, and the orange discs are the electrode panels. This type of actuator configuration will here-on be referred to as a "flat" configuration, focusing on the dimensions of the dielectric.

The flow field induced by the circular flat PSJA and the shape of the device lend this PSJA configuration to be easily coupled with Helmholtz resonators, while the straight line PSJA geometry does not. The shape of circular configuration allows for a natural fit when placed around the opening of the neck of a HR. However, the circular configuration requires one major alteration to integrate the plasma actuator with the neck of a HR: a hole in the center to allow air flow through the dielectric piece. The cross section in Figure 5.1 shows a continuous piece of dielectric separating the electrodes. A circular hole will be cut in the middle of the concentric electrodes through the dielectric and will double as an opening for the neck of the HR.

5.1.2 Initial Construction of PSJA

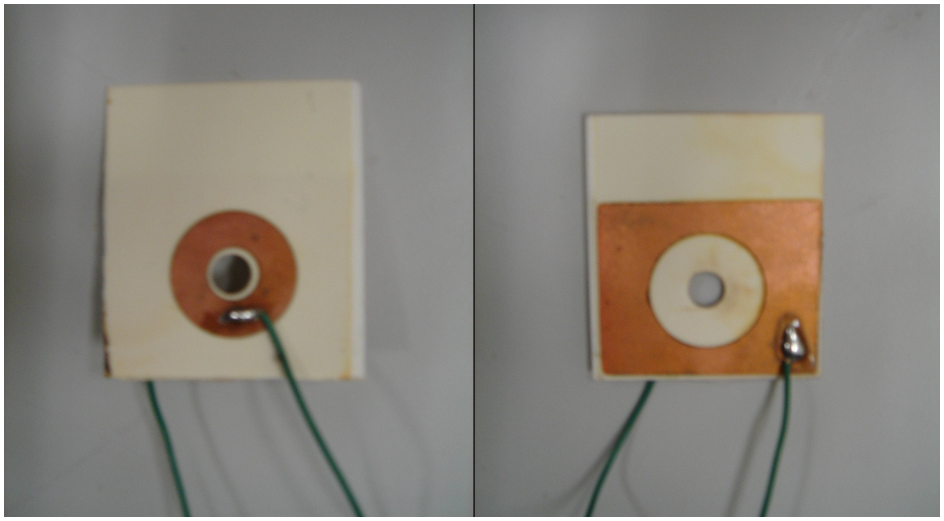

Figure 5.2: Both Sides of Early PSJA

The construction and experiments with the plasma synthetic jet actuators were preformed in the Vibrations and Acoustics laboratory of Virginia Tech. The raw materials used to manufacture the devices were alumina - copper sandwiched panels (with two layers of copper surrounding the alumina). Alumina is a common name for the dielectric, Aluminium Oxide, Al_2O_3. The panels were cut to the desired shapes that matched with constructed HRs. Figure 5.2 shows both sides of a completed PSJA. It embodies the shape that is outlined in Figure 5.1, with the addition of the hole in the dielectric. The shape of the smaller electrode directly mimics Figure 5.1, and the inner perimeter of the outer electrode on the opposite side also has the correct shape at the important interface. The square outer electrode around the perimeter will not affect the induced flow operation because the induced flow is controlled by the inner circular perimeter. This location is the shortest path for electrics to flow between the two electrodes. When the electrodes are charged with low differential voltages the dielectric will block the flow of electrons. At higher differential voltages, on the order of 1kV and greater [46], a break down in

the local air at this perimeter will occur, and some current will flow between the electrodes, despite the insulating properties of the dielectric [5] [46]. The glow discharge occurs in this region and this area is where the electro-hydrodynamic forces originate. A number of alternative electrode settings were attempted, but none showed improved results over this flat, circular configuration.

5.1.3 Hot Wire Anemometer

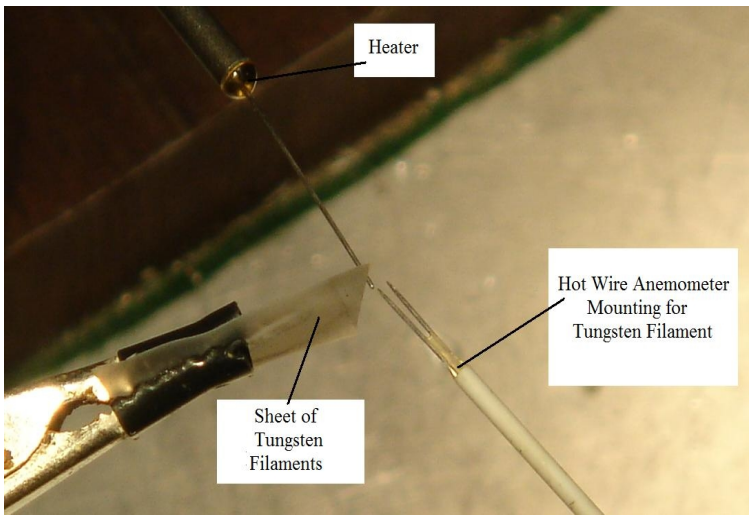

Figure 5.3: Mounting Filament on Hot Wire Anemometer

A hot wire anemometer measures the velocity of a fluid by measuring the change in the resistance of a thin filament at the tip of the probe. The sensor of a hot wire anemometer is composed of an extremely thin filament and a conductive mounting. The resistance in the thin wire, or filament, varies as heat is dissipated through convection by the motion of the fluid. A constant current is run through the thin filament while the fluid flows around it. Figure 5.3 shows a tungsten filament being mounted on the tip of the anemometer by a heater. Additionally,

a second hot wire probe was set up in order to calibrate the anemometer. A known flow speed was controlled and set at 21.52 m/s to assure accuracy of the hot wire.

5.2 *Hot Wire Anemometer Experiment with Flat Actuator*

A hot wire anemometer experiment was conducted to quantify the induced flow that the plasma actuator could produce. This section will highlight and explain the electrical workings of the components that were used to run the flat PSJA during the first hot wire anemometer experiment. Then, specific details of the experiments are followed by results insinuating further tests.

5.2.1 Actuator Circuitry

The PSJA requires high voltage to produce the glow discharge and induce the electro-hydrodynamic effects that are of key interest. A step up transformer with a high turns ratio is the ideal means by which to convert normal voltage levels to the higher levels required for plasma production. A single transformer that would step the signal from the amplifier up to the necessary >1kV level, was unavailable. Two transformers wired in series were used to obtain the necessary voltage levels for the actuators to operate. An audio amplifier was used to increase the power of the driving signal of the actuator. The glow discharge that the actuator produced was dependent on the gain the amplifier added to the system.

The source of the driving signal for the actuator originates from a desktop computer

running Matlab. A simple script was written in Matlab to control the actuator. The sound card is the interface between the software or the mathematical model of the signal and the actual signal flowing through the circuitry in the form of voltage and current (See Appendix C for example Matlab script). The script produced a single tone, which was output from the sound card of a laptop and wired into the amplifier. A concise summary of the electrical circuitry for the flat PSJA, hot wire anemometer experiment is visible in Figure 5.4.

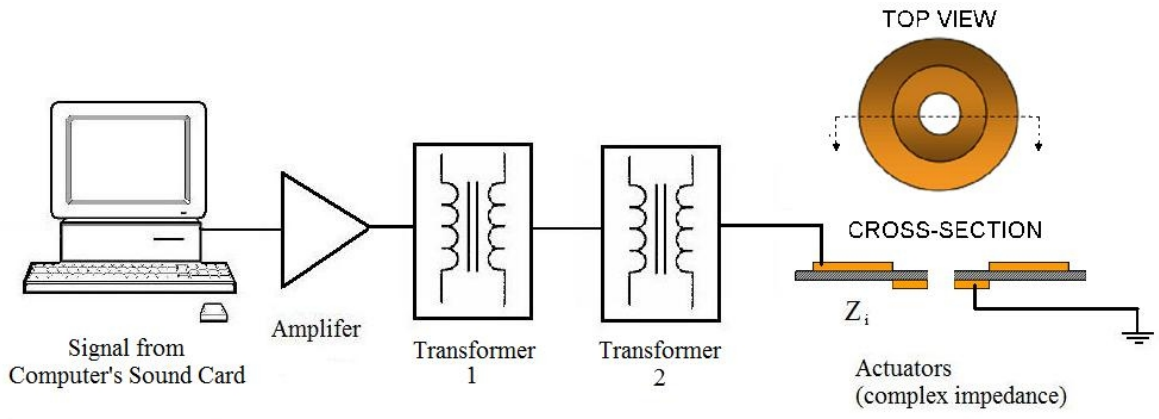

Figure 5.4: Hot Wire Anemometer Experiment for Flat Actuator with Two Transformers

5.2.2 Experimental Setup

The arrangement associated with the first set of experiments is presented in Figure 5.5. This figure shows the experimental setup with the hot wire anemometer positioned at the center of the flat actuator's opening, ½" from the surface of the actuator. The position of the anemometer was not changed throughout this experiment.

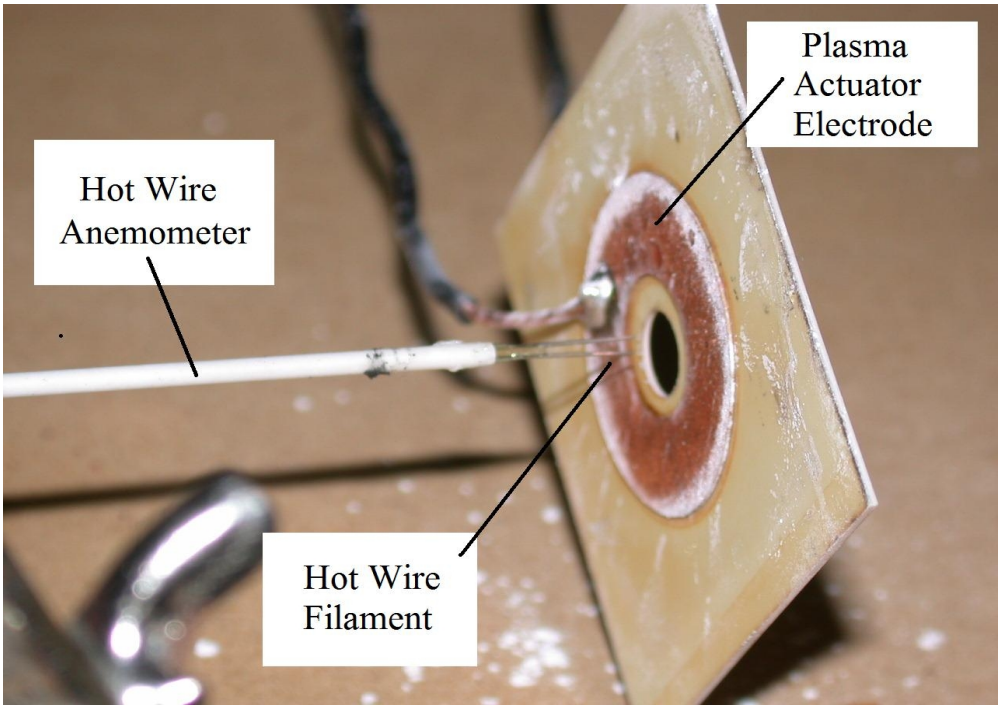

In order to obtain a standardized set of results, the hot wire anemometer was calibrated for each experiment. The calibration was dependent on the transducer. The available transducer was not designed to operate with flow speeds below 20 m/s. Not having a transducer that could operate reliably at lower flow speeds produced problems when data collection was conducted.

The actuator was activated by running the aforementioned Matlab script, which outputted a single tone from the sound card of a laptop. Subsequently, four sets of data were taken corresponding to four different pure tone frequencies of operation for the PSJA. Each signal passed through the circuitry described in Section 5.2.1, and a glow discharge was observed. The actuator usually ran for a period of 4-10 seconds before data was actually collected by the hot

wire anemometer. Four frequencies were tested: 500Hz, 600Hz, 700Hz, and 800Hz. The actuator and hot wire can be seen operating during a test in Figure 5.6. The characteristic glow discharge illuminates the actuator and local surroundings in this figure.

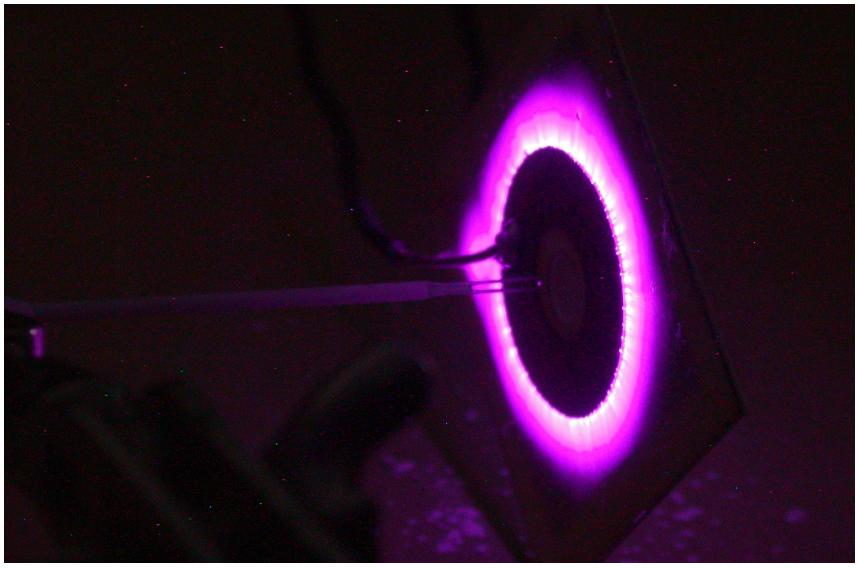

5.2.3 Experimental Results

As expected, a fast Fourier transform (FFT) of the collected data showed distinct, dominant peaks at the driving frequencies for each case. The data showed flow result values less than 0.5 m/s. The observed average flow speeds are shown in Table 5.1. The two orders of magnitude between the calibration flow speed of 21.52 m/s and the results is a significant problem. The flow values are below the point where the transducer can be expected to operated linearly. Furthermore, the values obtained are below the noise floor of the experimental probe.

Therefore, for all pure tone frequencies tested, the measured induced flow was nearly zero. This does not mean that the actuator did not induce any airflow. Rather the airflow induced was minimal and significantly less than values expected.

Freq. (Hz)	Speed (m/s)
500	0.39
600	0.32
700	0.29
800	0.13

Table 5.1: Initial Hot Wire Results

Despite the lack of quantifiable results, a number of lessons were garnered from this preliminary experiment. The induced flow is strongest at the driving frequencies. While this investigation was intended to characterize bias flow properties, it actually revealed the dominance of the oscillatory motion. This knowledge was combined with information collected from literature, to form a redesign of the actuator's layout. This redesign is better suited to couple with an HR, which is described in the following section.

5.3 *Hot Wire Anemometer with Embedded Tubular Actuator*

These effort acknowledge the shortcomings of the previous flat PSJA design. A redesign produced the tubular actuator configuration. Experimental considerations parallel the work conducted on the flat actuator. Section 5.3.2 will highlight and explain the electrical workings of

the components that were used to run the tube PSJA, with noted differences from the previous experiment.

5.3.1 Actuator Redesign

After multiple attempts at getting the flat actuator configuration to satisfy the needs of this specific project, a redesign of the plasma actuator was undertaken. The focus of the redesign was to move away from a two part system where the actuator acts in the local area of a resonator and move towards an actuator that would directly enhance the physical properties of HR operation.

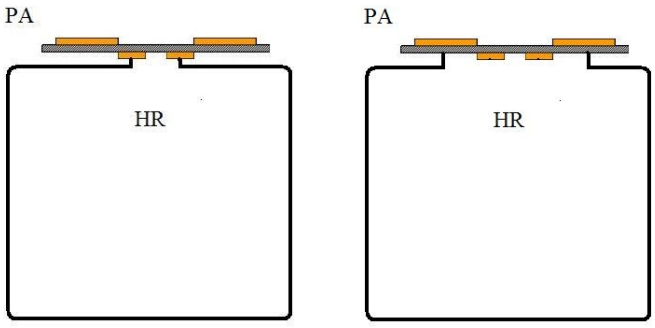

Figure 5.7: Original HR/PA Design

Initially, the design of the HR/PSJA system was going to involve attaching a flat actuator to the open end of the neck of a HR, seen in Figure 5.7. Although, the flow field of the flat actuator produces vortexes that induce flow, the majority of the flow occurs in areas that do not

directly affect the operation of a HR. This issue is illustrated in Figure 5.8. A simple solution to this problem is to keep the flat actuator configuration but place the actuator within the neck of the HR. A flow field visualization of the flat actuator set in the middle of a HR's neck is shown in Figure 5.9. Unfortunately, this design does not operate as intended. The actual neck opening of the HR is effectively only the opening of the PSJA. However, the induced flow has been directed in a more efficient and productive manner. The actuator acts as an input periodic force on the analogous spring mass system of the resonator.

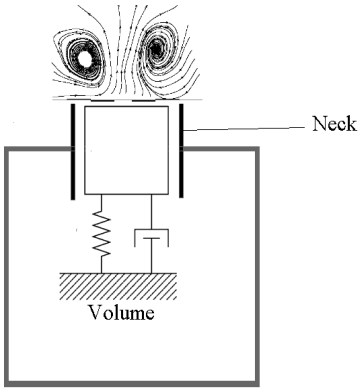

Figure 5.8: Spring Analogy with PA Flow Field

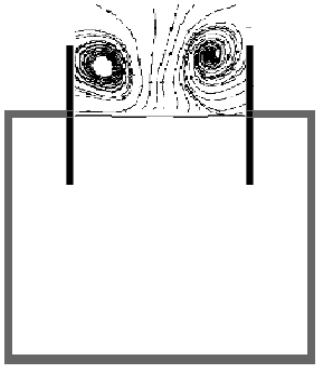

The previous actuators were composed of a flat Alumina piece with copper panels attached to both sides. The glow discharge from these PSJAs occur at small distance away from the opening of the HR neck. The configuration shown in Figure 5.9 continued to lack the direct flow field interaction that was desired, because the induced flow was still produced some distance away from the effective opening of the neck. The final configuration places the copper panels directly on the neck of a HR, rather than on the outside or in the middle of the neck. One copper panel is placed on the inside perimeter of the neck, and the other is on the outside perimeter, as shown in Figure 5.10. An example of an actuator built with this configuration is shown in Figure 5.11.

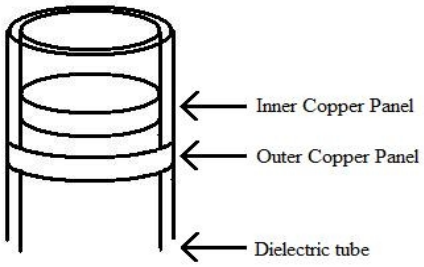

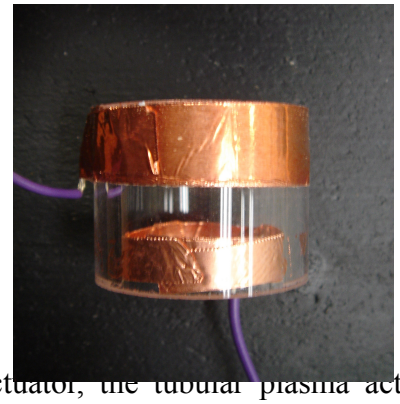

As with the original actuator, the tubular plasma actuator creates two areas of glow discharge. In this case, the glow discharge on the inside of the neck directly interacts with the oscillating air of the resonator. The glow discharge that occurs on the outside of the tubing can potentially be used to help excite the air inside the volume of the resonator that is also fluctuating. Figure 5.12 shows both configurations, with the resonator on the left not using the outside glow discharge and the resonator on the right using the outside glow discharge to excite the air in the volume of the resonator.

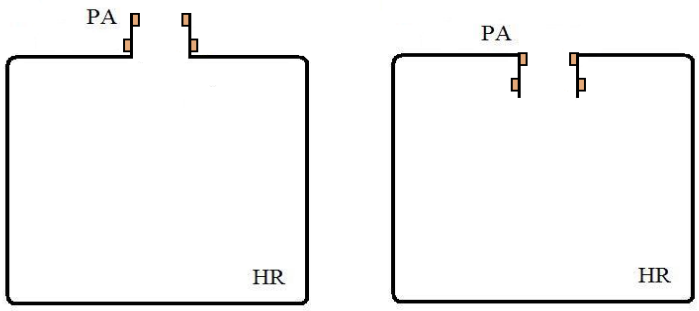

In addition to this new configuration, new dielectrics have been tested for usability. Fused Quartz is now the standard dielectric used for testing because it is readily available in a variety of sizes that allow for different tune frequencies for the resonators. The Fused Quartz has a dielectric strength of 5 kV/mm, while the Alumina has dielectric strength of 15 kV/mm (See Appendix A: Table of Tested Dielectrics). Changing the dielectric material will change the way the actuator responds to the electrical driving signal.

5.3.2 Actuator Circuitry

The early tests saw the refinement of the circuitry to a point where a given actuator could operate with a standardized set of electrical components. Instead of using two transformers that have a combined weight greater than 10kg (22 lbs), a single high voltage transformer was used. Figure 5.14 shows a picture of one of the high voltage transformers used. The design of the transformer makes it useful for a variety of specialized high voltage applications including:

"solid state Tesla coils, plasma displays, Jacob's Ladders, drivers for DC multipliers or [other] general purpose high voltage sources"[54]. The specifications for the transformer rate it at 10kV peak at 10mA. It has a large ferrite core, in a square frame shape with windings on opposite sides of the frame.

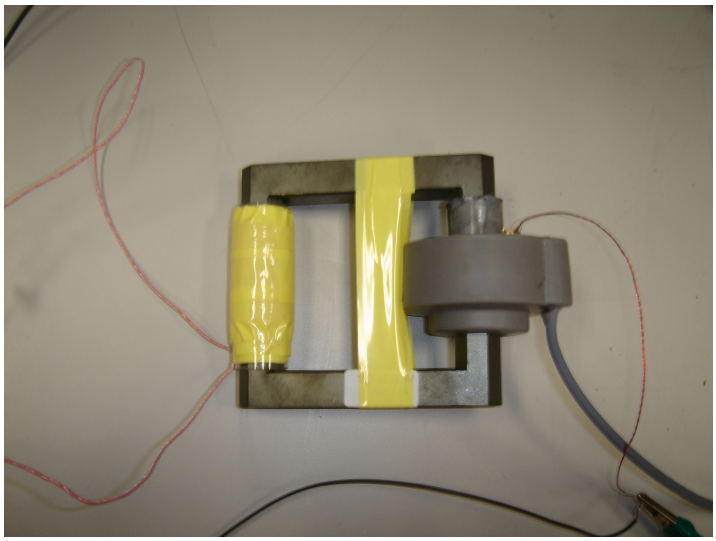

Figure 5.13: High Voltage Transformer

Like with many mechanical and electrical operations, a transformer is a dynamic system, and therefore has an associated resonant frequency. If the resonant frequency of the transformer is known, this value can be used to improve the output of the transformer to ensure the necessary voltage step-up is achieved. A test was completed to find the resonant frequency of the transformer. A frequency sweep was amplified and fed to the input terminals of the transformer, while the output terminals were connected to an oscilloscope, with a high voltage probe. Resonance for this particular transformer is 18 kHz.

Finally, the previously utilized Matlab script used to produce the signal for the system

was revised and utilized for this set of experiments (See Appendix A for example Matlab script). The script required two frequencies as input: one as the carrier frequency and the other as the modulating frequency. The resonant frequency of the transformer was set to be the carrier frequency at 18kHz. The modulated frequency was varied from experiment to experiment depending on what resonator/actuator combination was used. A filter removed frequencies greater than 100 kHz, added 10dB before the signal reached the amplifier, and smoothed the sound card output. A concise, visual summary of the electrical circuitry for a typical high voltage plasma actuator can be seen in Figure 5.15.

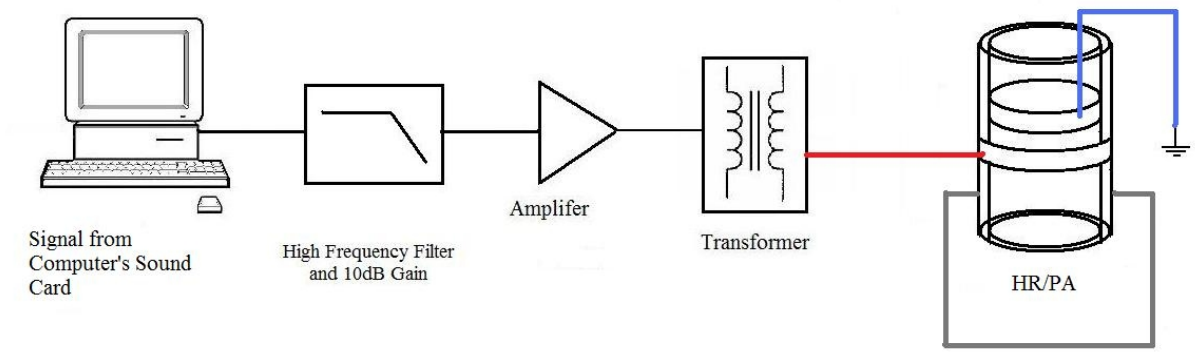

5.3.3 Hot Wire Anemometer Test for Tube Actuator

The new PA configuration was tested using a hot wire anemometer. The tungsten hot wire filament was placed 7/8" from an end of the actuator. This test incorporated the Helmholtz

resonator with the PA. Figure 5.16 shows the hot wire placement at the center of the tube opening. The actuator signal circuitry and the hot wire are independent (the filters and amplifiers are not shown).

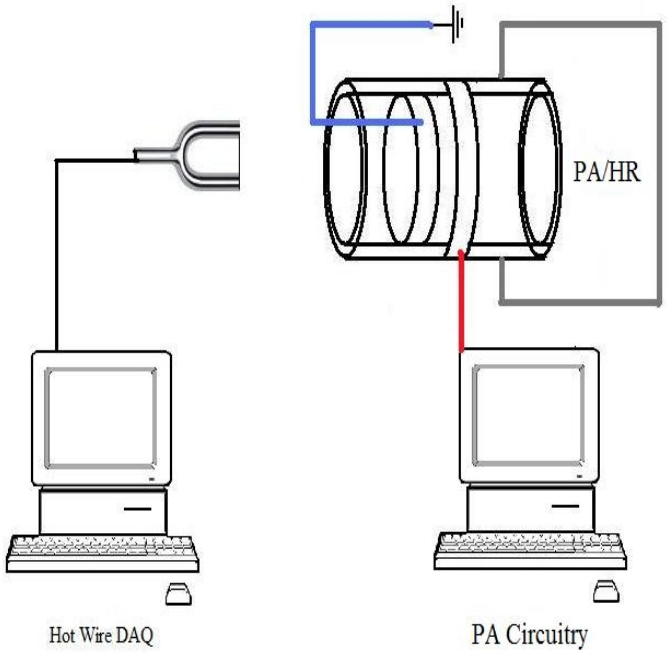

Figure 5.15: Tube Actuator Hot Wire Experiment

In this experiment, the hot wire was calibrated to a 2m/s air flow. This calibration was much more appropriate for the expected flow rates. This low flow calibration was made possible by the availability of a low voltage transducer.

5.3.4 Tubular Actuator Hot Wire Results

Since the actuator is run with an amplitude modulated signal, three major results are

expected. First, a net bias flow should be observable. Secondly, a fluctuating flow at the modulated frequency should be observed, and finally, another fluctuating flow at the carrier frequency is expected.

The experiment was run by operating the actuator at a variety of frequencies and collecting samples of data through the hot wire. A range of frequencies was tested to allow comparisons of flow depending on frequency of operation. The average of the induced flow speeds was recorded, and those values are plotted in Figure 5.17, which represents the average values of three samples. The highest magnitude of induced flow occurred at the lowest operational frequency tested, 1200 Hz. The range is less than 0.15 m/s across these frequencies. Additionally, the peak flow rate recorded during the test reached about 1.5 m/s for each frequency tested, showing that the maximum flow rate is independent of driving frequency. A flow vs. time graph of the raw data showed oscillations of the flow around the average value or bias flow value.

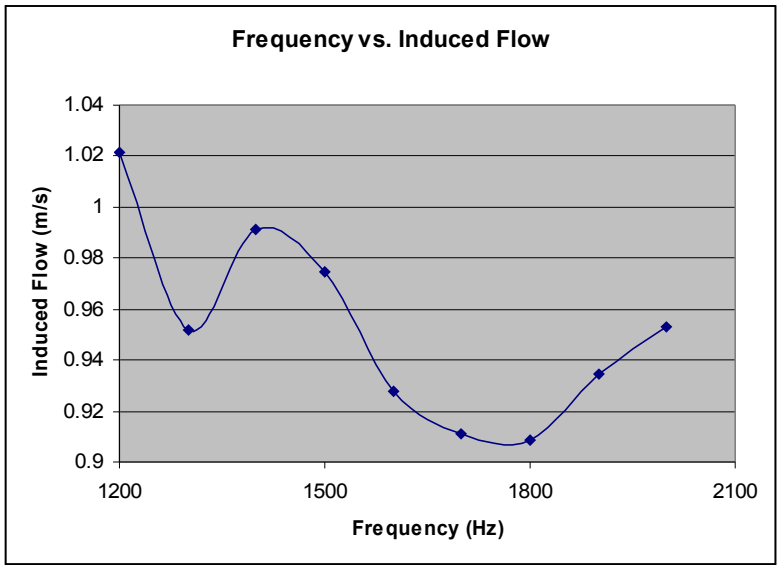

Figure 5.16: Frequency vs. Induced Flow

A test of the flow variation across the radius of the tube and beyond was also conducted. The measurements began at the center of the tube, progressing outward to 24 mm at discrete steps of 2 mm. The diameter of the tube plasma actuator was 25mm (radius = 12.5mm), so this range extended beyond the radius of the tube. The symmetry of the tube actuator design should create a symmetry in the flow field in the angular direction. Some variation is expected in the radial direction (Refer to Figures 5.8 and 5.9 for the actuator flow field). Three measurements were taken at every position and averaged. The results of this radial variation test are plotted in Figure 5.18, where the radial distance from the center of the tube for each measurement of the hot wire is indicated on the x-axis. R is the radial distance from the center of the tube for each measurement of the hot wire(R=0 corresponds to the center of the tube). For values within radius of the tube, the measured average flow rates are all larger than the recorded flow rates at

radii larger than the radius of the tube actuator. This fact indicates that the synthetic jet is concentrated within the tube's radius.

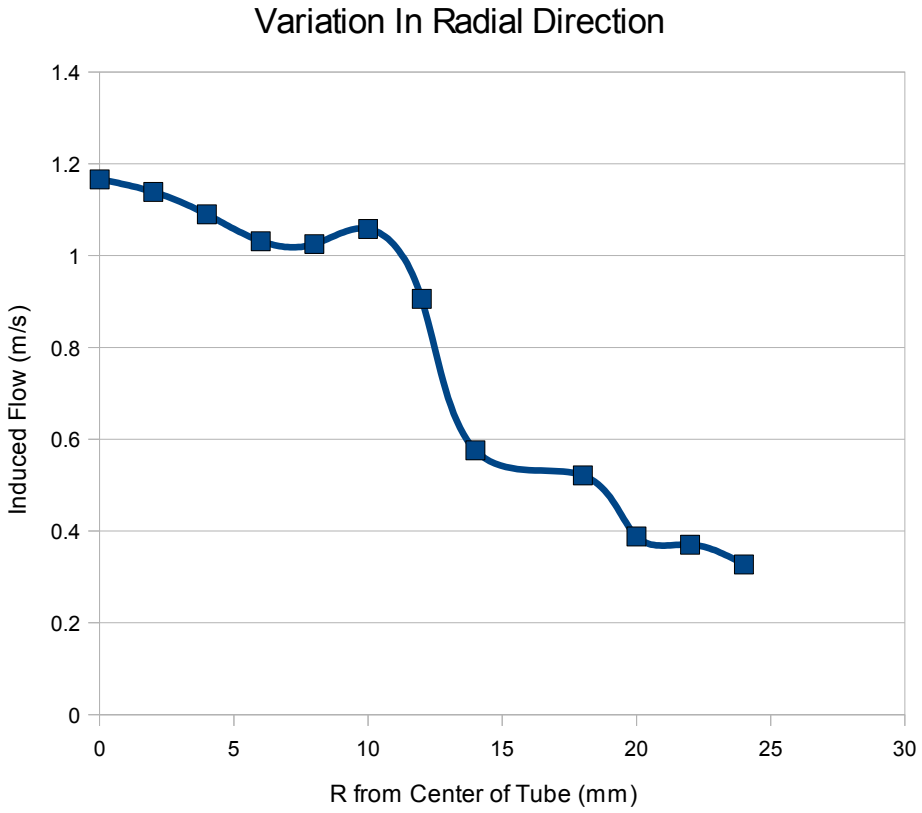

5.4 *Summary*

This chapter presented the early design of the flat Plasma Synthetic Jet Actuator, as well as the redesigned, tube actuator. Incorporating a plasma actuator with a Helmholtz Resonator required the redesign to aid the actuator's properties to better compliment the physical properties

of a Helmholtz resonator. Tests of the tube configuration actuator reveal low induced-flow rates, on the order of 1 m/s. While these flow rates are low they do reveal an induced flow caused by the operation of the plasma actuator. The next experiments present in Chapter 6 will test the combination of the oscillatory as well as the induced bias flow as a means to improve the performance of a Helmholtz resonator in a duct setting.

6 Concept Validation

This chapter presents the work done to test the tube plasma actuator in a setting which simulates a turbofan engine environment. A waveguide will simulate the engine nacelle environment with focus on the shape of the engine duct. The goal of this experiment is to study the effects the addition of an active plasma actuator will have on the performance of a Helmholtz resonator as an attenuating device.

6.1 *Experimental Setup*

6.1.1 Waveguide and Duct Design

To designed a waveguide with ideal properties for testing of the actuator-resonator the frequencies of interest were considered along with source and termination details. The experimental setup was designed to allow the acoustic pressure frequency range from 1kHz to 2kHz to operate without complication or modal interaction. Referring to Figure 2.1, the basic shape of the engine is a short, wide tube. A circular cross section shape for the waveguide duct was chosen to parallel the shape of the turbofan engine. The basic design of the wave guide is shown in Figure 6.1. While the primary noise source of a turbofan engine resides in the center of the duct, this experimental setup places a source speaker (also referee to as the disturbance

speaker) at one end of the waveguide. This placement allows for the noise to propagate down the duct, past the mounted actuator-resonator device, and dissipate at the anechoic termination.

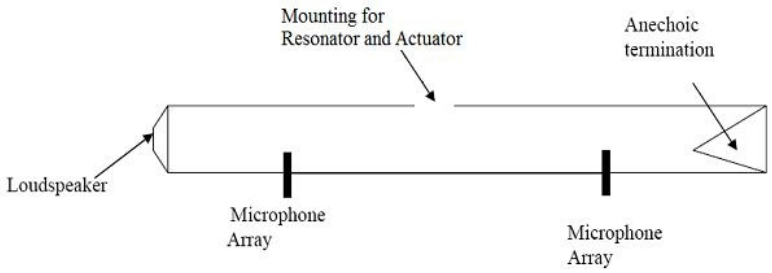

Figure 6.1: Waveguide Setup

For the material composition of pipe, construction grade PVC piping was chosen because it was rigid and readily available. The rigidity of PVC allows the perimeter of the inner tube to not absorb significant sound as a wavefront progresses down the waveguide. By allowing only plane waves to exits within the waveguide, the measurements and analysis will not have to consider modal excitation in the cross section of the pipe. The cut off frequency indicates the frequency at which he cross mode interaction should be a concern and can be calculated from the radius, a, of the pipe:

$$f_c = \frac{1.81 \cdot 343\text{m}/s}{2\pi a} \tag{6.1.1}$$

The highest frequency to be tested was 2.5kHz. Applying a factor of 1.5, to ensure the calculated value was conservative, gave 3750Hz as the target cut off frequency for the wave guide. The conservative radius, a, is calculated in Equation 6.1.2.

$$a = \frac{1.81 \cdot 343\text{m}/s}{2\pi f_c} = \frac{1.81 \cdot 343\text{m}/s}{2\pi\, 3750\text{Hz}} = 0.02634\text{m} \tag{6.1.2}$$

This radius corresponds to a diameter of 0.0527m, which is 2.0748 in. A 2" diameter pipe allows only plane waves to exist along the length of the pipe at frequencies well above 2.5kHz.

The speaker was 2" in diameter, to match the diameter of the PVC pipe, with 3.2 Ohm resistance. It was mounted on the inside of a PVC nozzle so that the face of the speaker was flush with the end of the 10ft pipe. If the microphones and test subjects are placed in the far field from the disturbance speaker, then special near field analysis is not necessary. Three criteria dictate the far field, and are shown in Equations 6.1.3-6.1.5

$$r \gg \frac{\lambda}{2\pi} \tag{6.1.3}$$

$$r \gg l \tag{6.1.4}$$

$$r \gg \frac{\pi l^2}{2\lambda} \tag{6.1.5}$$

With r standing for the distance from the source to the measurement position, λ is the wavelength, and l is the characteristic source dimension. The $\gg$ indicate that r should be at least three times greater that the other term in the inequality[13]. Using the outer bounds of the bandwidth of interest between 1kHz (λ =13.5 in.) and 2kHz (λ =6.78 in.) results in the following calculations.

$$r \gg \frac{13.5\,in.}{2\pi} = 2.15\,in. \tag{6.1.6}$$

$$r \gg 2\,in. \tag{6.1.7}$$

$$r \gg \frac{\pi(2\,in.)^2}{2(6.8\,in.)} = .93\,in. \tag{6.1.8}$$

The anechoic termination was made of a cone of fiberglass. Fiberglass, with a soft and fibrous composition, absorbs airborne sound well. The cone shape allows for the fiberglass to gradually occupy more of the waveguide cross section as an incident wave continues to progress toward the end of the pipe and is therefore ideal for an anechoic termination element. The conical shape of the fiberglass was supported by a wire mesh. A λ_{max} /4 length for the cone will suffice because any incident wave will be absorbed both while progressing toward the end of the waveguide and during any reflections that are not already effectively attenuated. This termination therefore acts as a full half wavelength absorber. The largest wavelength of concern occurs at 1 kHz (λ =13.5 in.).

$$L_{termination} = \frac{\lambda}{4} = \frac{13.5\,in.}{4} = 3.38\,in. \tag{6.1.9}$$

The anechoic termination used is shown in Figure 6.2.

Figure 6.2: Fiberglass Termination

The waveguide was 10ft. The speaker was rigidly attached to a open expansion joint. The fiberglass termination was also mounted on the inside of a PVC expansion joint. When inserted into the 10ft pipe, it extended 3.5” into the pipe, which exceeded the designed anechoic length. The termination mounted to the end of the waveguide can be seen in Figure 6.3.

The mounting for the test subject (Helmholtz Resonator and Plasma Actuator) is centered at 5ft from the speaker end. The opening for the mounting point measures 1.5” along the pipe and 1” across. Clay is used around the perimeter of the opening to grip the actuator when mounted on the wave guide. The mounting opening and clay are visible in Figure 6.4.

The microphone array had two microphones upstream and two microphones downstream of the mounting point. The reader is referred to Figure 6.1 for a global view of all of these parts of the waveguide.

6.1.2 Resonator Tune Test

A preliminary experiment was conducted on the actuator/resonator device before the actuator was activated. The test was conducted to find the resonator tune frequency. This frequency is then used to drive the actuator.

A PA/HR device was mounted on the waveguide. A hole, the size of the microphone element (< ½”), was drilled in the resonator's cavity. A microphone mounted in that hole collected the acoustic pressure data in the cavity of the resonator. A single microphone was placed in a similarly drilled hole at 2.5ft from the speaker and at 7.5ft from the speaker (Figure 6.1). Every microphone was mounted tightly in the hole which was drilled to size, and clay was used to assure the microphone mountings are air tight. These microphones were connected to a signal conditioning system which fed into a National Instruments Data acquisition board. A computer running LabView was used to collect the data.

In order to use a flat power spectral density input, white noise was played through the disturbance speaker at one end of the waveguide. The data from the microphone closest to the speaker was considered the reference data. The transfer function was then computed for the two signals from the resonator and downstream microphones. The transfer function between the reference noise and the resonator cavity microphone produces strong peaks at the resonant frequencies, and the transfer function between the downstream and upstream microphones will show a clear local minimum at the resonant frequencies of the HR. The transfer function between the resonator microphone and the reference microphone using Equation 6.1.10.

$$TF(f) = \frac{Output(f)}{Input(f)} \tag{6.1.10}$$

The "Output" and "Input" in this case refer to the cross correlation and auto spectrum, respectively. These parameters were calculated by the a LabView program, which will be referred to as "VAL DAQ". During all data collecting sessions which used VAL DAQ, a coherence plot was immediately checked after data collection ceased. If the coherence dropped below 0.95 for the bandwidth of interest, that data was not use for further analysis. The transfer function (TF) is shown Figure 6.5(a). The transfer function between the downstream microphone and the reference microphone data is also calculated, and the frequency response plotted in Figure 6.5(b).

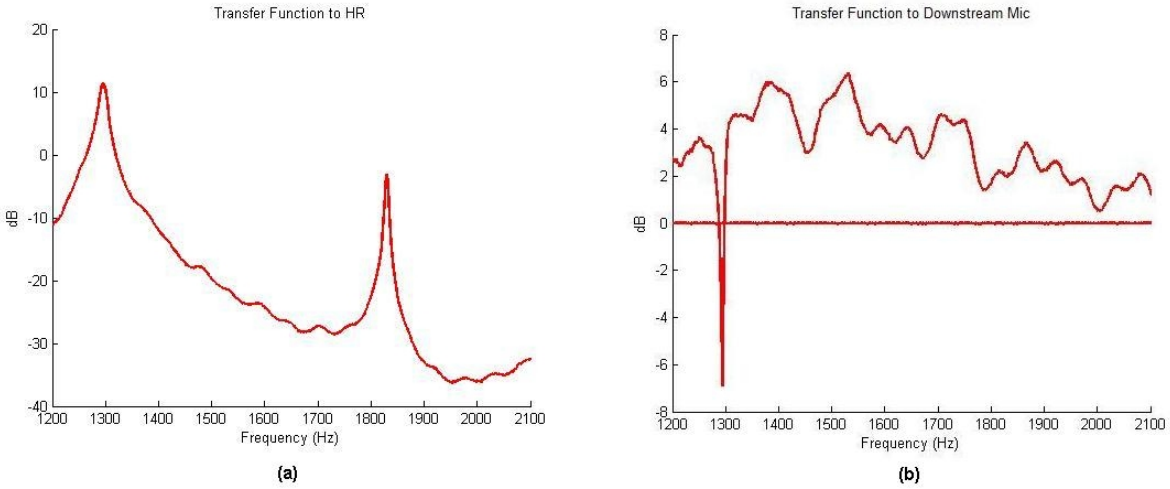

Figure 6.5: TF to HR(a) and Downstream(b) Mic

Two clear peaks are visible in Figure 6.5(a) at 1290Hz and 1830Hz. The 1290Hz peak in the resonator, is directly related to the 10 dB trough at the same frequency in Figure 6.5(b). The

rest of Figure 6.5(b), away from the resonator tune frequency, shows a complex shape. This test successfully revealed the resonator tune frequency, and showed that it is an effective 10dB passive attenuator.

6.2 *Actuator Experimental Operation*

During early experiments, preliminary results showed the actuator signal impinging on the reference microphone. This was tested by operating the actuator, while the disturbance speaker remained silent. The reference microphone picked up the actuator signal as clearly as the downstream microphone. This created a problem for data collection, because the reference signal was being corrupted by the actuator signal. This additional signal would have correspondingly altered the transfer function. To alleviate this undesirable situation, the experimental setup was altered. Instead of being taken from a microphone upstream of the test subject, the reference data was taken from the signal going into the speaker. This solution eliminated any possibility that the actuator signal was affecting the reference signal. A foreseeable drawback collecting the reference data before the signal is converted to pressure waves is that the speaker will have some shape to its transfer function. The assumption is made that the transfer function from the input electrical signal to the output acoustic signal, across the speaker, is relatively flat and does not have a adverse effect on the system as a whole.

The variation in the experimental setup is shown in Figure 6.6. When comparing the difference between this setup and the initial setup (Figure 6.1), the only difference is the

microphone arrays. The signal running to the actuator/resonator is provided by a sound card which output is controlled by a Matlab script. The script produced a modulated signal from the sound card with the carrier frequency as the resonant frequency of the transformer and the modulated frequency as the resonant frequency of the resonator. The disturbance speaker and the actuator signal were isolated by disconnecting each before the actual test was conducted. Data was collected for just the disturbance speaker and just the actuator. Gains for each device were altered until the magnitudes at the downstream microphones nearly matched.

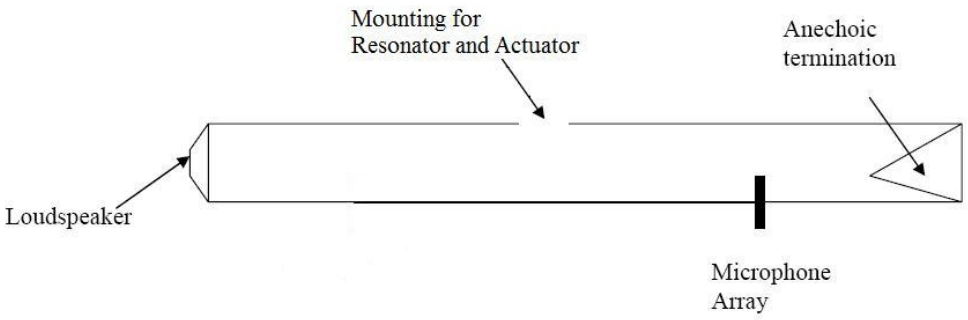

The data collection computer, used the VAL DAW program to collect the data. This program sampled the microphone signals at a frequency of 8192Hz., and averaged 20 sets of the data. The sound pressure level (SPL) at the microphone array was approximately 60 dB during data collection. Figure 6.7 shows the active device mounted on the waveguide.

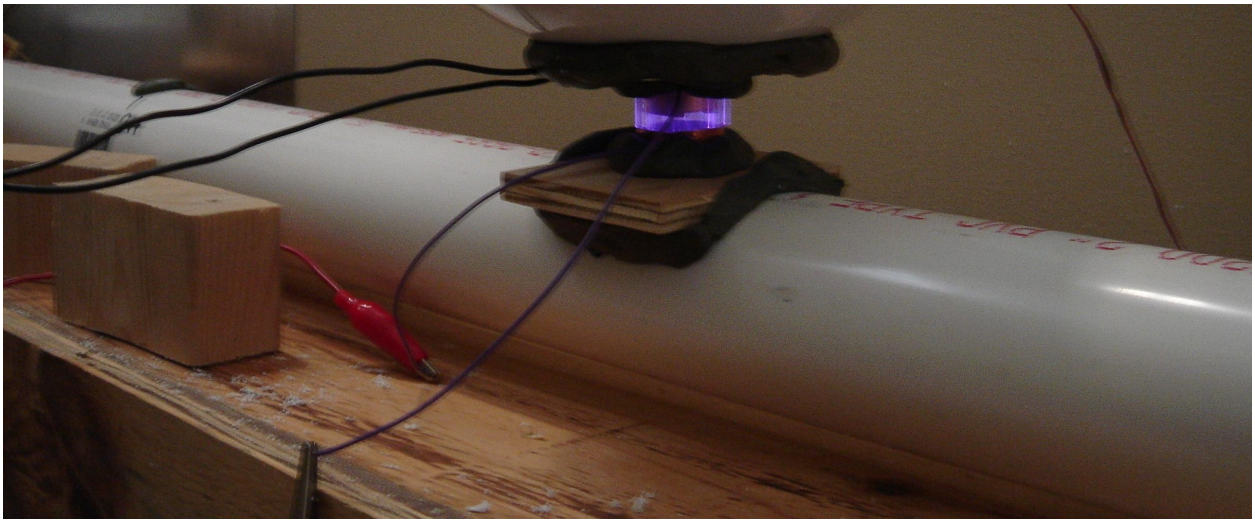

6.3 *Results*

Figure 6.8 shows a number of experimental results and is not calibrated to SPL. This series of data collections were taken one after another with the actuator running for 30 seconds during each sampling. After data was collected the actuator was stopped for 30 sec while the data was saved and the test setup re-examined. The process was repeated in this manner until a large number of results were collected.

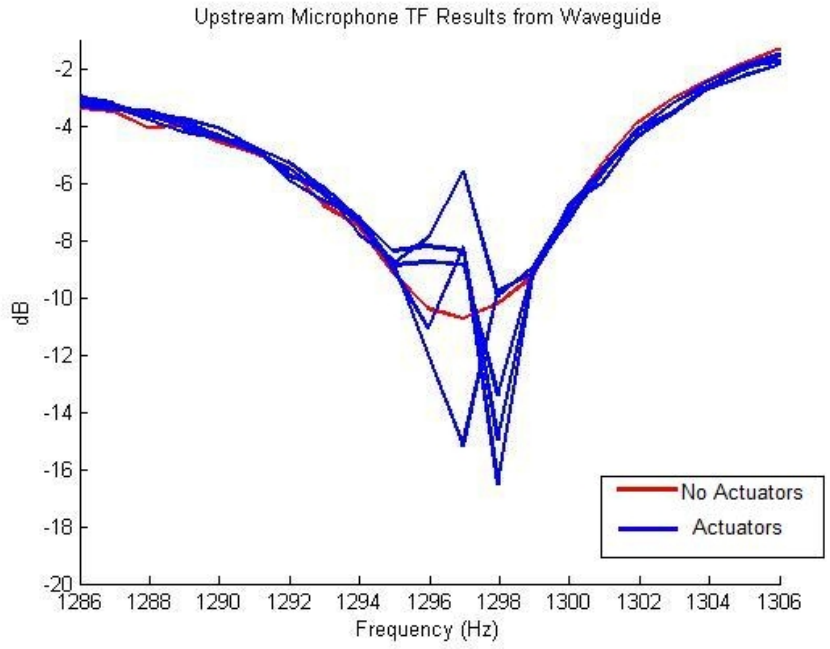

The red curve in Figure 6.8 is the dip at the resonant frequency of the resonator. That plot shows approximately 9dB of attenuation due solely to the passive resonator. The various blue curves shown in Figure 6.8 represent experimental runs with the disturbance speaker and plasma actuator operating at the resonant frequency of the HR.

The results show inconsistent data for how the actuator interacts with the system. It appears that some experimental results reduced the resonator's attenuation, and other runs improve the attenuation. Figure 6.8 shows that the actuator's operation affects a small range of frequencies surrounding the resonator's tune frequency. The actuator's effect is not necessarily consistent across the entire affected frequency range. Some of the blue curves affect the tune frequency in a “positive” manner for the lower affected frequencies, while the effect is “negative” for the higher affected frequencies. A key fact to note, is that the actuator always had

some effect. The effect was simply not consistent; sometimes improving the attenuation, and other times decreasing the attenuation. A phase plot of the data is shown in Figure 6.9.

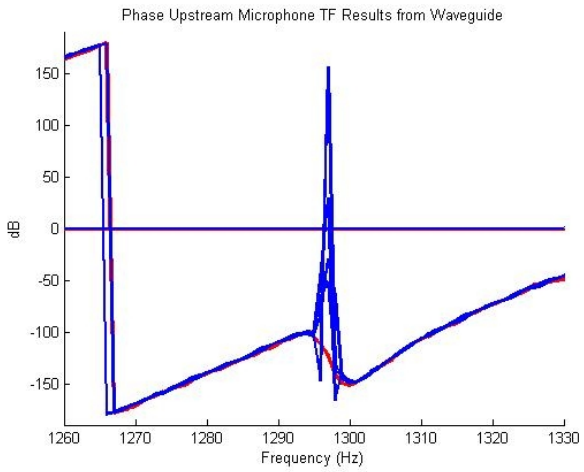

Figure 6.9 shows a clear phase variation at the operational frequency of the actuator.

6.4 *Comments and Conclusions*

The different results during different data collecting sessions point to the necessity for phase control. The two signals were controlled by separate devices, with no defined phase relationship between the signals. This waveguide test has proven that the addition of a plasma synthetic jet actuator as an embedded active device can affect the attenuation of a single Helmholtz resonator. The best explanation points to a variation in phase that might cause this effect. The next chapter presents work that will test this hypothesis.

7 Control Authority Test

The results of the previous waveguide experiment, suggested a phase locked excitation of the plasma actuator to the disturbance speaker would produce more favorable results. For an active control system to operate effectively the magnitude of the control signal must match the disturbance signal, and this was accounted for during the previously described experiment. The phase of the control signal must be shifted by 180° compared to the disturbance signal to produce optimal results. An experiment was designed and used to characterize the possible additional attenuation that a single plasma actuator can produce when coupled with the Helmholtz resonator with the phase control.

7.1 *Experimental Setup*

This experiment required the use of the waveguide, as well as the plasma synthetic jet actuator embedded in the neck of a Helmholtz resonator. The general setup of the experiment required a waveguide as a means of simplifying the acoustic elements of the experiment. The waveguide was the same one described in the previous chapter with a speaker at one end and an anechoic termination at the other end. See the previous chapter for discussion and further descriptions of the waveguide, the actuator, and the resonator. The key change in the experimental setup was in the source of the two signals. The signals originated from the same

computer, one signal coming from the right channel of the computer's sound card and the other from the left channel. Each channel was fed into a different amplifier. The speaker signal was then wired directly to the disturbance speaker. The actuator signal was low pass filtered under 10kHz. From the filter, the actuator signal was stepped up by a transformer and then connected to the actuator. The actuator was embedded in the neck of a resonator. This PA/HR was mounted on the waveguide at the mount point. Figure 7.1 shows the basic set up of the experiment.

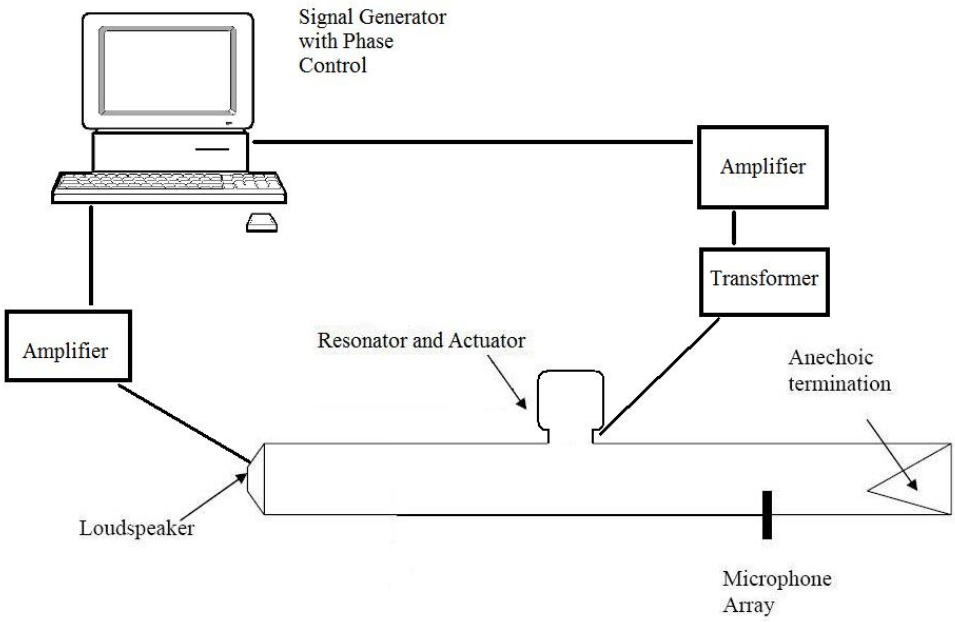

7.2 *Method*

The previous chapter showed that the active actuator has an impact on the performance of the resonator as an attenuator. This experiment aims to examine the effects of varying the phase between the disturbance speaker signal and the actuator single. This test was a feed forward test to confirm control authority over the system. The source signals originated at a computer sound card. The phase relationship between the two signals was systematically shift by 10° from 0° to 450°. The actuator signal continued to be amplitude modulated, as discussed in Section 5.3.2, and the phase shift was applied to the disturbance signal. Both signals were amplified, and the disturbance speaker signal was fed directly from the amplifier into the speaker. The PAs signal was stepped up using the high voltage transformer and then sent into the PA. A microphone on the termination side of the waveguide measured the acoustic pressure of the system at this point.

Before this experiment began, the resonator tune test (See Section 6.1.2) was conducted on a new actuator/resonator. This preliminary test revealed the resonator tune frequency to be 1260 Hz. The intent of this experiment was to see if the performance of the resonator could be improved by the addition of the actuator, and therefore this frequency became the focus of this experiment. A 1260 Hz signal was sent to the speaker, and an amplitude modulated 1260Hz signal with a 20kHz carrier (the resonance of the transformer) was sent to the actuator. Before data was collected, each sound signal was isolated by turning off the other signal's amplifier. The amplifiers were adjusted so the levels of the signals at the microphone were nearly the same.

7.3 *Results*

A transfer function was calculated between the signal going to the speaker and the signal from the microphone. The magnitude of that transfer function was recorded, and then the phase between the two signals was shift by 10°. The tone SPL in the duct when both the actuator and the speaker were operating was 76dB, and the results do not reflect this calibration. This operation was repeated to collect data across a full period of phase offset. The results are shown in Figure 7.2.

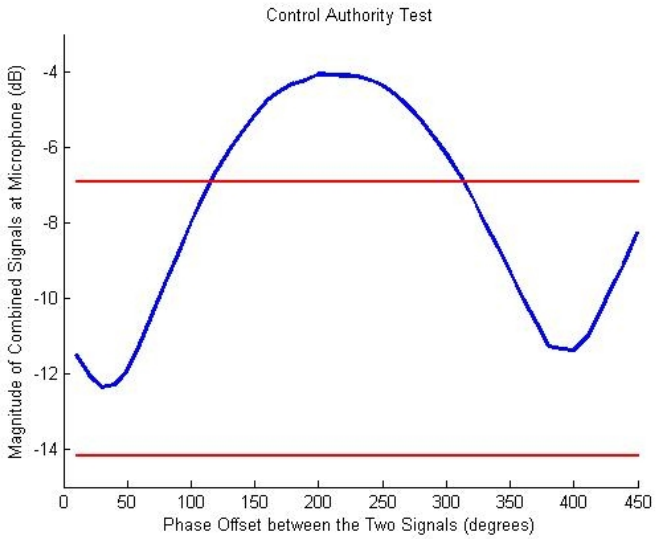

The blue line represents the magnitude of the sound signal at the microphone while both the disturbance speaker and the PA were operating. After all of the data for the phase offset had been collected, baseline data was taken for the speaker and PA, individually. The red line at -5 dB is the magnitude of the disturbance-speaker signal (with the PA off) at the microphone at the end of the experiment, and the red line at -14 dB represents the magnitude of the PA signal (with

the disturbance speaker off) at the microphone. These three lines demonstrate the relative magnitudes for each of the signals in relation to each other. For a phase offset between 0º and 120º and for the values above 310º the magnitude of the combined signals is less than the magnitude of the disturbance speaker alone. The maximum reduction due to the PA/HR appears to occur at about 35º phase offset with a 5dB drop compared to the disturbance speaker's signal.

It is noteworthy that the next trough at 390º phase offset does not return to the same the minimum value that is reached at 35º. This fact led the experimenter to repeat this experiment over a larger phase offset range. The results of this test are shown here:

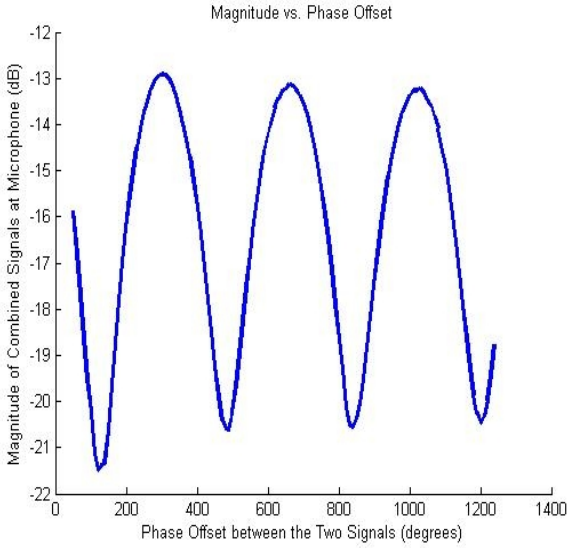

The amplitude of the function drops slowly as the phase offset increases. The process of testing for this experiment leaves the PA running for a long periods of time during data collection. A possible cause could be the ozone that is being created by the plasma discharge glow. The ozone might be filling up the HR volume and decreasing the effectiveness of the actuator/resonator to attenuate the signal. A second possibility is that the heat created by the plasma glow is changing the temperature of air in the HR in such a way that the effectiveness

drops. Rerunning the same test with an small openings in the volume of the HR may yield a better understanding of what is causing this drop in amplitude. These holes should allow for better ventilation of the heated air and the ozone produced.

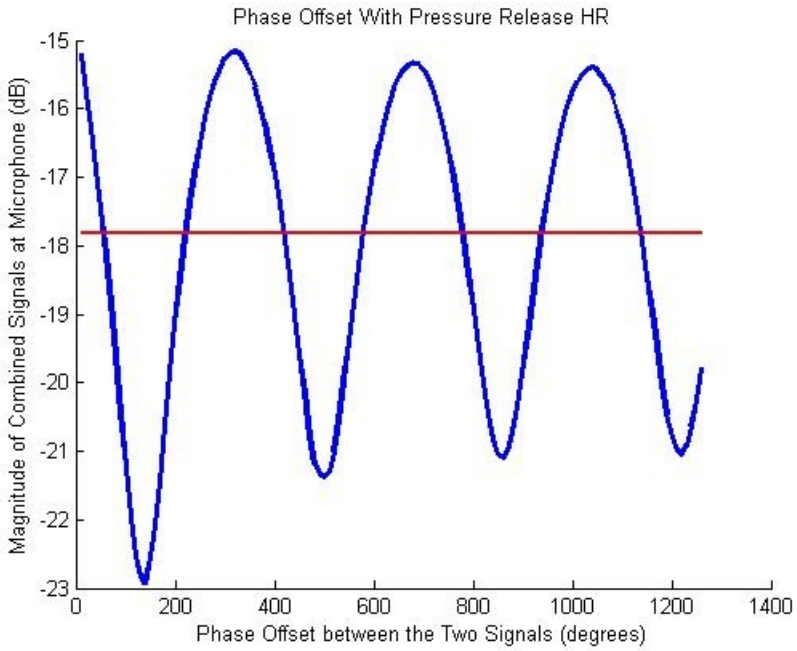

Figure 7.4: Phase Offset with Pressure Release HR

In this plot, the blue line shows the changes in the magnitude of the acoustic signal at the microphone as the phase shift is increased, and the red line represents the level due only to the disturbance speaker, with no PA operating. Again, as time passes the effectiveness of the actuator decreases.

7.4 *Conclusion*

The test for control authority confirms control over the system. This conclusion can be broadened by saying that a plasma actuator can be effectively employed as a active noise control

device. The effect stays approximately constant, adding or removing 3 dB of attenuation. The reduction in performance of the actuator did not change when ventilation holes were added. The variation is likely caused by microphone drift. The next step in researching the effects of the plasma actuators on turbofan liners is to test an array of resonators with operating actuators.

7.5 *Summary*

This chapter contains the work committed to the control authority test. The experiment was designed to show that with the correct phase relationship, the actuator effect can be controlled. Two signals were produced by a computer, and one of those signals was fed into the disturbance speaker, while the other entered the plasma actuator. The results showed that the downstream speaker saw an additional 3-4 dB reduction when the actuator operated at with certain phase shifts.

8 Array Testing

With control authority confirmed, the next experiment focused on applying the completed work to an array of actuator/resonators. Working on an array of resonators simulated an acoustic liner environment by using multiple resonators, instead of a single resonator. Testing an array of resonators/actuators allowed for investigations into issues that might occur during implementation. Building an array of resonators/actuators revealed the best circuitry configuration and a number of other nuances related to the powering of an array of active control actuator/resonators. This work provides a better understanding of the challenges and difficulties inherent to the implementation of these actuators in an acoustic liner.

8.1 *Actuator/Resonator Array - Experimental Setup*

A number of differences between the experiments and the turbofan acoustic liner systems are noteworthy. One of the differences is the spacial dimensions of the resonating cavity. If the open area of the resonator is used for comparison, the original resonators described in the previous experiments were a 20 times scaled model. This factor was reduced during array testing (described in this chapter) down to factor of 6.

Another difference between the previous experiment and acoustic liners is the number of

resonators in the system. The old device focused on the effects of a single actuator-resonator device, and the major focus of this experiment was the actuator/resonator *array* device. This multiple resonator system is coupled with the spacial differences already mentioned. The array of resonators in an acoustic liner, allows for a great number of individual resonators to be compacted into a tight space. So, along with dropping the scale factor of the experiment, additional actuator/resonator devices were wired together and closely (spatially) mounted. Figure 8.1 shows a sketch of the cross section of an actuator/resonator array, with all of the devices structurally connected by a the mounting. The neck of the resonators are composed of tube style actuators similar to the ones in Figures 5.10 and 5.11.

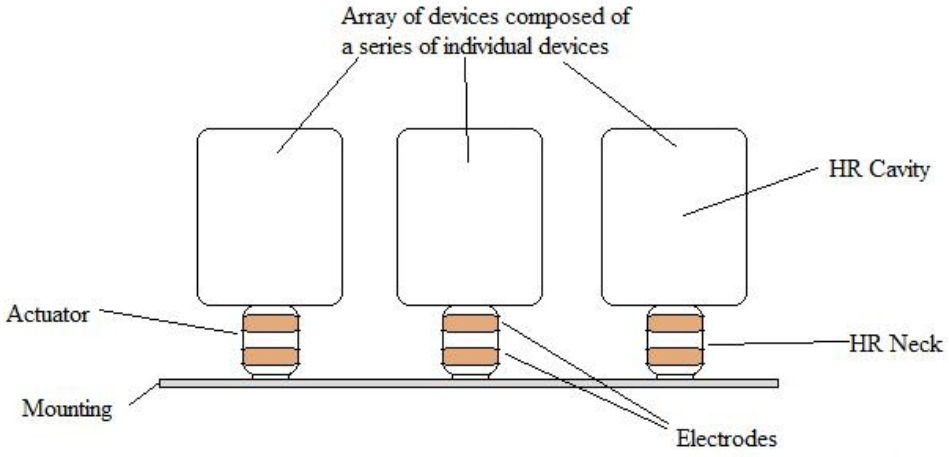

When considering the wiring of the array of actuators, the electrical impedance was based on the impedance of a high impedance capacitor. If the electrical impedance is assumed to be nearly the same for each actuator constructed, then the power dissipated by each actuator should be equal based on the linear addition equation used to describe a equivalent capacitor. Equation

8.1.1 shows how to calculate the equivalent capacitance for an number of capacitors wired in parallel.

$$C_{eqParallel} = C_1 + C_2 + C_3 + ... + C_n \tag{8.1.1}$$

If the power dissipated by each actuator element is the same, then the energy translated into air particle motion should be nearly the same for each actuator as well, assuming the local region has relatively similar characteristics. A parallel wiring configuration was initially adopted in order to expel electrical energy evenly across the array of actuators.

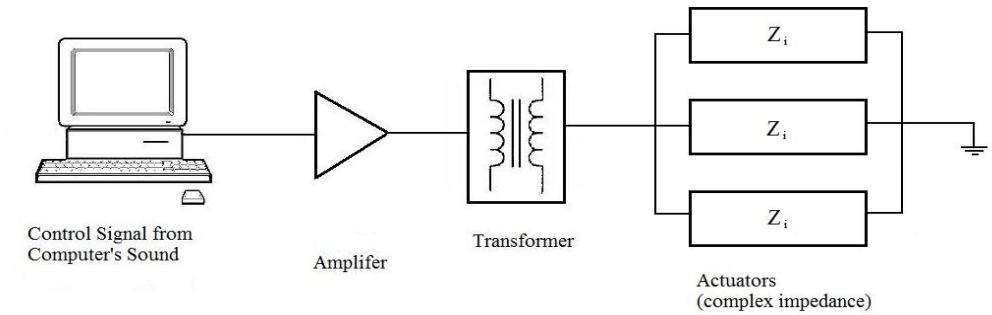

Running multiple actuators in parallel repeatedly produced the plasma formation glow (which has been used as an indicator of fluid excitation) at only a single actuator in the array. In actuality, the small variations in the constructed actuators likely cause a significant change in the electrical impedance. Beyond the dielectric material used in normal capacitors, the capacitance is also dependent upon the size of the electrodes, and the separation distance [55]. Small differences in electrical impedance between the actuators can cause a short at single actuator interface. This finding makes the parallel wiring configuration unfit for the actuator array.

A series configuration was investigated as a better wiring configuration. A series configuration would alleviate the issues encountered with the parallel wiring. The series wiring was setup so that all of the positive electrodes resided on the same side of the actuator (inner or outer perimeter). The actuators were mounted with all of the inner electrodes facing into the waveguide, and the outer electrodes facing on the cavity side of the neck. Figure 8.3 shows a schematic of the wiring path looking at cross sections of the tubular actuators.

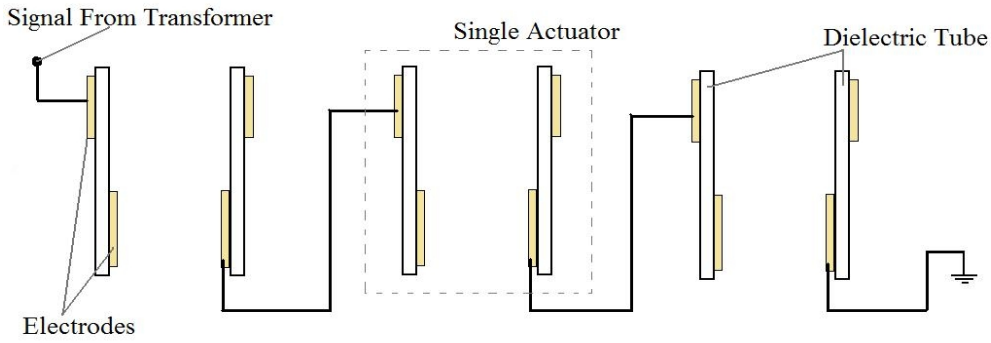

A picture of an actuator array without any cavities is shown in Figure 8.4. This figure shows a staggered actuator positioning on the mounting piece. The copper tape electrodes are positioned on the fuzed-quartz tubes in the manner shown in Figure 5.10 and pictured in Figure 5.11. The wiring of this array matches Figure 8.3.

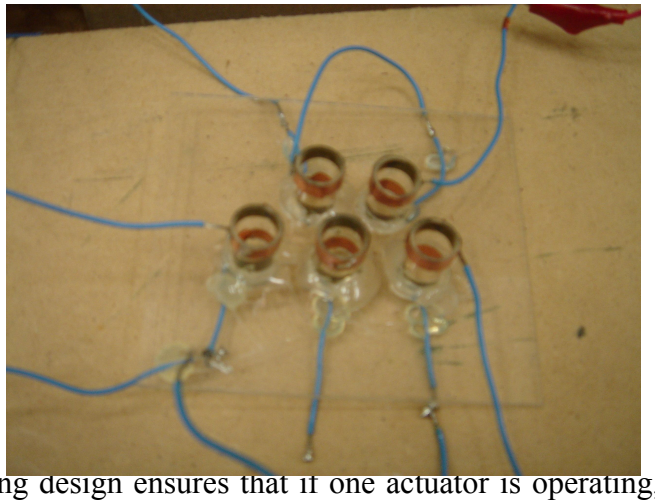

This series wiring design ensures that if one actuator is operating, then all the actuators are operating. However, it has operational some issues as well. This configuration is prone to the possibility of arcing between outside electrodes of adjacent actuators. Figure 8.5 shows arcing between actuators.

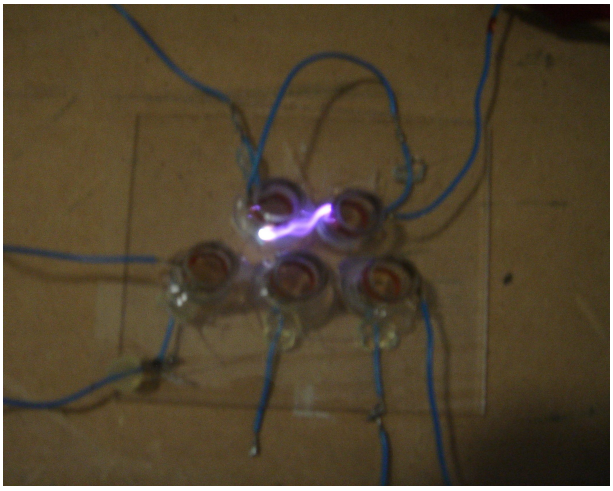

Figure 8.5: Inter-Actuator Arcing

The most efficient solution to the inter-actuator arching problem was to add a shielding dielectric tube. This tube had an inner diameter that was 1-2mm larger than the outer diameter of the actuator tubes. The actuator was then mounted with the "casing" tube as an additional barrier

to protect against the inter-actuator arcing. Figure 8.6 shows a sketch of how the actuator was surrounded by another fuzed quartz tube.

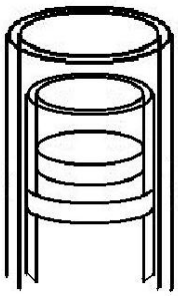

Figure 8.6: Actuator With Casing

The final working array had 6 resonator/actuators. The 6 elements had fused quartz tube actuators as the necks with the shielding tubes installed. The wiring design connected only pairs of actuators. The pairs of actuators which were connected were located at the same distance down the waveguide, so their acoustic phase information was synchronized. This connection required each pair of actuators to receive a separate signal line, with different phase offsets. The phase relationship between the signals was controlled by the source computer in LabView. The cavities of the resonators was composed of PVC pipe ends in the same manner used for previous experiments. The final resonator/actuator array is pictured in Figure 8.7 and Figure 8.8, already mounted on the experimental waveguide.

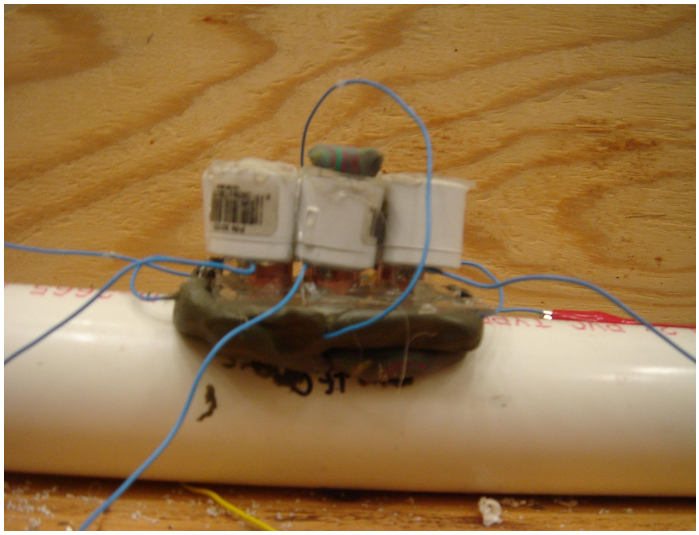

8.2 *Experiment Operation*

The experiment ran with 4 channels of signal originating out of the control computer. The first signal was set the same as the resonant frequency of the HR. The bulk of experimentation focused on the improvements in the already present attenuation of an Helmholtz resonator device. This specific frequency was, like in previous experiments, the main focus of

the experimentation. The three other signals were designated for each of the pairs of actuators embedded in the necks of the resonators. The actuator signals received amplitude modulation at the resonant frequencies of the transformers that were in the respective lines. A preliminary transformer resonance test was conducted prior to this array testing. The results revealed the resonance of each transformer, and that resonant frequency was used as part of the amplitude modulation to ensure an adequate step up in voltage on the actuator side of the transformer. The magnitude of each individual signal was checked individually before testing. Each signal was set to have nearly the same magnitude at the downstream microphones.

The method to find the overall effect of the actuators on the resonator array consisted of adding one pair of active actuators at a time. Step by step this process is outlined in Table 8.1.

Step	Process
1	Find Tune Frequency of Passive Resonator Array (See Section 6.1.2)
2	Find the Phase Angle which Minimizes the Downstream Propagation of Sound for the First Pair of Actuators (Similar to the experiment described in Section 6.2)
3	Find the Phase Angle which Minimizes the Downstream Propagation of Sound for the Second Actuator Pair with the First Pair Operating
4	Find the Phase Angle which Minimizes the Downstream Propagation of Sound for the Final Actuator Pair with the First and Second Pairs Operating
5	Confirm Addition of Each Actuator has Reduced the Downstream Propagation of Sound

Table 8.1: Array Steps

For clarity, Figure 8. shows a cross section of the waveguide with three pairs of

resonator/actuators mounted on it. The cross section does not indicate that a pair of devices is composed of two, with only one shown. Figure 8.8 clearly shows the pairs at the same length along the waveguide.

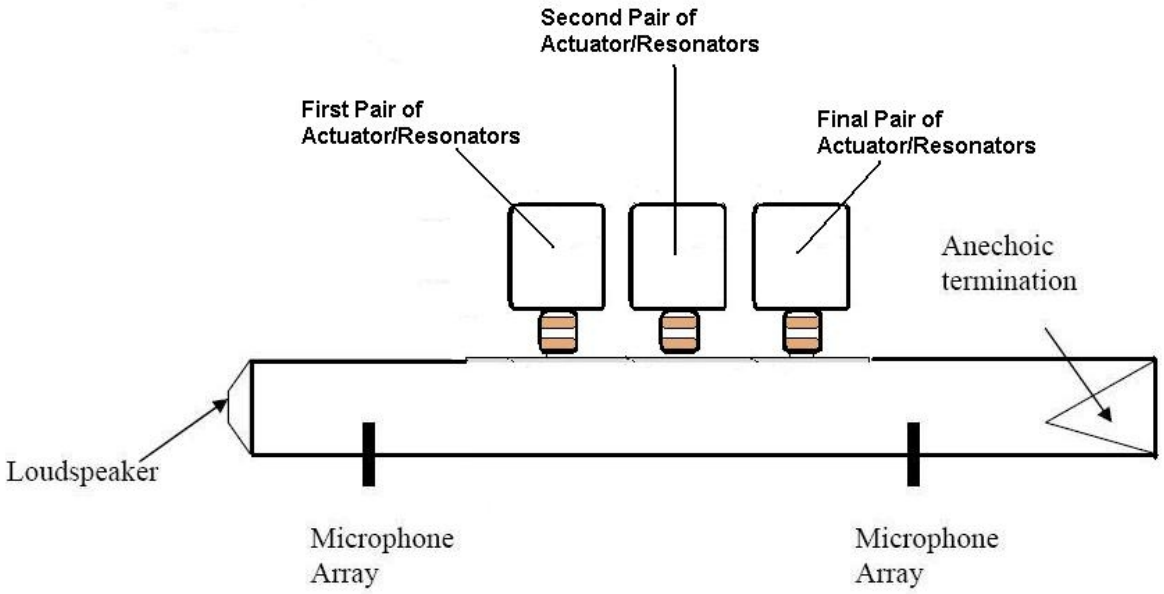

Figure 8.9: Cross Section of Array Mounted on Waveguide

The two microphone arrays shown in Figure 8.9 allowed for the breakdown of the pressure data at these points into upstream and downstream traveling waves. The method used is based on the work of Olivieri, Bolton, and Yoo [56]. Using two microphones spaced a short distance along the waveguide, the two signals at both upstream and downstream are broken down to two waves propagating upstream and downstream. Figure 8.10 is from the work of Olivieri *et al.* and shows many similarities between their experimental set up and the setup used for experiments in this thesis.

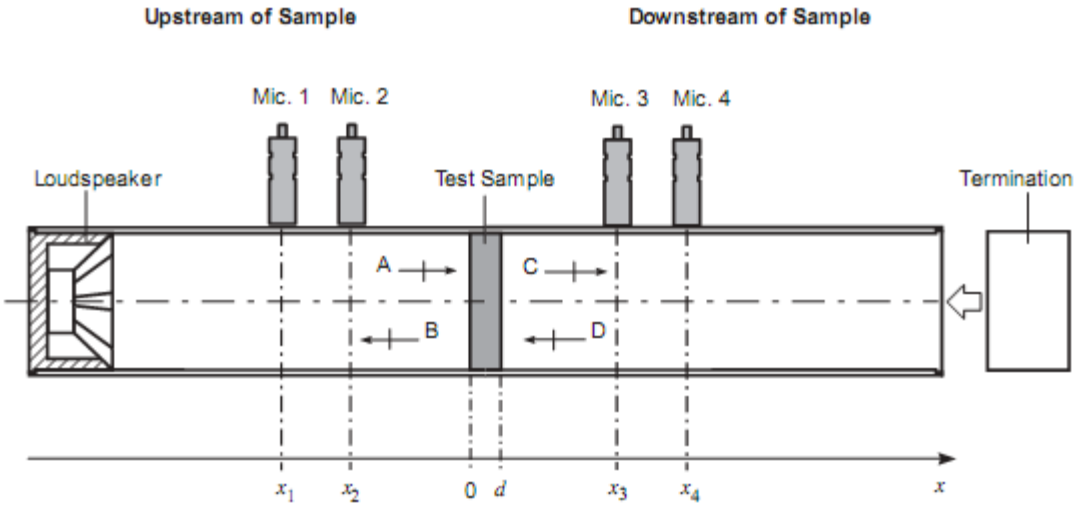

Figure 8.10: Four Microphone Method Setup[6] used with permission of J. Stuart Bolton and Bruel & Kjaer, 2010

Two terminations were necessary to fully characterize the the waves the anechoic cone termination was used, as well as an open termination.

8.3 *Results*

The method used to collect data and analyze that data focused on transmission loss [56], but insertion loss is a more appropriate metric for comparison. The results presented in this section were collected by following the methodology described in Table 8.1. The SPL at the microphone array due to the disturbance speaker with the passive resonator array mounted was 74dB for the tone of interest. The results of the tune frequency test for the resonator array showed the resonant frequency at 1280Hz. With the experiment setup complete, the first set of data collected with an active actuator is plotted in Figure 8.11. Subsequent results for the

second and final pair of actuators are plotted in Figure 8.12 and Figure 8.13. Figure 8.11 shows the best phase angle for that signal, where the IL is a maximum. The plot covers insertion loss results for phase angles from 120º to 560º.

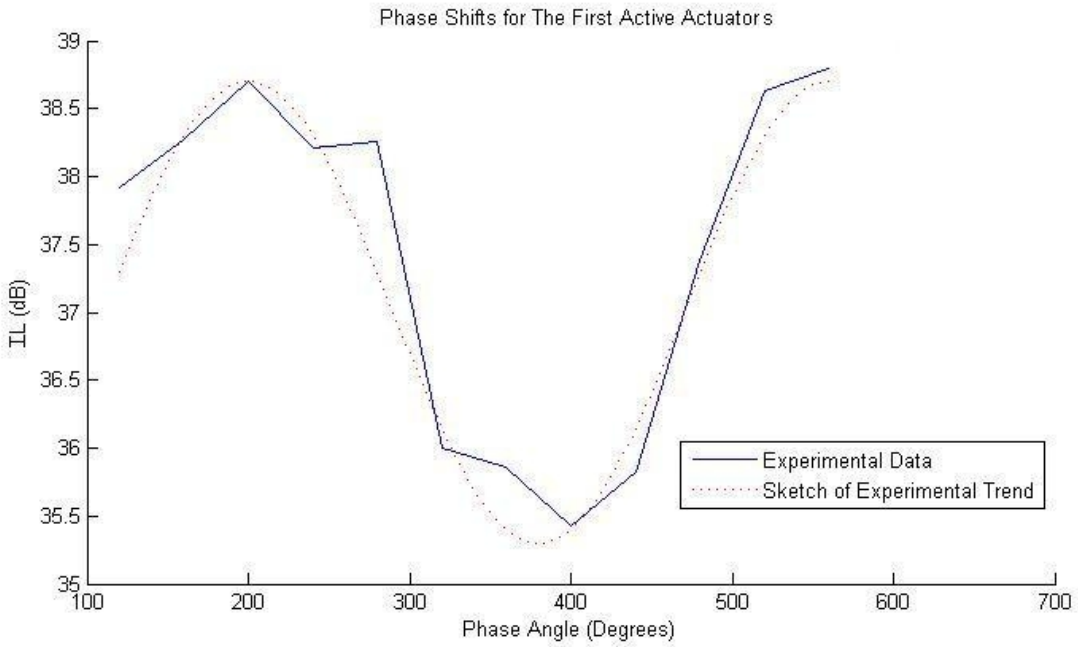

A higher the insertion loss produces a lower sound propagation downstream, therefore the peaks are the ideal operational phase for maximum attenuation in each of these figures. The experimental results appear somewhat jagged, due to the fact that data points are taken every 40Hz. A smoother curve could be expected if more phase angle data points are collected.

The results show two peaks approximately 360º apart, as expected. The lower frequency peak occurs at 200Hz, and this will be the operational phase angle during the testing of the other two pairs of actuators. There were some noted arcing problems with the first actuator, these issues may have reduced the effectiveness of this first pair actuators.

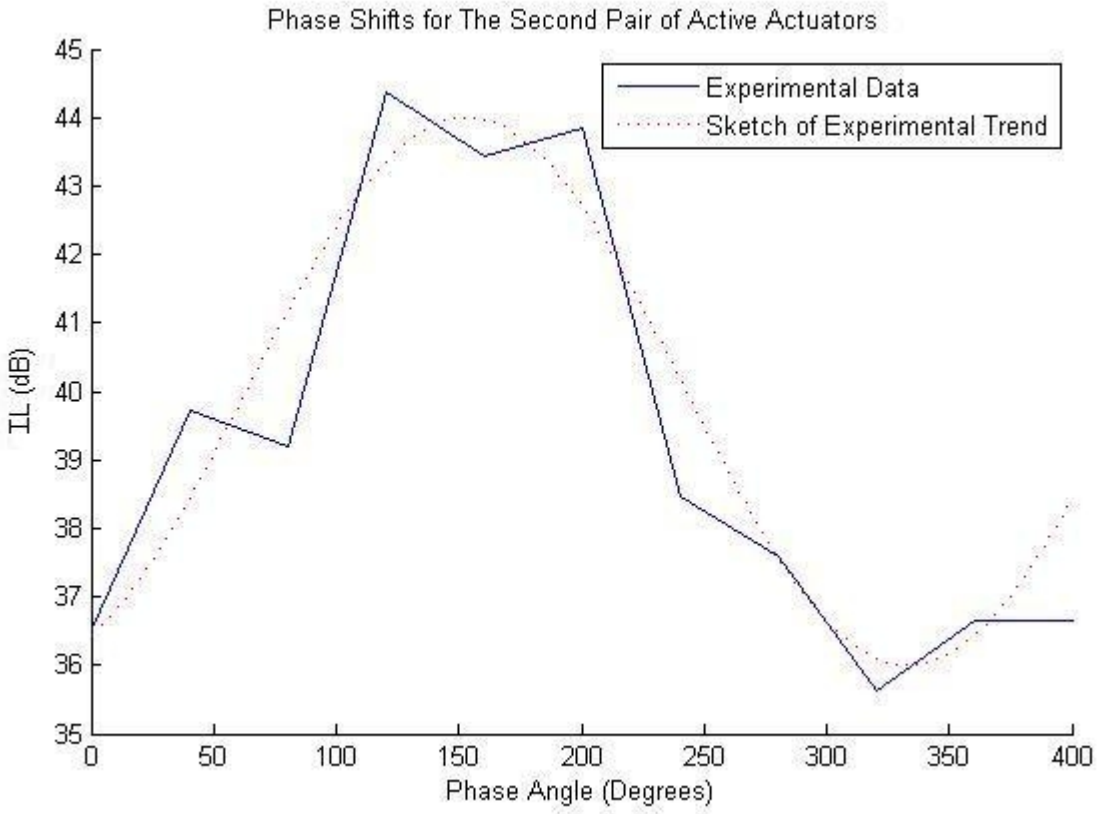

Figure 8.12: IL vs. Phase Angles for Second Pair of Active Actuators

Figure 8.12 shows the same type of trend as Figure 8.11, but the over-all insertion loss values (36-44 dB) have increased with the addition of the second active actuator set. The phase angle (for the second set of actuators) creates a maximum IL at 160º. This phase angle will be the operational value for the rest of the data collection.

Finally, Figure 8.13 shows the IL of the device with all actuators active. The variation in the phase angle of the final actuator pair is a controlled variable and is plotted on the x-axis, in the same manner as Figures 8.11 and 8.12.

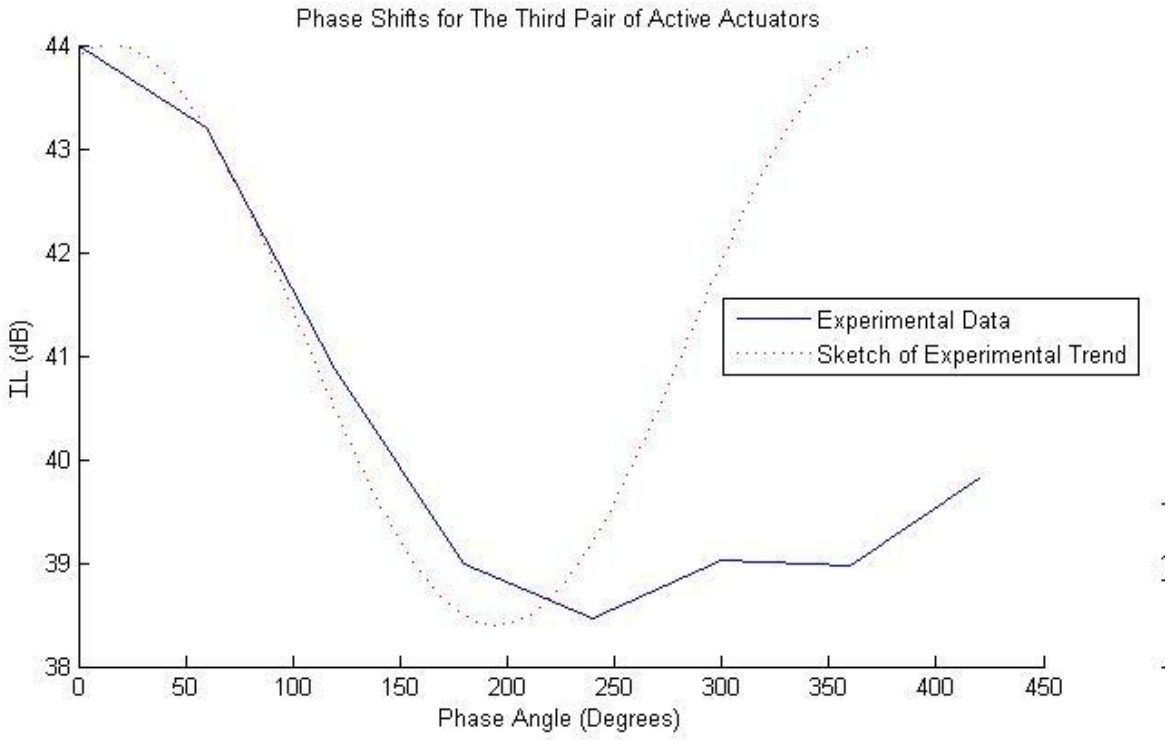

Figure 8.13: IL vs. Phase Angles for the Third Pair of Active Actuators

The addition of the final actuator did not significantly improve the IL. Arcing problems also occurred with this pair of actuators during experimentation. Figure 8.13 shows the actuator phase angle effect on the IL. The variation from the expected trend at phase angles above 200º is unusual compared to the results for the other two actuator pairs. The likely cause of the deviation in trend is the arcing problem. The dropping of the amplitude after long experimentation has been seen in earlier experiments with the plasma actuator.

8.4 *Conclusions*

Plasma actuators embedded in the necks of an array of resonator have shown a ability to improve the attenuation performance. The actuators require a sophisticate control system to allow the active components to effectively interact with the disturbance signal. The constructed device has simulated the workings of a turbofan liner reasonably well. The waveguide has also been designed with considerations for the turbofan engine environment. The implementation of the plasma actuator in the necks of four resonators showed improvement in the attenuation when phase relationships were controlled. The final pair of actuators did not show the same improvement that the previous two pairs of actuators produced. The 6dB variation in insertion loss is a smaller range than the 10dB created by varying the second pair of actuators.

9 Applicability

Throughout this research experience, many vital details that pertain to the applicability of this technology have been uncovered. This chapter will highlight the most important aspects that would be involved in employing the plasma actuator technology as an active addition to turbofan acoustic liner.

9.1 *Arcing Problems*

The fragile glow discharge-arcing boarder line was breached many times during testing. To avoid arcing problems, the plasma actuators must be very robust when employed as an addition to an acoustic liner. This robustness is necessary to prevent the positive glow discharge effects from being spoiled by a small impurity. The appropriate control system required to run the actuators is a difficult and costly system to integrate into a turbofan engine. The plasma actuator while a plausible choice is truly a difficult and costly technology to implement in this environment.

Throughout the progression of this research, arcing between electrodes has been a concern. The glow discharge, which is characteristic of operating plasma actuators, can easily convert to an arc discharge. The arc discharge occurs when the high voltage electrodes have an effective “short”. Arcing focuses all of the current through one dense path, while the glow

discharge is able to spread the ionization across more space. When dealing with the simple Helmholtz resonators, the plasma discharge should aid in the vibration of the air in the neck. If a single arc path is produced, it is unlikely it will be able to move large amounts of the air uniformly. Glow discharge is better suited to induce air flow within an actuator.

The arc discharge occurs when impurities or cracks are present in the dielectric of a plasma actuator. The high voltage electrodes discharge through the path of least resistance when an impurity is present. Poor wiring configurations also cause arcing issues. These two issues should be addressed when designing the perforated sheet with embedded plasma actuators for the acoustic liner.

9.2 *Embedding Actuators In Perforated Sheet*

The current acoustic liner uses a simple perforated sheet at the necks of the resonators. This sheet will require a number of design considerations in order to apply the plasma actuator technology. The dielectric will have to be able to withstand the environment inside the turbofan engine without fracturing. Beyond simply embedding the electrodes at each opening, a sophisticated control system is also necessary.

9.3 *Transformer/ Actuator Additional Weight*

The step up transformers used for testing weigh 1.3kg to 2.3 kg (3lb - 5lb). Those transformers are composed of a ferrite core and wire windings. They operated with AM signals to take advantage of the resonant frequency of the transformer.

Separate transformers were used for each channel during the Array Testing experiment, but it is conceivable that a single transformer could be used. This would require high voltage phase control on the actuator side of the transformer.

9.4 *Power Consumption of Actuators*

The power consumed by the actuators is another important design consideration. Labergue et. all report values of power consumption between 10 W/m to 100W/m for their plasma actuators [57]. The units have a length component to account for the length of the electrodes. Roth and Dia's conference paper [7] contains a great amount of information on plasma actuator operation. A number of power per unit length plots allow for comparisons to voltage and frequency of the signals for different actuator configurations.

9.5 *Ozone Production*

Implementation of the plasma actuator comes with an environmental issue. The operation of the actuator creates ozone. During experimentation, the ozone was perceivable by smell within a few moments of onset.

10 Summary/ Conclusions

10.1 *Overview of Work*

This thesis contains a summary of the work on the application of plasma synthetic jet actuators to turbofan acoustic liner. The goal of this research was to investigate the potential for improvement of turbofan acoustic liner performance by using this plasma actuator technology as a fluid flow control device. As a passive device, acoustic liners have improved the radiated noise levels which propagate from turbofan engines [58]. Previous work showed the applicability of plasma actuators as flow control devices in a number of situations [29] [31] [5]. Two types of flow produced by the plasma actuator were identified as mechanism for improvement: the bias flow and the oscillatory flow. Previous work on bias flow improvements [20] in acoustic liners indicated that this method could effectively improve liner performance. Active noise control methods also stand out as the other possible mechanism for improvement of the liner with by using oscillatory flow. The entirety of this work, especially the active noise control experiments, leads to a principle conclusion:

- A plasma synthetic jet actuator can be effectively used as a acoustic source.

10.2 *System Considerations*

The model and experiments focused on a simplification of the turbofan engine environment. A circular duct replaced the short-length and wide-diameter cylindrical housing of a normal turbofan engine with a scaled small-diameter duct. Special considerations were given to ensure plane wave propagation within both the modeled and experimental ducts for the bandwidth of interest. As construction of actuator/resonator devices progressed, the scaling factor between normal liner dimensions and the experimental device was improved. Initially, the constructed devices were approximately 20 times the dimensions of a normal liner, and by the final experiments this factor had been reduced to six.

10.3 *Modeling*

Models to estimate the active control mechanism were constructed. At the time of the model construction, a preliminary test to evaluate the bias flow mechanism had already been conducted. The results indicated that the one-directional flow control of the plasma actuator did not produce the necessary flow speeds to alter the attenuating characteristics (see Section 5.2). This fact obscured the rationale for modeling the bias flow mechanism of liner improvement. Further improvements in plasma actuator technology are necessary before the bias flow mechanism can be fully realized as a method of liner performance improvement.

The constructed model relied solely on the active control mechanism, which was the main focus of the later experiments (See Chapter 7 and 8) described in this thesis. The modeling

relied on finite element analysis to analyze the actuator/resonator waveguide system. The model reflected many of the dominant attributes that were built into the experimental setups.

The plasma actuator model offers a possible means to improve the performance of acoustic liner. A summary of the conclusions relating to the modeling is shown here:

- As much as 40dB of additional insertion loss was calculated at the re-tuned resonant frequency by the FEA. This value is unlikely to be fully realized during experimentation but can be noted as a theoretical ceiling on the improvement of the liner performance.
- The tune frequency of the resonators can be shifted by the activation of the actuators. Modeling results showed a 200Hz (12%) shift in tune frequency.
- The FEA model showed that retuning the resonant frequency of an array of actuators was possible by shifting the actuator firing times or the phase of the bandwidth of interest.
- The same series of simulations showed that other bandwidths (0.8kHz-1.2kHz and >1.6kHz in Figure 4.13) had increased energy reaching the virtual microphone.

10.4 *Actuator Redesign*

The goal of combining the plasma actuator technology with the acoustic liner technology required a deviation from the standard actuator configuration studied by Arvind Santhanakrishnan and Jamey D. Jacob [5]. Initially, their flat circular plasma synthetic jet actuator was the actuator configuration tested. However, the bias flow produced by the flat

actuator was unable to induce flow speeds necessary for significant attenuation improvement. A hot wire anemometer test showed that air flow speeds did not exceed 0.5 m/s. Consequently, the oscillatory flow became the focus. Applying the flat actuator assembly to the neck of a resonator did not prove to function as initially anticipated. Altering the flat line actuator design to cover the perimeter of a tube allows for better implementation as the neck of a Helmholtz resonator. In order for the oscillatory flow to produce consistent results, the phase must be controlled.

The research fell short of the goal of applying the plasma actuator technology to an actual piece of acoustic liner, but dramatic improvements were seen as constructed resonators progressed closer to actual liner dimensions. The actuator array was constructed from PVC pipe ends (as cavities) and fuzed quartz tubes (as necks), instead of a honeycomb core and a perforated sheet, which are the normal components of an acoustic liner. The other major research goal that was not achieved is the automatic generation of the plasma actuator drive signal. The control authority test provided some insight into the design of an active control system, but it does not consider the full scope of turbofan engine parameters necessary to implement such a system. Lastly, the array experiment attempted to bridge the gap between the experiments and an actual acoustic liner by deploying a number of actuators and resonators to better simulate an acoustic liner.

10.5 *Experimental Conclusions*

Initially, the dominate mechanism for acoustic liner improvement was unknown and two possibilities were identified: improvement by bias flow and the active noise control mechanism. The initial tests showed the bias flow produced by the plasma actuator was less than expected. This result drove the research towards focusing on the active control mechanism, which was further reinforced with the initial waveguide test. The results from this early waveguide produced two important conclusions:

- A plasma actuator can alter the performance of a Helmholtz resonator (by as much as 6dB).

The experiment showed as much as 6dB of added attenuation due to the plasma actuator during some data collections. During this same experiment as much as 5dB of added noise was recorded. The actuator had degraded the performance of the resonator in this situation. This extreme variation in results pointed to the need for phase control of the actuator signal. The following experiment addressed this parameter by phase locking the disturbance speaker and actuator signals. Again the improvement in the attenuation of the resonator was 5dB. This experiment also confirmed that driving a plasma actuator produced an acoustic tone at the driving frequency. A control authority test was conducted, and the results confirm a major characteristic of active noise control:

- The phase of the actuator driving signal plays an important part in the active control implementation of the plasma actuators within a Helmholtz resonator.

The next major experiment focused on applying the confirmed control authority to an array of actuator/resonators, simulating an acoustic liner environment. Testing in this situation allowed for investigations into issues that might occur during implementation. Examples of iteratively improved methods include the layout of the circuitry, powering, and driving of an array of active control actuator/resonators. Therefore, a better understanding of the challenges and difficulties inherent to the implementation in a turbofan were developed. Findings related to array construction and operation are summarized as:

- Wiring of the actuators in series ensures that all actuators operate.
- The inter-actuator arcing was alleviated by shielding individual outer perimeter electrodes. This method reduced arcing between neighboring actuators in the array.
- A large array of actuator/resonators will require specific phase information for each actuator.

10.6 *Final Remarks*

Commercially applying the plasma actuator technology to acoustic liners would prove to be costly. The feasibility of this device would require further development of a reliable face sheet and honeycomb core assembly. Once this scaling issue is addressed, the control system within the engine would require microphones and a feedback loop. The normal turbofan engine environment is harsh, so developing sensors that can effectively operate in this space will be necessary.

If the bias flow induced by the plasma actuator had been greater, then the need for phase control would be obsolete. Therefore, if some breakthrough in the plasma actuator technology dramatically improves this feature, then this work has produced an excellent basis for refining the attenuation capabilities of an acoustic liner with embedded plasma actuators. Without a greater bias flow speed, the oscillatory flow stands as the dominate mechanism for liner improvement.

Appendix A: Table of Dielectrics

This table of Dielectric materials and their properties was compiled by J. Reece Roth and Xin Dai and published in their conference paper, "Optimization of the Aerodynamic Plasma Actuator as an Electrohydrodynamic (EHD) Electrical Device" [7]. It is best used as a starting reference point when designing the dielectric portion of a plasma actuator.

Material	Mass density $\rho(kg/m^3)$	Dielectric constant (ε_r) (room temperature)	Dielectric Strength (E) (room temperature)	Dielectric loss tanδ (1MHz)	Loss Factor ε_r·tanδ	Reference
Teflon™	2160	2.1	11.2kV/mm	0.0001	0.00021	DuPont
Quartz	2200	5	25kV/mm	0.00001	0.00005	CEVP Ltd.
Aluminum Oxide	3700	9.4 (1MHz)	15kV/mm	0.0004	0.00376	KYOCERA
Glass	2600	3.8	10kV/mm	0.004	0.0152	MatWeb
Lexan™	1190	2.9 (1MHz)	16kV/mm	0.0085	0.02465	GE Plastics
Mica	2800	4~9	25kV/mm	0.0013	0.0052~0.0117	McMaster
Pyrex® glass	2530	4.1 (1MHz)	15kV/mm	0.005	0.0205	Corning
PC Board	1690	5	16.8kV/mm	0.005	0.025	DuPont
Bakelite	1420	5~22	24kV/mm	0.02	0.1~0.44	MatWeb
Kapton™	1420	3.5	154kV/mm	0.009 (100kHz)	0.0315	DuPont
Garolite G10/FR4	1820	5.2	20kV/mm(62mil)	0.0048	0.025	K-mac plastics
Garolite® G7	1680	4.2	15kV/mm(62mil)	0.00071	0.003	K-mac plastics

Appendix B: Simulation Transfer Function Plots

Transfer functions (TF) of simulation results are presented here.

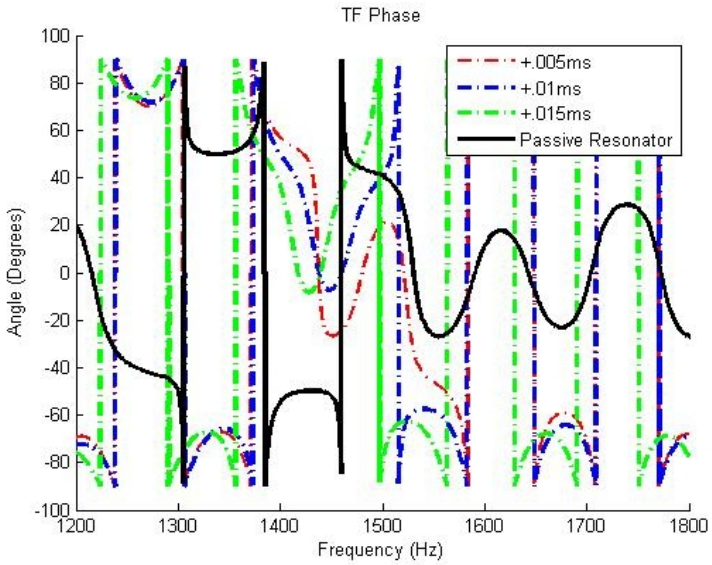

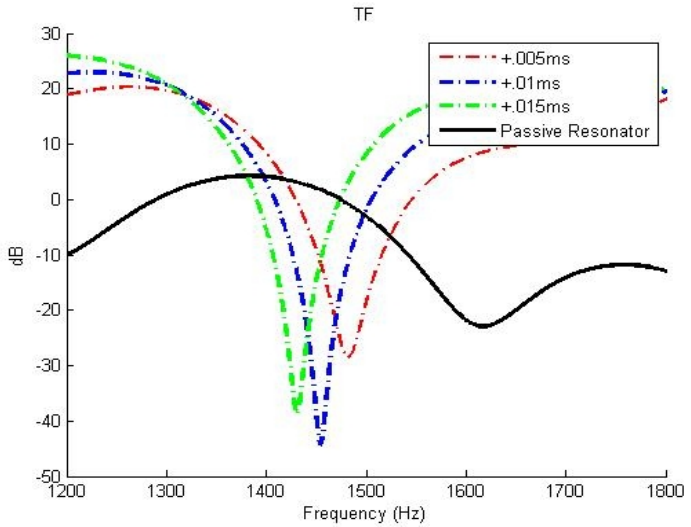

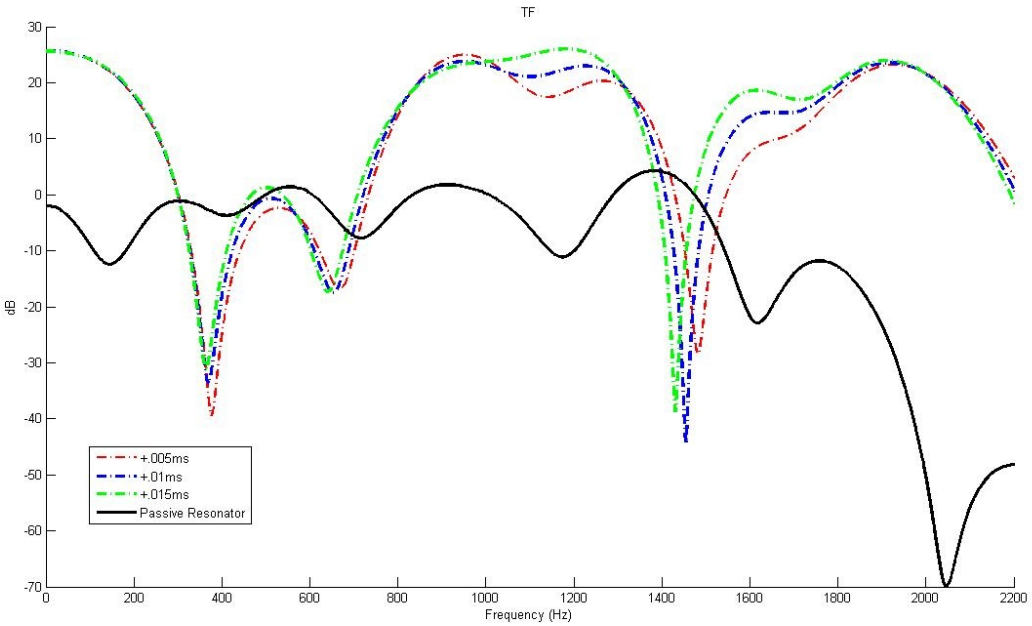
TF
dB
Frequency (Hz)
+.005ms
+.01ms
+.015ms
Passive Resonator

Appendix C: Matlab Actuator Script

This matlab script controlled the disturbance speaker and a actuator during early experiments and the control authority test.

```
clear all
close all

fs=48e3;
T=1/fs;
Tmax=30;
t= 0:T:Tmax;

fc = 18e3; %carrier frequency
fi = 1520; %Resonant Frequency of HR used

phase = 0; %phase offset between signals. in degrees
phas = phase*pi/180;
mu = 0.9;

      x1=(0.5 + mu * 0.5*cos(2.*pi.*fi.*t)) .* cos(2*pi*fc*t);

      x2=(cos(2.*pi.*fi.*t + phas));

      x = [x1' x2'];

plot(x(1:100,:))
soundsc(x, fs)
```

Bibliography

1. MacNeil, J. *GE 90 Turbofan Cut Away 3D Model.* 2007 [cited 2009 Oct 11]; http://www.fallingpixel.com/product.php/4330].
2. M. G. Jones, T.L.P., W. R. Watson, *Comparison of Acoustic Impedance Eduction Techniques for Locally-Reacting Liners,* in *9th AIAA/CEAS Aeroacoustic Conference and Exhibit.* 2003 Hilton Head, SC. p. 11.
3. Howe, M.S., *Acoustics of Fluid-Structure Interactions.* 1998, New York: Cambridge University Press.
4. Henriksson, J., *TownsendVI.png,* TownsendVI.png, Editor. 2007.
5. Arvind Santhanakrishnan, a. J.D.J. *Development and Characterization of Plasma Synthetic Jet Actuators.* 2005 Novermber 18, 2005 [cited 2009 Jan]; http://www.engr.uky.edu/~jdjacob/fml/research/plasma/index.html].
6. J. Stuart Bolton, T.Y., Oliviero Olivieri, *Measurement of Normal Incidence Transmission Loss and Other Acoustical Properties of Materials Placed in a Standing Wave Tube,* in *Bruel and Kjaur Technical Review.* 2007.
7. J. Reece Roth, X.D., *Optimization of the Aerodynamic Plasma Actuator as an Electrohydrodynamic (EHD) Electrical Device,* in *44th AIAA Aerospace Sciences Meeting and Exhibit.* 2006: Reno Nevada.

8. *Noise Pollution and Abatement Act of 1972*, in *Public Law No. 92-574, 86 Stat. 1234* FAA, Editor. 1988.

9. Helmholtz, H.v., *On the Sensations of Tone*. 1954, New York: Dover.

10. Rayleigh, L. *The Theory of the Helmholtz Resonator.* In *Proceedings of the Royal Society of London.* 1916L The Royal Society.

11. White, F.P. *The Period of a Spherical Resonator with a Circular Aperture.* In *Proceedings of the Royal Society of London.* 1916: The Royal Society.

12. Lawrence E Kinsler, A.R.F., Alan B. Coppens, and James V. Sanders, *Fundamentals of Acoustics.* 1999, New York: Wiley.

13. David A. Bies, C.H.H., *Engineering Noise Control; Theory and Practice.* 2003, New York: Spon Press.

14. Harold C. Lester, a.J.W.P., *Optimal One-Section And Two-Section Circular Sound-Absorbing Duct Liners For Plane-Wave And Monopole Sources Without Flow.* 1976, NASA: Washington D.C. p. 54.

15. Baumeister, K.J., *Optimized Multisectioned Acoustic Liners,* in *17th Aerospace Sciences Meeting.* 1979: New Orleans. p. 10.

16. J. Atvars, R.A.M., *Parametric Studies of the Acoustic Behavior of Duct-Lining Materials.* Journal of the Acoustical Society of America, 1970. **48**: p. 815-825.

17. Quentin Gallas, M.S., and Louis N. Cattafesta III, *Design Optimization Tool for Synthetic*

Jet Actuators Using Lumped Element Modeling. 2005, University of Florida. p. 21.

18. Michael G. Jones, M.B.T., Willie R. Watson, and Tony L. Parrott, *Effects of Liner Geometry on Acoustic Impedance.* AIAA, 2002. **2446**: p.10.
19. Watson, W.R., *Circumferentially Segmented Duct Liners Optimized for Axisymmetric and Standing-Wave Sources,* NASA, Editor. 1982: Hampton, Virginia. p. 51.
20. Tony L. Parrott, W.R.W., and Michael G. Jones, *Experimental Validation of a Two-Dimensional Shear-Flow Model for Determining Acoustic Impedance,* NASA, Editor. 1987: Hampton, Virginia. p. 51.
21. Keith S. Peat, J.-G.I., and Seong-Hyun Lee, *The Acoustic Impedance of a Circular Orifice in Grazing Mean Flow: Comparison with Theory.* Journal of the Acoustical Society of America, 2003. **114**(6).
22. Houston Wood, J.F., *Optimization and Control of Acoustic Liner Impedance with Bias Flow.* 2000, University of Virginia: Charlottesville. p. 22.
23. Betts, J.F., *Experiments and Impedance Modeling of Liners Including the Effects of Bias Flow,* in *Mechanical Engineering.* 2000, Virginia Polytechnic Institute and State University: Blacksburg p. 212.
24. Dean, P.D., *On the "In-Situ" Control of Acoustic Liner Attenuation.* Journal of Engineering for Power, 1976. **Paper No. 76-GT-61**
25. K. K. Ahuja, P.C., J. Geata, *Sound Absorption of a 2DOF Resonant Liner with Negative*

Bias Flow. 2000, Georgia Institute of Technology. p. 35.

26. Robinson, M., *Movement of Air in the Electric Wind of the Corona Discharge.* AIEE Trans, 1960. **80**: p. 143-150.
27. Robinson, M., *A History of the Electric Wind.* American Journal of Physics, 1962. **30**(5): p. 366-372.
28. Ashpis, L.S.Ha.D.E., *Demonstration of Separation Delay With Glow-Discharge Plasma Actuators.* AIAA, 2003. **41st Aerospace Sciences Meeting and Exhibit**: p.10.
29. Timothy I. J. Goodenough, P.W.G., Sylvia M. Goodenough, *The Efficiency of Corona Wind Drying and its Application to the Food Industry.* Journal of Food Engineering, 2006. **80**(4): p. 1233-1238.
30. F. Yang, N.E.J.-L., D.L. Brown, K. Pendergrass, D. A. Parker, I. A. Krichtafovitch, A. V. Mamishev, *Corona Driven Air Propulsion for Cooling of Electronics,* in *XIII th International Symposium on High Voltage Engineering.* 2003: Netherlands.
31. Xun Huang, S.C., Xin Zhang, *Atmospheric Plasma Actuators for Aeroacoustic Applications.* IEEE Transactions on Plasma Science, 2007. **35**(3): p. 693-695.
32. Sammie Chan, X.Z., Steve Gabriel, *Attenuation of Low-Speed Flow-Induced Cavity Tones Using Plasma Actuators.* AIAA 2007. **45**(7): p. 1525-1538.
33. Roth, J.R., *Electrohydrodynamically Induced Airflow in a One Atmosphere Uniform Glow Discharge Surface Plasma.* IEEE International Conference on Plasma Science

2003. **10**(5): p.1166-1172.

34. Moreau, E., *Airflow Control By Non-Thermal Plasma Actuators.* Journal of Applied Physics, 2007. 40(3): p. 605-636.
35. Amitay, A.G.M., *Synthetic Jets.* Annual Review of Fluid Mechanics, 2002. **34.**
36. Hansen, C. H., *Understanding Active Noise Cancellation.* 2001, New York: Spon Press.
37. M. C. J. Trinder, P.A.N., *Active Noise Control in Finite Length Ducts.* Journal of Sound and Vibration, 1982. **89**(1): p.95-105.
38. HVNTechnology. ADQ Systems. 2009.
39. A. S. Hersh, B. W., M. Bucha, *Effect of Grazing Flow On The Acoustic Impedance Of Helmholtz Resonators Consisting of Single and Clustered Orifices.* AIAA, 1978. **78-1124.**
40. Jeff D. Eldredge, A.P.D., *The Absorption of Axial Acoustic Waves by a Perforated Liner with Bias Flow.* Journal of Fluid Mechanics, 2003(485): p.307-335.
41. Xiaodong Jing, X.S., *Experimental Investigations of Perforated Liners with Bias Flow.* Journal of Acoustical Society of America, 1999. **106**(5): p. 5.
42. Elert, G. *Dielectric Strength of Air.* 2000 [cited 2010 Jan]; Available from: http://hypertextbook.com/facts/2000/AliceHong.shtml
43. Cobine, J.D., *Gaseous Conductors, Theory and Engineering Applications.* 1941, New York: McGraw-Hill. 606.
44. R. S. Sigmond, I.H.L., *Mass and Apecies Transport in Corona Discharge.* High

Temperature Chemical Processes, 1993. **2**: p. 221-229.

45. Ari Glezer, M. A., *Synthetic Jets.* Annual Review of Fluid Mechanics, 2002. **34**: p. 503-529.
46. Arvind Santhanakrishnan, J.D.J., *On Plasma Synthetic Jet Actuators.* AIAA, 2006. **AIAA Aerospace Sciences Meeting and Exhibit**(44th): p. 19.
47. C. L. Enloe, T.E.M., Robert D. VanDyken, K. D. Kachner, Eric J. Jumper, Thomas C. Corke, M. Post, O. Haddad, *Mechanisms and Responses of a Single Dielectric Barrier Plasma Actuator: Geometric Effects.* AIAA, 2004. **42**(3): p. 595-604.
48. Inman, D. J., *Engineering Vibration.* 1996, New Jersey: Prentice Hall.
49. Ingard, U., *On The Theory And Design of Acoustic Resonators.* Journal of Acoustical Society of America, 1953. **25**(6).
50. T. L. Parrott, M.G.J., *Parallel-Element Liner Impedances for Improved Absorption of Broadband Sound In Ducts.* Noise Control Engineering Journal, 1995.
51. Jacob Fish, T.B., *A First Course In Finite Elements.* 2007: Wiley. 336.
52. Bathe, K.-J., *Finite Element Procedures.* 1996: Prentice Hall.
53. Simulia. *Abaques 6.8 Documentation.* 2009 [cited 2009; Available from: http://www.esm.vt.edu/v6.8/
54. *Transfromers.* 2008 [cited 2008]; Available from: http://www.amazing1.com/transformers.htm.

55. Tipler, P.A., *Physics For Scientists and Engineers.* Vol. 3rd ed. 1995: Worth Publishers.

56. Oliviero Olivier, J.S.B, Taewook Yoo, *Measurement of Transmission Loss of Materials Using a Standing Wave Tube,* in *Inter-Noise.* 2006: Honolulu, Hawaii.

57. A. Labergue, E.M., N. Zouzou, G. Touchard, *Separation Control Using Plasma Actuators: Application to a Free Turbulent Jet.* Journal of Physics, 2006. **20**.

58. A. McAlpine, R.J.A., V.J.T. Hii, N.J. Baker, A.J. Kempton, *Acoustics scattering by an axially-segmented turbofan inlet duct liner at supersonic fan speeds.* Journal of Sound and Vibration, 2006. **294**.